

Physics of electrophotography

Damodar M. Pai and B. E. Springett

Xerox Corporation, Webster, New York 14580

Electrophotography is one means of arranging 100 million pigmented plastic particles on a sheet of paper to faithfully replicate an original. It is based on many diverse phenomena and employs many properties of matter. These include gaseous ionization in the charging step; photogeneration and charge transport through disordered solid-state materials in the latent-image-formation step; triboelectricity in the particle-charging step; mechanical, electrostatic, and magnetic forces to detach particles in the development and transfer steps; and the application and transfer of heat in the fixing step. In addition, it relies on a precise balance of thermorheological, chemical, and mechanical properties of large area films and small particles. This article reviews the physics of the latent-image formation and development steps.

CONTENTS

I. Introduction	163
II. Overview of the Electrophotographic Subsystems	165
A. Charging subsystem	166
B. Exposure subsystem	167
C. Photoconductor subsystem	169
D. Development subsystem	169
E. Transfer subsystem	172
F. Fusing subsystem	173
G. Cleaning subsystem	174
H. Erase subsystem	174
I. Print quality considerations	174
III. Charge-Image Formation in a Photoconductor	175
A. Photoconductor requirements	175
B. Brief survey of photoreceptors	175
C. Photoinduced-discharge curve	176
D. Photoinduced-discharge curve: field-dependent supply	177
E. Photoinduced-discharge curve: mobility-limited discharge	183
F. Measurement technique	189
IV. Development Fields	190
V. Contact Electrification	194
VI. Toner-Carrier Adhesion Forces and Detachment of Toners	198
VII. Tone Reproduction Curve	202
VIII. Color Electrophotography	203
IX. Gain: Photography Versus Electrophotography	203
X. Conclusions	204
Acknowledgments	205
Appendix: Other Electrophotographic Imaging Systems	205
1. Electrofax	205
2. Overcoated xerography	206
3. Ionography	206
4. Photoelectrophoresis and particle migration	206
5. Thermoplastic electrophotography	207
6. Magnetography	207
References	207

I. INTRODUCTION

The invention of electrophotography has ushered in a worldwide revolution in document processing. It is the technology that underlies the operation of virtually all office copiers and laser printers. In the annals of modern

technology, the invention and development of electrophotography is unique. It is the creation of a lone inventor, Chester F. Carlson, whose early experiments leading to the invention were conducted in the kitchen of an apartment in New York City (Dessauer, 1971). As originally patented by Carlson, the process was referred to as "electrophotography." When it was commercialized the process came to be known also as "xerography." In this article "electrophotography" and "xerography" are used somewhat interchangeably. The name "xerography" has its origin in the Greek words *xeros* (dry) and *graphos* (writing; Schaffert and Oughton, 1948). The invention is based on the synthesis of a variety of phenomena, some of which were very obscure and poorly understood, such as the charge exchanged by surfaces in contact and moving relative to each other (triboelectrification). Chester Carlson disclosed and demonstrated the crude process to 20 major U.S. corporations, whose help he sought in developing a practical commercial process of his invention. He is later supposed to have remarked that he met with "an enthusiastic lack of interest" from these companies (Gundlach, 1989). Figure 1 illustrates something of the quality of Carlson's initial demonstration and also records the date of his first real success. Finally, the commercial development of the process took place first in a small independent laboratory, the Battelle Memorial



FIG. 1. Chester Carlson's first image, consisting of the date and location (Astoria, NY), which he used as a successful demonstration of the electrophotographic process (after Carlson, 1942).

Institute, and subsequently at Haloid Company (now Xerox Corporation), which was at the time a small company in upstate New York. The work at Battelle resulted in major improvements in the photoconductor-charging device, in the image-development step, in the transfer of the developed image to paper, and in the introduction of a photoconductor based upon amorphous selenium (Schaffert and Oughton, 1948; this paper contains the word "xerography" in the title and states that the object is "to introduce the subject of xerography.") The basic process at this point involved creating an electrostatic charge pattern on a photoconductor with light and attracting charged dry ink (toner) to this pattern to develop it. Refinements and rapid strides in understanding the physics of the process began almost immediately upon publication of the Schaffert and Oughton paper. For a view of the involvement of the scientific community in the developments, see Pake, 1992.

It would be 21 years after the invention by Chester Carlson before the first automated copier was introduced in the marketplace. Today the xerographic process makes over 5 billion copies every day, an amount that is being augmented by the rapidly growing field of electronic printing in both black and white and color. The new industry created as a result of this invention today employs over 500,000 people worldwide and has an annual revenue base of over \$100 billion (Gundlach, 1989). The dry ink, or toner, accounts for some \$4 billion and photoreceptors some \$5 billion of this total. Since the invention of xerography by Chester Carlson in 1938, a variety of imaging systems under the generic title "electrophotography" (see the Appendix) have been invented and some developed into commercial products (Carlson, 1940, 1942; Dessauer and Clark, 1965; Schaffert, 1975).

A xerographic image consists of on the order of 100 million pigmented plastic particles arranged on a sheet of paper to replicate an original image. The xerographic process begins with the creation of a charge pattern, replicating the original optical image, formed on a photoconducting film. Charged, pigmented thermoplastic particles, called toner (the dry ink), are selectively attracted to the charge pattern, thereby developing it. The toner image is then transferred to paper and fixed by softening and fusing the toner to the paper. The process is designed to be repetitive and to operate at printing speeds greater than 100 pages per minute. It is the purpose of this review to describe this process much more fully and, in particular, to focus on the electrostatic image creation and development steps. We shall begin the discussion with brief descriptions of each of the steps in the imaging process in order to illustrate the scientific understanding that must be brought to bear to fully characterize each step, and to illustrate the interconnectivity of these steps (Sec. II). This section closes with a commentary on print quality and the considerations that must be kept in mind in order to design a successful copying or printing system. This section will be followed by a more detailed discussion and description of the typi-

cal photoconductors in use today and their role in the electrostatic image-forming step (Sec. III). Next come four sections (Secs. IV–VIII) that describe the processes by which toner is charged and how it interacts with the electrostatic charge pattern to develop the image. Before elaborating on some conclusions (Sec. X), we comment on the extension of the electrophotographic process to color (Sec. VIII) and compare it to photography (Sec. IX). Lastly, in the Appendix, we very briefly describe some major variants to the generic electrophotographic process.

There are many useful books dealing with various aspects of electrophotography. A historical perspective and an early survey of the field can be found in the first book published on the subject, *Xerography and Related Processes*, edited by J. H. Dessauer and H. E. Clark (1965). *Electrophotography*, by R. M. Schaffert (1975), contains details on the technology of the subsystems and is a useful source of patent literature. *The Physics and Technology of Xerographic Processes*, by E. M. Williams (1984), and *Electrophotography and Development Physics*, by L. B. Schein (1988), are two very useful books for scientists and engineers who might wish to enter the field. *The Anatomy of Xerography, Its Invention and Evolution*, by J. Mort (1989), gives very useful insights into the science and technology that resulted in Carlson's invention. The latest book on materials for electrophotography is *Handbook of Imaging Materials*, edited by A. S. Diamond (1991). There are other books and review articles on various aspects of electrophotography, and they are referenced as the article proceeds.

It is pertinent to ask what this review adds to the literature base, since several books have been written about aspects of the subject matter. Most books (and articles) focus on more specific details of certain parts of the process, or are more descriptive than this short review. This review is also limited, with the intent being to focus on some of the specific physics of the image-forming process. This focus is intended to implicitly emphasize several points not typically stressed. They are the fact that the image-forming process itself is dependent on a balance of interactions between distinct solid states of matter, radiation, and electric and magnetic fields, with the resulting need for a strongly multidisciplinary approach to understanding basic mechanisms; that quite simple physical ideas lie at the root of the process; and, lastly, that much of the physics takes place on a scale of microns and milliseconds and is very dependent on events at material surfaces. Accordingly, this review makes only little use of equations and detailed theory and illustrates the ideas by reference to experiments in a wide variety of materials. The level of the material is such that by and large it should be accessible to final-year undergraduate or first-year graduate students.

The development of electrophotography and its related variants is not yet a closed book. Because of its commercial importance and multidisciplinary nature, advances and improvements in understanding are not usually re-

ported in the regular scientific literature. It is also true that reports by industrial scientists and technologists dominate the literature. Accordingly, apart from the books and review articles referenced in this review, the reader is referred to the following journals and proceedings where regular reports on various aspects of the subject may be found: *Journal of Imaging Science & Technology*; *Proceedings of the International Conferences on Non-Impact Printing* (published by the Society for Imaging Science & Technology); *Journal of Electronic Imaging*; *Proceedings of the Annual Joint SPIE/IS&T Conferences* (published by SPIE); *Electrophotography* (in Japanese, published by the Japanese Society for Electrophotography); and the United States, European, and Japanese patent literature.

II. OVERVIEW OF THE ELECTROPHOTOGRAPHIC SUBSYSTEMS

As already stated, the process of creating a hard-copy image electrophotographically involves using electrostatic forces to achieve the image-development step. Before discussing how, specifically, the electrostatic image is created, it is useful to consider the generalities of the electrostatics of the situation. Imaging systems based on the movement of electrically charged toner particles and their deposition on a substrate are described by

$$F_e = QE, \quad (1)$$

where F_e is the force exerted on the toner particles, Q is the charge on the toner particles, and E is the electric field acting on the toner particles. The image formation itself is based on the spatial variation δF of the force F_e on the toner particle and is given to first order by (Schmidlin, 1972)

$$\delta F = Q\delta E + E\delta Q, \quad (2)$$

where δE is the spatial variation in electric field applied to the toner particle and δQ is the variation in charge on the toner particles. The first term in Eq. (2) defines the imaging system envisioned by Chester Carlson. In this system particles with essentially constant charge move in a field pattern that replicates the subject to be imaged. The differential force δF on the toner particles produces a developed real image, since larger fields transferred more toner to the electrostatic latent image than smaller fields. Imaging systems based on the second term, such as those employing photoelectrophoresis and particle migration (Tulagin, 1969), have also been developed. These processes rely on the electrophoretic motion of charged pigment particles in a liquid or near-liquid dielectric medium under the influence of a constant electric field. The charge on a pigment particle, and hence its motion, is controlled by absorbed light. Specifically, the charge δQ is photogenerated in the pigment and exchanged with the dielectric medium.

In another form of electrophotography, termed "dipole

xerography" (Bean and Miller, 1978; Chen, 1982), the uncharged toner particles are polarized by the field gradient, $\text{grad } E$, above the photoconductor surface. The induced dipole moment p is also proportional to the electric field E . The force exerted on the toner particles is given by

$$\begin{aligned} F_e &= p \cdot \text{grad } E \\ &= \alpha E \cdot \text{grad } E \\ &= \frac{1}{2} \alpha \text{ grad } E^2. \end{aligned} \quad (3)$$

The image is based on the variation of force

$$\delta F_e = \frac{1}{2} \alpha \delta (\text{grad } E^2). \quad (4)$$

For narrow line images, a strong-field gradient exists over the image. In order to create a dipolar force over a solid-area image, a periodic or modulated charge pattern has to be created. The methods employed to accomplish this include screened exposure, screened corona charging, or a specially fabricated photoconductor structure with a dot pattern on the substrate (Bean and Miller, 1978).

Other imaging principles employed in electrophotography include electrofax, thermoplastic and overcoated xerography, and ionography (Pell and Teegarden, 1969; Rice and Schaffert, 1972; Weigl, 1977). The discussion in this article is devoted to xerography, which is one form of field variation electrophotography on which most of the commercial electrophotographic systems are based. Other electrophotographic and related systems are summarized in the Appendix.

When Chester Carlson demonstrated his process in 1938, it was little more than a feasibility demonstration. He employed a primitive photoconductor consisting of a layer of sulfur on a zinc plate. The charging was done by rubbing the sulfur surface with a cotton handkerchief. The charged photoconductor was then exposed to light to create a latent electrostatic image. He developed the image by dusting the surface with lycopodium powder and transferred the powder image by pressure to a sheet of waxed paper. Some of the early important improvements, as well as technical control of the individual process steps, were done initially at Battelle, and later at Haloid, in the late '40s and early '50s. These first major improvements involved the use of a fine wire held at a high voltage to effect the charging step ("corona emission"), the use of toner and carrier beads in an agitated state to achieve toner charging triboelectrically, the use of electrostatic fields to transfer the "toned" image to paper, and, as already mentioned, the introduction of amorphous selenium as the photoreceptor to give a much improved photosensitive response. This was well before all the steps were understood at a scientific level (Gundlach, 1989, Mort, 1989). Major advances have subsequently been made based on an increased understanding of the mechanisms of these particular process elements (Comizoli *et al.*, 1972; Schaffert, 1975; Mort and Pai, 1976;

Watson, 1979; Scharfe, 1984; Williams, 1984; Schein, 1988).

The design of an imaging system based on these ideas requires a method of converting the light image into an electric-field pattern and a means of charging the toner particles. To fix ideas and to visualize the process, consider Fig. 2, which has been drawn to have some parallels with the photographic process steps. It is also drawn to roughly parallel the steps as used by Carlson in his demonstrations. Steps 1 and 2 show the corona charging device (a corotron) moving across the photoconductor plate to create a uniform surface charge (in this case negative). Step 3 shows the use of a single lens to image the "original" (the dark "E") onto the charged photoconductor. Step 4 shows the photoconductor with a charge pattern (in the form of an "E") on it being developed by toner, which in this case is positively charged. Note that no charge exists where light arrived at the photoconductor. In step 5, a piece of paper has covered the image and a corona charging device lays down a uniform charge (again negative) to electrostatically attract the positively charged toner to the paper. Step 6 shows the paper with toner image on it being separated from the photoconductor and subsequently being fused by a heating process in step 7.

To be commercially viable this whole process needs to be packaged so that it can be done repetitively at high speed. So in practice the photoconductor is what moves, and an erase step is introduced in order to refresh the photoconductor. The other steps are adjusted to cope with the relative motion of the photoconductor. The basic steps and machine configuration in a commercial xerographic process are shown in Fig. 3. The steps are conceptually identical to those originally proposed by Carlson and illustrated in Fig. 2. The only difference lies in the sophistication of the individual steps (Berger *et al.*, 1979; Williams, 1984; Schein, 1988; Pai and Melnyk, 1989; Scharfe *et al.*, 1989; Diamond, 1991). The charge pattern, which is produced by the imagewise photo-discharge of a charged photoconductor film, produces an electric field outside the photoconductor surface. The

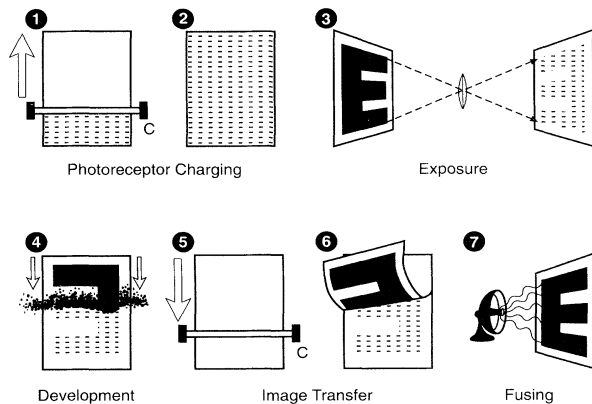


FIG. 2. Electrophotographic process drawn to parallel roughly the steps used by Carlson.

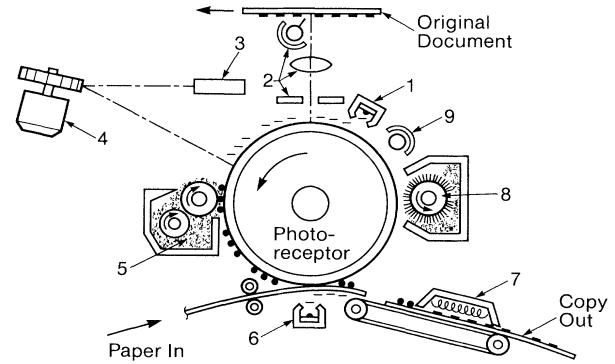


FIG. 3. Xerographic reproduction machine indicating the important process steps: (1) corona charging; (2) exposure with light and lenses; (3) laser; (4) rotating polygon; (5) development; (6) transfer; (7) fixing; (8) cleaning; and (9) erasing (after Pai and Melnyk, 1989).

toner is charged by repeated contacts with larger particles (the carrier) of a different material. The phenomenon of charge transfer by contact or rubbing is termed "contact electrification" or "tribocharging" (the term "tribo" comes from the Greek work meaning "to rub"). The charged toner is attached to the oppositely charged carrier particle by means of Coulombic and short-range van der Waals adhesive forces. The imaging system also requires a method of delivering the carrier particles with the attached toners in the region of the electric-field pattern above the photoconductor surface where those patterned fields detach the toner from the carrier and deposit them on the photoconductor surface to replicate the image. Some of the characteristic features of the electrophotographic images are determined by the penetration of the field pattern in the space above the photoconductor surface, the sign and magnitude of the charge on the toner, and the system employed to deliver the carrier-toner mixture.

We turn now to a more detailed discussion of each of the steps mentioned above and shown disposed around the photoconductor in Fig. 3. Note that the photoconductor may, in fact, be an elongated flexible belt rather than a rigid cylinder.

A. Charging subsystem

The first step in the xerographic process, shown in Fig. 2, is to charge the photoconductor. This can be accomplished in several ways. The most common method is to charge with a corotron or scorotron (Dessauer *et al.*, 1955; Dessauer and Clark, 1965; Schaffert, 1975). A corotron is essentially a thin wire ($< 100 \mu\text{m}$ in diameter) to which a high voltage is applied. A high voltage of from 3 to 8 kV generates a large electric field around the wire which, in turn, generates a plasma immediately sur-

rounding the wire by accelerating randomly created electrons from cosmic rays, field, or thermal emission (Waters and Stark, 1975). Ions then drift from the plasma under the action of the external and space-charge electric fields to the surface of the photoconductor, thereby charging the photoconductor. Further details of these corona discharge processes can be found in Loeb (1965) and Sigmond and Goldman (1981).

In the case of a positively biased wire, electrons and negative ions in the surrounding air are drawn to the wire, causing secondary ionization consisting of electrons and positive and negative ions in the vicinity of the wire. Positive ions, consisting primarily of hydrated protons, $(\text{H}_2\text{O})_n\text{H}^+$ (Shahin, 1969), are repelled from the plasma surrounding the wire and driven by the electric field to the shield and photoconductor. In the case of a negatively biased wire, electrons are emitted from the wire and ionize the air. The electrons attach to molecules so that the charge deposited is ionic, dominated by hydrated $(\text{CO}_3)^-$ (Shahin, 1969). In both cases, the plasma is confined to the neighborhood of the wire, extending out to a radius of some 3–5 times that of the wire, and is clearly visible in the dark; most of the light emission is from atomic nitrogen. The plasma chemistry is exceedingly complex, and a wide variety of chemical species are created therein, including ozone, oxides of nitrogen, and ammonia (see, for example, Naidis, 1992).

A scorotron is similar to a corotron, except that a control grid is placed between the ion-emitting wire and the photoconductor. The control grid is used both to improve charge uniformity and to limit the charging of the photoconductor (Schaffert, 1975; Tateishi and Hoshino, 1981). Control is accomplished by applying a voltage to the grid approximately equal to the required final potential on the photoconductor. Ions pass through the grid and deposit on the surface of the photoconductor until the photoconductor surface potential equals the grid potential. At this point, the ions will flow only to the control grid, since the electric field between the grid and the surface of the photoconductor has approached zero. This device acts therefore somewhat like a triode.

Photoconductors can also be charged by pins, i.e., needles with sharp points. The pins are biased to a high potential that produces a strong electric field at the point of the pin where the radius of curvature is extremely high. The air breaks down in this region, producing an ion sheath that can be used to charge the photoconductor. Uniform, large-area charging is produced by several pins spaced at regular intervals along the length of the charging device.

As a simple example of this step in the process, Fig. 4 shows an idealized response curve of a scorotron (the geometry is shown in the inset.) When a photoconductor passes beneath this device at a velocity v , the resulting exit voltage V_s on the surface of the photoconductor is given by

$$V_s = V_G [1 - \exp(-I_0/V_G C v)] + V_i \exp(-I_0/V_G C v), \quad (5)$$

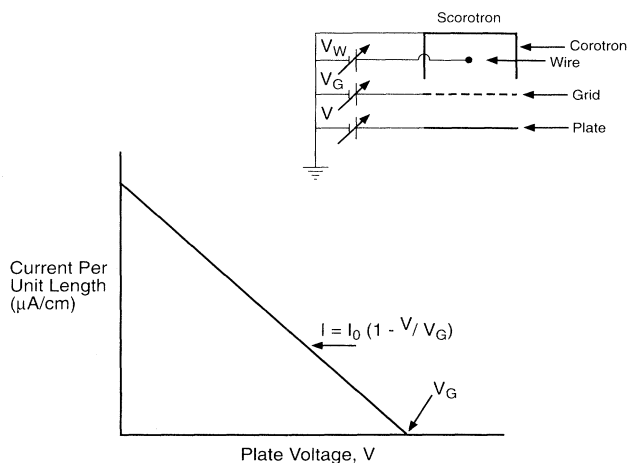


FIG. 4. Idealized current-voltage response curve of a scorotron. The geometry is shown in the inset.

where C is the photoconductor capacitance per unit area, I_0 is from the scorotron response curve (initial current), V_i is the incoming voltage, and V_G is the grid voltage. This equation shows how V_s approaches the grid potential, V_G . Both the scorotron and the photoconductor properties enter into this process. As can be seen, I_0 needs to be increased as v increases in order to keep V_s constant for a given photoconductor. For more complex computations, these devices may be modeled using well-known techniques (Springett *et al.*, 1978; Watanabe *et al.*, 1991).

The corotron wire may also be excited by an ac voltage (Cheung and Springett, 1981). This is usually done in order to provide an alternating flow of positive and negative charges in order to erase an electrostatic image on the photoconductor which has lots of fine detail without using a secondary photodischarge step. It is also often a convenient way to neutralize the charge on isolated toner particles.

B. Exposure subsystem

The charged photoconductor is imagewise light-exposed to form an electrostatic latent image. Copiers with drum photoreceptors require scanning optics that project a moving narrow strip of the original image through a slit onto, and synchronously with, the moving photoreceptor surface. Many techniques have been used to accomplish this. One is to project the original image through a lens on a rotating mirror that scans the image across a slit synchronously with a photoreceptor motion. Another is to scan the original image with moving lamps and mirrors, projecting the image through folded optics that maintain the original focus on the photoreceptor through a slit. In small, personal copiers, another approach is to move the original document with rollers or a translating platen while keeping the optics stationary.

One advantage of the latter is the use of very low cost fiber optics in a bar, called "selfoc lenses," in place of lenses and mirrors. Early copiers, with amorphous selenium photoconductors, which are primarily sensitive in the blue wavelength region of the visible spectrum, had fluorescent tube lamps in scanning optics and xenon flash lamps in full-frame exposures employed in high-speed duplicators. In flash exposure systems, the full image is projected on a flat area of a belt photoreceptor with a xenon flash lamp to freeze the image on the moving belt. Present-day copiers with scanning optics tend to have high-temperature incandescent (tungsten-halogen) tube lamps in place of fluorescent lamps. These systems are also capable of 60% to 150% image reduction or magnification (i.e., a zoom feature).

In xerographic printers the photoreceptor is discharged digitally with light spots that are turned on or off (Vahtra and Wolter, 1978; Starkweather, 1980). The differences between analog and digital copying are shown in Fig. 5. The complexity of digital copying comes from the added computing power embedded in the copier. This complexity adds cost, but it also increases the image manipulation flexibility of the device. A printer is obtained by simply leaving out the scanning system and providing a direct connection to a computer. Intermediate exposure, gray-scale imaging, is also possible. Digital imaging is performed in several ways. The majority of xerographic printers use a laser and a rotating polygon flying spot light exposure. The laser light beam is projected onto a rotating polygon mirror which causes the light beam to be repetitively swept across the photoreceptor. By timing the sweeps to repeat after the photoreceptor has advanced the width of the beam spot, the surface of the photoreceptor is raster scanned much like the electron beam in a television tube. The beam is turned on or off by an optoacoustic modulator (Gotlieb *et al.*, 1983) or

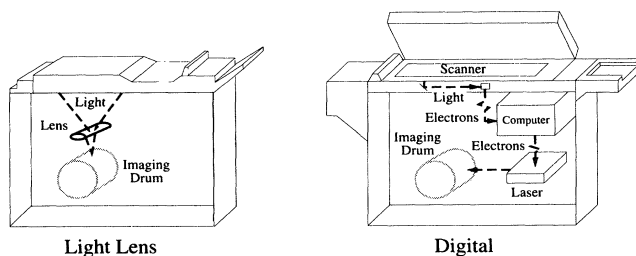


FIG. 5. Light lens (left) and digital electrophotography (right). Light-lens copiers capture an image with a lamp and a lens and hold the image on the drum while copies are made. Digital units capture hard-copy images with scanners and convert the images to digital form for electronic printing. The digital information is employed to modulate a laser beam. Only high-volume printers have the capability of scanning and digitizing the image. Low-volume printers generally receive the digitized image either from a workstation or from a scanner at a remote location. A digital document can be manipulated prior to printing in ways not possible with a lens-and-lamp system.

by directly modulating a solid-state diode laser. Other approaches used are image bar arrays of individually addressable light-emitting diodes (LED), or liquid-crystal and magneto-optic light valves (Williams and Hall, 1978; Ross, 1979; Haas, 1983). The two most commonly used lasers, HeNe and GaAlAs, emit at 633 and 780 nm, respectively, while the LED's used in image bars emit from 660–680 nm. However, the use of gas lasers is currently in decline. Hence the photoreceptors for the xerographic printers require photosensitivities in the red to near-infrared part of the spectrum.

The schematic of a digital exposure system using a 12-sided polygon and a solid-state laser are shown in Fig. 6. The sides, or facets, of the polygon reflect the laser light. The number of facets on the polygon and the rotational speed of the polygon determine the resolution, also known as pixels per unit length. Printing speeds of 100 pages per minute or more can be generated with this scheme.

The optical density of an image is defined through

$$D = -\log_{10}(X_i/X_{bg}), \quad (6)$$

where X_i is the light reflected from the image and X_{bg} is the light reflected from the background on which the image is superimposed. X_{bg} also includes non-image-forming light, or flare, which is often a nearly uniform light over the whole image. In normal copying and duplicating, input images usually consist of typewritten characters, pencil or pen writing, continuous-tone photographs, and halftone images, while the background is usually the "white" paper on which the images are superimposed. As suggested above, an input image can be described in terms of its size and optical density. For example, a typewritten character is typically 200–300 μm

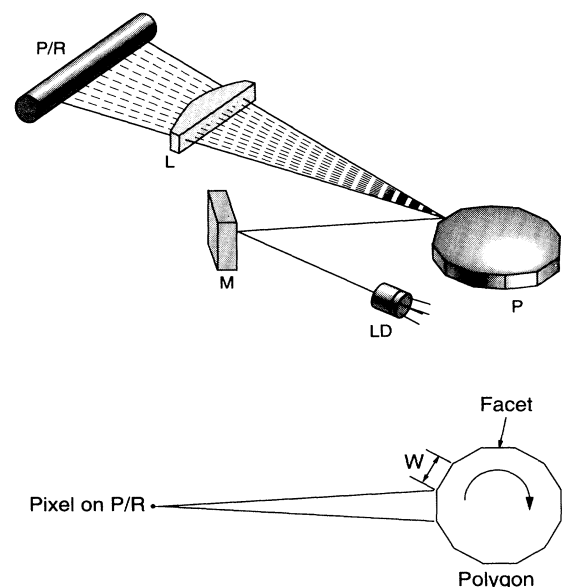


FIG. 6. Digital exposure system employing a 12-sided polygon and a solid-state laser. LD, P, M, L, and P/R denote laser diode, polygon, mirror, lens, and a photoreceptor.

wide, with an optical density of slightly greater than 1. A sharpened No. 4 lead pencil produces an image that is approximately $250 \mu\text{m}$ wide at a density of 0.3. Such small, sharp images are typically referred to as "line images." Of course, images vary in size and width from very narrow lines to large "solid-area" patches. Even typewritten characters vary greatly in this regard as point size or font is changed; indeed, different languages present differing requirements in terms of their image characteristics. It will be shown later that image size, shape, and density are critical parameters in determining the developability of a given input image. For the present discussions, only two input images will be considered: line images $250 \mu\text{m}$ wide and large solid-area patches.

The input exposure to the photoconductor is obtained from Eq. (6) by solving for X_i :

$$X_i = X_{\text{bg}} 10^{-D}. \quad (7)$$

A density of 1.0 reflects 10% of the light that is reflected from the white background, while a density of 2.0 reflects 1% of the light. In printers, the light image is electronically generated, by a raster scanning beam of laser light, for example, and is normally a binary exposure corresponding to $D=0$ and $D=\infty$. It is evident from Eq. (7) that the input image exposure is dependent only on the intensity of the illumination source and on the optical density of the input image, although there are second-order subtleties related to the spectral content of the light source and the spectral dependence of the reflectivity of the original document.

C. Photoconductor subsystem

The photoconductor, often referred to as the "photoreceptor," is the transducer that converts the light pattern into an electrostatic pattern. At a minimum, it consists of a photoconductive layer on a conductive substrate. The essential steps of photoreceptor operation are electrostatic charging of the photoreceptor surface to produce a uniform electric field across the device, imagewise photogeneration of charge carriers in the photoreceptor, and the transport of the photogenerated carriers across the layers. The photogenerated charges drift across the photoconductor, neutralize the surface charge in the illuminated areas, and so produce the electrostatic image. The photogeneration and charge-transport steps may be performed in separate material layers, which are optimized for their respective functions. In addition to the charge-generation and charge-transport layers, other layers for adhesion or charge blocking (to minimize charge injection from the conductive substrate into the photoconductor) may also be present.

The earliest photoreceptor was a flat plate, similar to a photographic plate, and required manual handling. Drums enabled automatic, repetitive imaging, embodied in machines of the type shown in Fig. 3. Flexible pho-

toresceptors initially were fabricated as sheets of film (Electrofax ZnO; see Young and Grieg, 1954), later as scrolls, and more recently as seamed belts. Belts enable full-frame flash exposure that increases the printing speed of duplicators.

The essential characteristic of the photoreceptor is the photoinduced-discharge curve (PIDC), which relates the voltage on the photoreceptor to the light exposure. The shape of this curve is governed by an electric-field-dependent quantum efficiency, the mobility of the photogenerated carriers, and charge trapping. These concepts and their impact on the PIDC will be discussed in detail in a later section.

Figure 7 shows the generic structure of a typical organic photoconductor found in today's electrophotographic copiers and printers. Also indicated are the functions each of the layers performs. There are many variants of the materials constituting each of these layers. In fact, in 1991 over a hundred U.S. patents were issued on the single topic of organic photoconductors for the imaging industry.

Table I describes very briefly the principal manufacturing processes for the photoconductors in major use today. A wealth of chemical engineering know-how has built up around these processes. Typically, the defect rate on a page-size image is required to be less than 1 part per million, where a 300 spi (spots per inch) laser printer is used as a basis. Thus all coating is typically done in Class 100 clean-room conditions.

D. Development subsystem

The electrostatic image is developed into a visible image with toner particles. Toners are charged, pigmented polymer particles that are attracted to the charge image by the electric field which emerges above the surface of the photoreceptor due to the charge pattern created by the modulation of the exposure intensity from the image (or "original").

Unless an electrode is placed close to the photorecep-

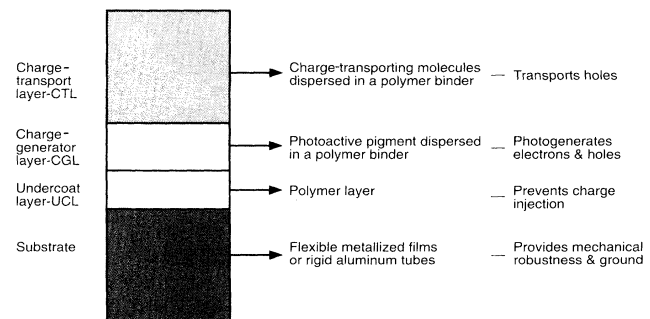


FIG. 7. Generic structure of a typical organic photoconductor found in today's copiers and printers. The functions of the different layers are indicated on the right. This type of design permits flexibility in the choices of materials in order to optimize overall device performance.

tor, the electric field will be very weak above a large charged area. With a distant electrode, strong fields extend into the space outside the photoconductor only at the edges of lines or solid patterns. Since development takes place by the attraction of the charged toner particles along the field lines, toner is attracted only to the fringe of wide (solid) image areas. To develop solid image areas it is necessary to introduce a development electrode. Generally the electrode is biased to a voltage higher than the white image background potential to prevent toner development in the white areas by creating a reverse field in these regions.

The various types of development systems are defined by the method by which the toner is transported to the charge image. These include cascade development, powder-cloud development, liquid or electrophoretic development, two-component magnetic-brush development, and single-component development. A typical developer consists of a black or colored powder called "toner." Toner consists of thermoplastic particles, typically 5–25 μm in size, containing 5–10% pigment to give the

desired color. The thermoplastic can be fused to fix the image to the paper by heat, pressure, or a combination of the two. Commonly employed thermoplastics are random copolymers of styrene and methacrylates or acrylates. Molecular weights range from 30,000 to 100,000, and glass transition temperature ranges from 60 to 65°C (Nelson, 1984). Black toner contains a pigment dispersion of carbon black (Julien, 1982), about 1 μm in size, while color toners contain mixtures of dyes and pigments of the required color (Macholdt and Sieber, 1988; Diamond, 1991).

The commonly used two-component developer is a mixture of a few weight percent of the toner with larger-size (about 80–700 μm) metal (steel) or metal oxide (ferrite) magnetic carrier beads. In order to develop solid areas, carrier beads are conductive or partially conductive to enhance the field due to the developer electrode. Carrier beads serve two functions: they provide a method of mechanically transporting the fine toner powder and a means for charging the toner. Fine powders are difficult to control, and their leakage con-

TABLE I. Photoreceptor manufacturing processes.

Photoreceptor	Process description
Selenium & alloys	Vacuum deposition from the alloy melt contained in an ohmically heated crucible onto a rotating aluminum tube; 1–3 distinct layers; batch process, 45–60 minutes per batch, 16–180 units per batch.
Amorphous silicon (<i>p</i> - or <i>n</i> -type doping)	Plasma deposition onto a rotating aluminum tube with dc or ac/rf discharge in the gas phase (silanes, boranes, etc.); multilayers achievable; batch process; 4–8 hours per batch; 1–12 units per batch.
Organic belt	Coating from a solution containing final layer materials extruded from a slotted head onto a moving metallized polyethylene terephthalate web (0.3–0.6 msec^{-1}), with a subsequent oven drying; 3–6 layers, semicontinuous process; webstock robotically slit and welded into belts.
Organic drums	Dip coating onto nonrotating aluminum tube by withdrawal from tanks containing final layer solutions, with subsequent oven drying; 1–4 layers; batch process for dipping made semicontinuous by robotics; 8–32 units per batch; 2–8 minutes per batch.
Organic drums	Spray coated, with electrostatic assist, onto a rotating aluminum tube, with subsequent oven drying; 1–4 layers; batch or semicontinuous process; 2–5 minutes for complete coating pass.

taminates the xerographic machine. To minimize this problem, toners are triboelectrically attached to the much larger and heavier carrier beads. With agitation, charge is exchanged between the toner and the carrier bead, charging the toner by triboelectrification. As many as 10^3 toner particles may be attached to a carrier bead. A photomicrograph of a carrier bead with attached toner particles is shown in Fig. 8. The operational measure of the toner charging process is the achieved charge-to-mass ratio per toner particle.

The toner is charged to a polarity opposite to that of the photoreceptor in charged-area development (CAD), which is employed in photocopying. The high potential areas are developed black, while partially discharged areas produce gray densities. Printers also can employ discharge-area development (DAD), wherein the polarity of the toner is the same as that of the photoreceptor and the low-voltage or discharged areas are developed.

The differences between these two imaging schemes is shown in Fig. 9 for a negatively charged organic photoconductor (OPC). The original motivation for using DAD for printers was to reduce the on time of the solid-state imaging devices in order to counteract heat dissipation and reliability problems. Advances in solid-state device reliability have rendered this motivation moot, but there remain some overall system latitude reasons for retaining DAD development.

Magnetic-brush development is the most widely used toner development process and consists of a series of magnets inside a nonmagnetic shell (Gaimo, 1957; Young, 1957). As the photoreceptor moves into the development zone, the toner-covered carrier beads are transported by a counter-rotating shell (Fig. 10). The

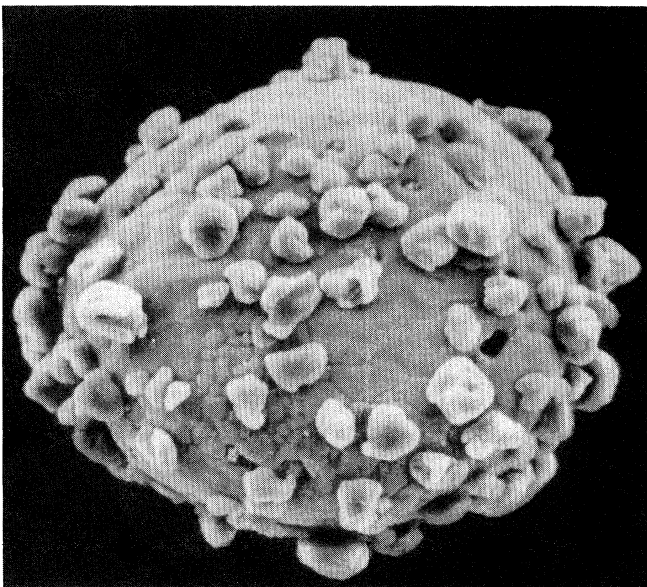


FIG. 8. Photomicrograph of a charge developer bead. Toner particles are held to the polymer-coated carrier bead primarily by electrostatic forces. Toner diameter is 5–20 μm . Carrier beads are 50–150 μm in diameter (after Scharfe *et al.*, 1989).

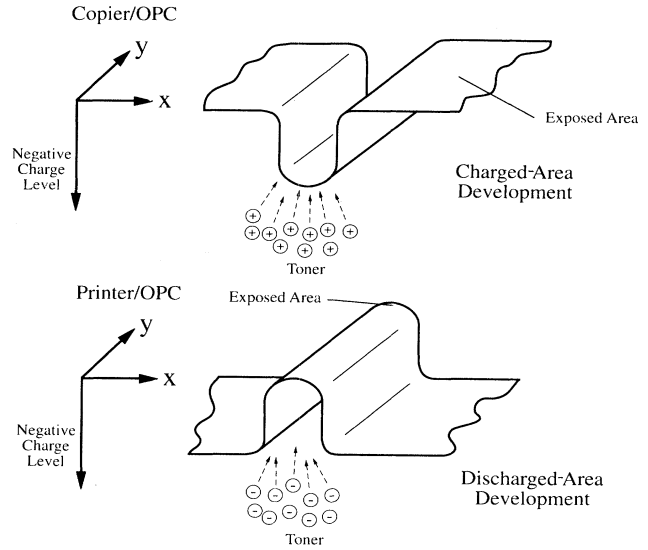


FIG. 9. Difference between charged-area development (CAD) and discharged-area development (DAD) for a negatively charged organic photoconductor. The toners are charged to a positive polarity in the CAD scheme and to a negative polarity in the DAD scheme. See Sec. IV for further details on this process.

magnetic carrier beads tend to form brushlike filaments along the magnetic lines of force, hence the name “magnetic-brush development.” The toner is stripped from the carrier beads by the electric field of the charge pattern, and the toner-depleted carrier beads are returned to the mixing region. The carrier beads are coated with a low-surface-energy polymer to optimize toner charging,

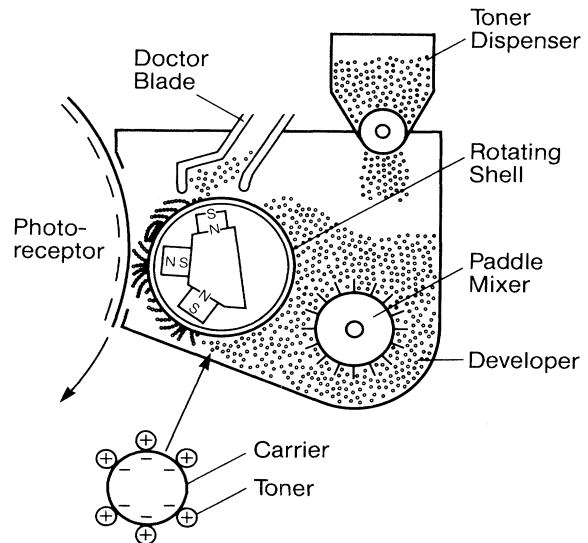


FIG. 10. Magnetic-brush development. Carrier beads tend to form chainlike bristles in the presence of the magnetic field due to the transporting magnets (after Scharfe *et al.*, 1989). Each carrier bead carries from 100 to 1000 toner particles.

to minimize permanent adhesion of the toner to the carrier, and to control the conductivity of the mixture. The effective development electrode spacing, which controls the field in large solid-area development as discussed above, can be reduced from the developer roll surface-to-photoreceptor distance by the conductivity of the carrier beads. By varying the shape and size of the carrier beads and the degree of polymer coverage on the carrier surface, the toner-carrier mixture can be made to vary from insulating (called "insulating magnetic brush," Schein, 1975a, 1975b; Hays, 1977, 1978; Folkins, 1985) to conducting (called "conducting magnetic brush;" see Jewett, 1977; Kasper and May, 1978; Hays, 1987). The former enhances fringe-field development, which is useful for fine lines, while the latter enhances solid-area development.

Cascade development is an older two-component development technology not used today (Walkup, 1952; Wise, 1952; Sullivan and Thourson, 1967; Bickmore *et al.* 1970; Thourson, 1972). The mixture of carrier beads and toner beads is tumbled (cascaded) over the photoreceptor surface by gravity. Because the carriers used for this system are large, heavy beads of glass or steel, their size limits the developer electrode spacing to distances greater than 500 μm , making it more difficult to generate adequate solid-area densities.

Mixing the thermoplastic polymer with magnetic iron oxide makes the toner itself magnetic, eliminating the need for carrier bead transport in a magnetic-brush development system (Takahasi *et al.*, 1982). The toner, in this single-component development process, is charged by induction or triboelectric charging against a donor roll. Single-component development enables smaller and lighter developer transport hardware, commonly used in personal copiers and printers, since the system of carrier beads and mixing hardware requires more space and heavy magnets. Because the magnetic oxide is brownish red, it limits the ability to produce bright color toners. Nonmagnetic insulative single-component developers have also been commercially employed. In this case the toner is charged triboelectrically by a development roller, attached to the roller, metered, and brought into contact with the photoreceptor (Demizu *et al.*, 1987).

Aerosol development, also called "powder-cloud development," is one of the earliest forms of single-component development (Bickmore *et al.*, 1960; Lewis and Stark, 1972). In one embodiment, the toner particles were charged by blowing them through fine bore tubes constructed from metal or ceramic. Submicron-size toner particles enabling very high resolution have been employed with this development system. A shortcoming of this process is that the toner charge distribution is broad and not easily controlled. This process is especially suited for developing x-ray images in xeroradiography or mammography where continuous gray scale, high-resolution images are required to enhance slight differences in contrast potentials.

Liquid development relies on charge exchange between

micrometer-size toner particles and the liquid medium in which they are suspended to charge the toner (Metcalfe, 1955; Dessauer and Clark, 1965; Dahlquist and Brodie, 1969; Schaffert, 1975; Larson, 1988; Gibson *et al.*, 1991; Schmidt *et al.*, 1991). The liquid may be purified kerosene or isopar, to which is added charge control agents. Liquid development produces high-resolution images, since the particle size is small (0.2–2.0 μm) and the counterelectrode can approach the image very closely. A disadvantage is the carryout of the objectionable residual solvent on the copy. High-speed machines employing liquid development require a solvent recovery system. The physics of the various development systems is discussed in detail in the book *Electrophotography and Development Physics* (Schein, 1988).

E. Transfer subsystem

The developed image is transferred from the photoconductor by placing the paper or other copy medium (transparency, label stock, etc.) in contact with the developed image on the photoreceptor and applying a charge by corona or conducting roller to the back side of the paper opposite in polarity to the toner charge. The reversed electric field breaks the adhesion between the toner particles and the photoreceptor surface, transferring the particles to the paper (Yang and Hartmann, 1976; Schluesener, 1991). The adhesive force of the toner to the photoconductor surface is inversely proportional to its size. Therefore some toner size classification occurs during the transfer step. The average toner size transferred to the copy medium is larger than the average toner size on the developed image (DePalma, 1982). In fact, the increased adhesion of the smaller-size toner particles to the photoconductor is one of the factors that sets a lower limit to the size of the toners that can be employed in electrophotography.

An optimum charge-to-mass ratio is required for efficient transfer. The generally observed transfer efficiency of toner from the photoreceptor to the paper is in the range of 80% to 85% (Hida *et al.*, 1982). Higher transfer efficiencies are achievable with the aid of some pressure applied to the back of the paper. The electric field that can be applied is limited to about 35 V/ μm by air breakdown. The difficulties encountered in controlling and understanding this step are related to (a) the highly variable dielectric properties of the paper, (b) the highly variable surface roughness of the paper, (c) the uncertain packing geometry of the toner on the photoreceptor, (d) the spatially varying dielectric properties in the gap between the paper and the photoconductor due to the image structure, and (e) lateral conduction effects of various kinds (Fletcher, 1991). Roller charging of the paper is employed in several machines; this helps in applying pressure and controlling the paper. The roller consists of a high-resistivity polymer coated on a metal core. Charging is achieved by air breakdown in the nip between the roller and the paper (Kamimura and Itoh,

1991; Zaretsky, 1991). Such partially conducting rollers have also been used to charge the photoreceptor (Nakamura, 1991). After creating the electric field by placing charge on the paper, the paper must be separated from the photoconductor. The geometry of this process is such that as the air gap widens in the separation process, there exists the danger of image disturbance due to air breakdown in the gap. To avoid this, a further reverse charging device is often employed in order to reduce the field as the paper separates.

The transfer step is critical for maintaining high levels of print quality, because it is an area where image disturbance can easily occur, where partial transfer reduces image density, and where remnants of the previous image can propagate through to the next image.

F. Fusing subsystem

Four types of fusers are employed in commercial copiers: hot roll, cold pressure roll, radiant, and flash. Toner rheological requirements, such as melting point and melt viscosity, are different for the four types of fusers, and toner design has to take the fuser type into account. Hot roll fusing is the most common process and consists of a pair of rollers, one of which is heated internally with a quartz lamp (Lee, 1975; Prime, 1983; Kuo, 1984). The toner image spends as little as 5 to 10 msec in the fusing region and has to reach temperatures substantially higher than the glass transition temperature to penetrate the paper fibers. To prevent the melted toner from sticking, the rollers are either precoated with a low-surface-energy material such as Teflon[®] or repeatedly coated with a release agent such as silicon oil (Seanor, 1978). Alternatively, the release agent, usually a low-molecular-weight wax such as polyethylene or polypropylene, can be incorporated into the toner, eliminating the need for external application of release agents. Image gloss, an important consideration in the appearance of the copy, may be controlled by the fuser coating. A non-compliant coating such as Teflon[®] usually produces a

high-gloss image, whereas a compliant coating such as Viton[®] usually produces a low-gloss image (Scharfe *et al.*, 1989). The gloss level can also be influenced by the specific polymer design, insofar as this influences the value of T_g and the temperature dependencies of the viscosity and surface tension. Control of the level of gloss is necessary to achieve appealing images, especially for color images. The generic set of processes during fusing and the factors governing them are depicted in Fig. 11. These steps include melting, coalescence and flow, paper penetration along capillary channels, and solidification.

Besides achieving sufficient fix of the toner to the paper, it should be recognized that (a) the paper itself has nonlinear thermal properties due both to its structure and to absorbed water, and (b) the cooled toner has built-in mechanical stress resulting from thermal contraction. The net result is that the "copy" will not exit the machine perfectly flat unless some control is exercised over it. The degree to which this is a problem depends on the area covered by the image and is thus usually most severe for color copiers or printers; for black and white text at about 5% area coverage, this is not usually a difficulty with any of the fusing types discussed above. As can be appreciated from the above, understanding and controlling the fusing process requires a considerable amount of measurement of toner and fuser roll thermal and rheological properties.

In cold roll fusing the toned paper passes between two polished steel rolls at room temperature, and the image is fused by pressure alone (Bhateja and Gilbert, 1986). The main advantage of cold roll fusing is low power consumption, with no need for standby power. However, gloss is usually high and the paper background may become smooth and shiny (termed "calendaring"). In radiant fusing, the toner paper passes under a heated coil or quartz lamp while in contact with a heated platen. The residence time required for radiant fusing is between 200 and 500 msec, much longer than for roll fusing. Flash fusing is similar to radiant fusing, except that the toner is

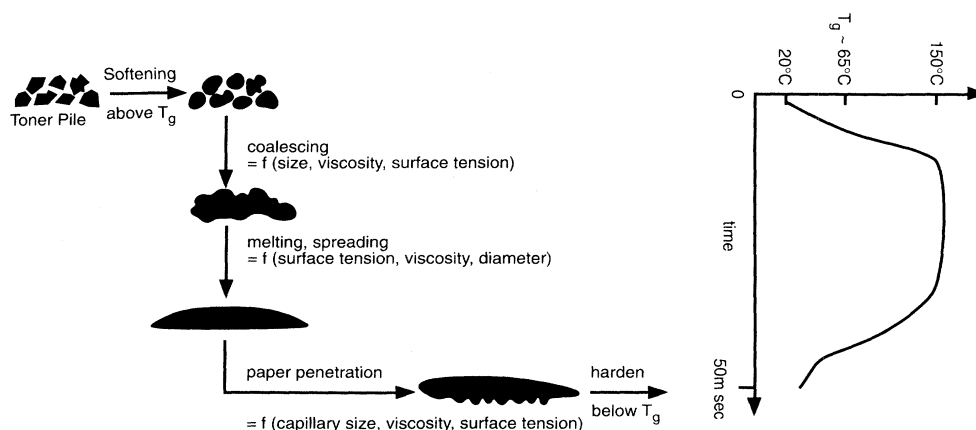


FIG. 11. Generic set of processes and the factors governing them during the fusing process.

fused by a high intensity light flash of approximately 5 msec duration (Gruber *et al.*, 1982; Narusawa *et al.*, 1985). Finally, it is also possible to fuse the toner to the paper by exposing it to solvent vapors.

G. Cleaning subsystem

Before repeating the imaging cycle, the photoreceptor has to be cleaned of residual charge and toner. Residual toner is removed by a brush, a wiper blade, or a magnetic roll (similar to that used in development). Some of the same forces that are at play in the transfer step, that is, adhesive and electrostatic, also come into play in the cleaning process. The essential feature of any cleaning subsystem is that it must physically disturb the toner, which is why intimate physical contact is required. In order to reduce the forces holding the toner to the photoreceptor and thus to reduce the energy input required to disturb and remove the toner, an ac corotron is often used to neutralize the charge on the toner particles. The process in turn may be aided by further light discharge of the photoreceptor. Once disturbed, the toner, which at this point can be considered to be isolated particles, must be carried away by the cleaning system. The cleaning system may have an auger or a vacuum system that collects the removed toner and, in some cases, may circulate it back into the developer system. Some elements of a cleaning system are shown schematically in Fig. 3 for the case of a brush cleaner. Since the toner is a thermoplastic, the cleaning system has to be designed so as not to smear the toner onto the photoconductor due to too much pressure or heat being generated. If the photoconductor surface is damaged, image degradation will result. Despite safeguards to protect it, a typical organic photoconductor loses as much as 5 μm of material in 100,000 prints.

H. Erase subsystem

Residual charge on the photoconductor is usually removed by flood exposure from an erase lamp. The surface potential on the photoconductor is generally low at this point. Thus the fields available for further photodischarge are also low. Typically 10 or more times the amount of light than that in the initial exposure step is required to reduce the remaining electrostatic images to a uniform low level in preparation for the next charging step. This amount of light can also create fairly long-lived metastable excited states in the photogenerating material which can decay to charge pairs under the action of an electric field. Thus the "color" of the erase lamp, its temporal distance from charging, and its intensity are all important for the stable operation of a given photoconductor.

I. Print quality considerations

Print quality is as much a perceptual issue (psychophysics) related to properties of the eye and cultural experience as it is a matter of measurement. In so far as measurement is concerned, the focus is on such things as line resolution (the ability to discriminate between closely spaced fine lines), edge sharpness (optical-density gradients at edges), edge raggedness (optical-density variations along an edge), gray density range, gray and color density uniformity, background (white) cleanliness, gray or color density noise, and gray or color density reflectance. There are other special considerations that come into play for transparencies.

The above properties of the image are controlled by many factors. Each step of the process can enhance or degrade the copied or printed image. These factors include the voltage levels on the photoconductor as a result of photodischarge, the size and tribocharge distributions of the toner, the resolving properties of the exposure system, the method of delivery of toner to the electrostatic image, and the set-points for transfer and fusing. The copy or print adjustment buttons on office machines provide for user adjustment of the electrostatics and exposure system. Some modern copiers maintain copy quality by sensing and adjusting the electrostatics and developed densities by a system of feedback loops. Toner must be constantly added to the developer mixture to maintain a constant toner concentration. Too much leads to background printout (dirt) and dark copies; too little leads to light copies. Most large copiers and printers have sensors that measure toner concentration or image density and control the toner feed system. Carrier beads are not consumed in the process, but they deteriorate and need to be replaced over regular intervals, since constant use causes surface damage and changes the toner charging characteristics.

All of the above apply equally to digital and analog (light-lens) imaging. There are certain special problems that are encountered in digital imaging. Basically, for laser scanning systems, the image is being written with a light spot whose intensity profile is approximately Gaussian with a FWHM (full width at half maximum) of a maximum value of about 80 μm . These spots of light must be overlapped in such a way as to minimize the ripple in surface potential upon photodischarge; simultaneously, they have to be manipulated so as to yield appealing edge structure to lines and text as well as to give uniform (i.e., noise-free) gray scale for pictorial rendition. These considerations add another layer of complexity to the image-forming process.

From the foregoing descriptions, it is apparent that certain of the subsystems play a key role in the process of reproducing the image (either analog or digital) on the photoreceptor. The remainder of the subsystems can be viewed as preserving the integrity and quality of that and subsequent images in the process of achieving a hard copy, that is, an image on one or both sides of a piece of

paper or other substrate.

Accordingly, the rest of this article will deal with some important aspects of the physics of charge-image formation in a photoconductor and the electric-field pattern in the space between the photoreceptor surface and a voltage-biased electrode, the physics of triboelectrification between two materials when brought into contact with each other, and the physics connected with the detachment of the toner from the carrier bead and the transfer to the latent image on the photoconductor. The goal is to demonstrate how the exposure, photoconductor, and development subsystems combine to produce the image on the photoconductor. For this exercise it is assumed that the developed image on the photoconductor can be perfectly transferred to paper and fused without any degradation. This, of course, is not true, since transfer and fusing steps influence the toner material selection and image quality (Yang and Hartmann, 1976; DePalma, 1982).

III. CHARGE-IMAGE FORMATION IN A PHOTOCONDUCTOR

A. Photoconductor requirements

To be useful in electrophotography, a photoconductor should meet several criteria.

(1) The photoconductor film should hold corona charge prior to the exposure step and maintain the charge pattern replicating the image exposure during the time between the exposure and the development steps. This requires trapping the surface charge and, in some cases, a blocking contact between the conductive substrate and the photoconductor. Additionally, this means that the rate of loss of charge in the dark, called dark discharge, must be minimized.

(2) The photoreceptor should discharge efficiently at all wavelengths in the visible spectrum in a copier application. In printer applications, the wavelength of the laser or exposure system is key (for example, 780 nm for GaAlAs lasers). The figure of merit is the efficiency of photogeneration, which in general is less than unity but increases with the electric field.

(3) The photogenerated charge carriers must traverse the photoreceptor in times short compared to the time between exposure and development. This sets a lower limit to the charge carrier mobility (velocity per unit electric field) and dictates something about the device thickness.

(4) The charged, partially discharged, and residual voltages must remain stable, i.e., have highly repeatable values, with repetitive cycling during a multiple copy or print run. A condition termed "cycle-up" results from a buildup of residual voltage caused by accumulation of trapped charge through repetitive use. A condition termed "cycle-down" results from increased dark discharge with repetitive use. Charge trapping is caused by certain impurities, which places stringent require-

ments on purity ($< 10^{13} \text{ cm}^{-3}$) or ≤ 1 ppb.

(5) The photoreceptor materials must be capable of being fabricated into large-area (from 0.1 to 2 m²) defect-free films. The materials must be sufficiently stable to perform in a chemically reactive corona environment containing ozone, oxides of nitrogen, water, and other effluents as well as to withstand wear and abrasion by the development and cleaning processes.

B. Brief survey of photoreceptors

Amorphous selenium (*a*-Se) photoreceptors, consisting of vacuum-deposited 20–100- μm -thick films on aluminum drums, were the first commercially used photoreceptors and continue to be widely used in xerography (Bixby, 1961). *a*-Se meets most of the photoreceptor requirements except sensitivity throughout the whole of the visible spectrum; it is highly sensitive to blue light only. The addition of Te to *a*-Se increases the red sensitivity, and multilayer devices consisting of a thick *a*-Se charge-transport layer overcoated with a thin, red-sensitive Se-Te layer are commonly used as photoreceptors (Neyhart, 1966; Kiyota *et al.*, 1980; Cheung *et al.*, 1982; Springett, 1988). Another weakness of *a*-Se is that it readily crystallizes at not much above room temperature ($\sim 60^\circ\text{C}$), and crystallized Se is very conductive. Arsenic is added to *a*-Se to retard the rate of crystallization and to increase red-light sensitivity (Felty, 1967; Melnyk, 1980). Photoreceptors containing 40% As and 60% Se have high sensitivity in the entire visible spectrum and are employed in high-speed printers with He-Ne lasers. They are much more stable, as they are close to the stoichiometry of As_2Se_3 . A more recent addition to the family of inorganic photoreceptors is hydrogenated amorphous silicon (Spear and LeComber, 1975; Shimizu *et al.*, 1980). *a*-Si:H is also sensitive in the entire visible spectrum and has sufficient 780-nm sensitivity to be used with GaAlAs lasers. *a*-Si:H is vacuum coated by chemical vapor decomposition of SiH_4 . Similar to crystalline Si, *a*-Si:H can be made positively or negatively conducting by doping with boron or phosphorus.

When Chester Carlson invented xerography, he experimented with sulfur and anthracene as photoconductors, and the initial commercialization of his idea relied on inorganic photoconductors (Carlson, 1940, 1942). The current trend is toward use of organic photoconductors (OPC) because of their material variety, economy, flexibility, and environmental safety. High-speed copying machines use belts coated with multilayered organic photoconductors, while personal copiers employ aluminum drums dip-coated with multilayered organic photoconductors. A large number of organic materials are good either at photogenerating charge or at transporting it. The concept of dual-layer devices (Fig. 7), in which the functions of photogeneration and transport of charge are carried out by different materials, has gained wide acceptance (Regensburger, 1968; Mort and Pfister, 1978; Mort and Pai, 1987). A thin charge-generation layer (CGL) of

organic pigment capable of photogenerating charge efficiently is combined with a thicker charge-transport layer (CTL). The CTL is fabricated either from a charge-transporting polymer or from a binary solid solution of a charge-transporting molecule dispersed in an inert polymeric binder. The CTL is generally fully transparent to light in the wave band 450–1000 nm.

The dual-layer concept of separating the photogeneration and transport functions combined with the concept of molecular doping to transport charge has resulted in the identification of new classes of photoconducting materials for electrophotography. Some of the materials that have been employed as CGL's include perylenes (Schlosser, 1978); thiapyrillium dyes (Light, 1971); squarilium dyes (Melz *et al.*, 1977); azo compounds; and phthalocyanine pigments such as metal-free and vanadyl phthalocyanines (Burne and Kurz, 1967; Weigl, 1972; Smith *et al.*, 1973; Burne, 1974; Khe *et al.*, 1984; Loutfy *et al.*, 1987). Generally, in some of these pigments, geminate recombination (the recombination between electron and hole produced by the same photon) appears to limit the photogeneration efficiency. The efficiency is further limited by a barrier to injection between the pigment and the charge-transporting material in the CTL (Melz *et al.*, 1977).

As mentioned before, the CTL generally consists of films of inert insulating polymers doped with active molecules. This concept provides flexibility to vary independently the photoelectronic and mechanical properties. To be able to transport holes, the molecule in a binary solid solution has to have a low ionization potential. The transport process is initiated by the transfer of an electron from a neutral molecule to a photoexcited hole in the generator layer. The neutral molecule is now converted to a radical cation. The hole transport process then consists of a field-driven chain of electron transfer events from the neutral molecule to the radical cation derivative. One factor governing the rate of charge transfer or the formation of the cation radical is the ionization potential. Lower ionization potential gives higher hopping mobilities, but lower ionization potential molecules also tend to be very unstable in a corona environment, due to the highly oxidative character of the environment. Some of the electron donor molecules employed to date include oxadiazoles (Schlosser, 1978), pyrazolines (Melz *et al.*, 1977), hydrazones (Kakuta *et al.*, 1981), and substituted triphenylamines (Pfister, 1977; Borsenberger, Mey, and Chowdhry, 1978) or biphenyldiamines (Stolka *et al.*, 1984). The structure and properties of some of these molecules are described later. The binder employed is generally a polycarbonate. The choice of binder is based on the solubility of the molecules in it, as well as other properties, such as durability.

C. Photoinduced-discharge curve

A photoconductor with no charge carriers in the bulk (perfect insulator in the dark) and with perfect blocking

contacts charges as an ideal capacitor. The potential V across the device is related to the charge density σ placed on the surface by the corotron and is given by

$$\sigma = CV = \frac{\epsilon_s}{s} V, \quad (8)$$

where C is the geometrical capacitance per unit area of the device, and ϵ_s is the dielectric permittivity of the photoreceptor layer of thickness s . We define $\epsilon_s = \kappa_s \epsilon_0$ where κ_s is the dielectric constant of the photoreceptor material and ϵ_0 is the permittivity of free space. Finite bulk conductivity can affect the charging in two ways. Free charge carriers generated from shallow centers will be swept out of the film during the charging process, causing what is known as depletion charging (Amick, 1959; Pai, 1989). Carriers generated from deeper centers after the charging process create dark decay (Melnyk *et al.*, 1977).

The role of the optical exposure subsystem is to transform the optical density of the input image into a light exposure on the charged photoreceptor. The exposure subsystem in a copier includes the exposure lamps, the optics (lenses, mirrors, aperture slits, etc.), and the document handlers required to produce a focused image of the document on the photoreceptor [see Eq. (7)].

The charge photogeneration and transport processes of the photoreceptor transform the light-exposure image into a voltage or charge image, sometimes referred to as the latent image. The absorbed photons from the light exposure create electron-hole pairs. These free charge carriers drift out of the photogeneration region, reducing the electric field. The relationship between the surface potential and the light exposure is called the photoinduced-discharge curve, or PIDC. Assuming a flux I_0 (photons $\text{cm}^{-2}\text{sec}^{-1}$) and absorption A within the photogeneration region, the rate of change of the electric field is given by

$$\frac{dE}{dt} = \frac{e\eta_s AI_0}{\epsilon_s}, \quad (9)$$

where η_s is the supply efficiency, defined as the efficiency with which an input photon will generate a free electron and a free hole which will contribute to the discharge of the photoreceptor. In the case of single-layer a -Se and a -Si photoconductors, in which the hole is the majority carrier, the photoconductors are charged to a positive polarity, and the exposure light is absorbed in a thin surface region ($< 1 \mu\text{m}$) of the layer. These layers are at least tens of microns thick; so η_s is the number of holes emitted into the bulk per absorbed photon [Fig. 12(a)]. η_s in this case includes both the photogeneration processes and any loss suffered by the photogenerated holes due either to surface recombination or recombination in the absorption region. In the case of a two-layer organic photoreceptor [Fig. 12(b)], the device is usually charged to a negative polarity and the imaging light is absorbed in the pigment contained in the charge-generation layer (the

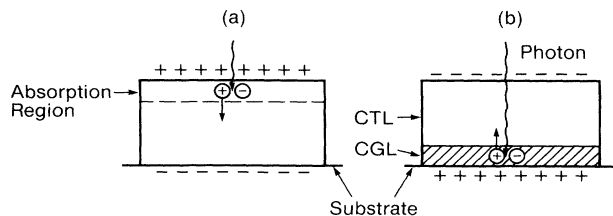


FIG. 12. Photoreceptor structures. (a) Single-layer inorganic photoreceptor in which light absorption occurs in a thin region near the top surface, and (b) dual-layer organic photoreceptor consisting of a conducting substrate, a thin ($< 2 \mu\text{m}$) charge-generation layer (CGL), and a thicker charge-transport layer (CTL). Light is absorbed in the CGL.

transport layer being transparent). The photogenerated hole is injected into the charge-transport layer, and η_s includes the photogeneration process, recombination losses, and loss suffered during the injection process. Equation (9) assumes that the transit time $t_T (=s/\mu E)$ of the photogenerated carriers across the film or the transport layer is short compared to the time interval over which the measurement is performed (μ is the drift mobility of the mobile carrier). In some organic photoconductors, charge carrier mobilities can be so low as to break this rule and, as a result, the photodischarge rate is reduced. The discharge governed by lower mobility is termed "mobility limited" and is discussed later in this section.

If η_s is independent of the electric field, integrating Eq. (9) over the exposure time gives (Melnyk and Pai, 1990)

$$E = E_0 - \frac{S}{s} X, \quad (10)$$

where

$$S = \frac{e \eta_s A s}{\epsilon_s} \frac{\lambda}{hc}.$$

S is the photosensitivity in units of volts per microjoules cm^{-2} , E_0 is the electric field for no light exposure, and X is the light exposure given by

$$X = \frac{hc}{\lambda} \int_0^t I_0 dt, \quad (11)$$

where h is Planck's constant, c is the velocity of light, and λ is the wavelength of light. Note that the factor hc/λ , the energy per photon, has been introduced to express the light exposure in energy units of, for example, microjoules per cm^2 . As can be readily seen from the parameters entering into the photosensitivity S , the value of S is dependent on the properties of the pigment via band-gap or first excited singlet-state energetics, and on the kinetics of photon adsorption, as well as on the more macroscopic properties such as effective dielectric constant and layer thickness. The photoconductor designer thus has two basic levers available to modify or improve the properties necessary for overall system optimization.

The PIDC is obtained by integrating Eq. (10) over the thickness of the photoreceptor. In most practical photoreceptors, the light is absorbed in a depth small compared to the thickness of the photoreceptor; hence we can assume both signs of charge exit the photogeneration region instantly. However, that is not necessarily the case for the entire photoreceptor layer and

$$V = Es, \quad (12)$$

where V is the measured voltage on the photoreceptor surface, E is the electric field in the photogeneration region, near one surface and proportional to the surface charge. This charge is due to photogenerated charge carriers still in transit through the photoreceptor. Thus the PIDC is given by

$$V_{\text{PIDC}} = V_0 - SX \quad (13)$$

and does not necessarily discharge to zero potential. The potential remaining at the end of the discharge is termed "residual potential" V_R and results from the trapping of charge carriers in the bulk of the film.

The most important characteristic of a photoreceptor is the plot of surface potential as a function of input exposure. This plot, the *photoinduced-discharge curve* (PIDC), is linear in exposure when there is no trapping or range limitation ($V_R = 0$) and η_s is a constant. The carrier range ($=\mu\tau E$) is the distance the carrier transits before becoming immobilized in a deep-trapping state. τ is the deep-trapping lifetime, which is the time it takes for a carrier to fall into a trap. This situation is indeed the case for hydrogenated amorphous silicon, which exhibits a field-independent supply efficiency coupled with a high mobility and long carrier range (Pai, 1989). Amorphous silicon is, however, an exception. For most practical photoreceptors, the supply efficiency decreases as the field is reduced. This has a significant impact on the shape of the PIDC.

D. Photoinduced-discharge curve: field-dependent supply

Thus far, no distinction has been made between quantum efficiency and supply efficiency. The quantum efficiency is the number of free carriers photogenerated per absorbed photon. This step could have a field dependence arising from geminate recombination, which, as explained before, is the recombination between the electron and hole produced by the same photon. Supply efficiency is defined as the number of carriers injected from the photoabsorption region near the free surface of the photoreceptor into the bulk. In the absence of any other loss process within the photoabsorption region, the supply efficiency is equal to the quantum efficiency. In the presence of free-carrier recombination, the supply is less than the quantum efficiency.

The characteristics of photogeneration efficiency in amorphous selenium and many other photoconductors

employed in xerography are explained by the Onsager mechanism for the effect of the electric field on geminate recombination and charge separation (Melz, 1972; Pai and Enck, 1975; Borsenberger, Contois, and Hoesterey, 1978; Kinemitsu and Imamura, 1990). Although experimental data are available for only a few materials, it can be said with some degree of confidence that the mechanism of photogeneration discussed here, known as the Onsager mechanism (Onsager, 1934a, 1934b; Batt *et al.*, 1968; Geacintov and Pope, 1971; Melz, 1972; Pai and Enck, 1975; Borsenberger, Contois, and Hoesterey, 1978), should appear in one form or another in low-mobility materials. A schematic of a Coulombic barrier between oppositely charged carriers being lowered by the applied electric field is shown in Fig. 13. According to the Onsager model, an absorbed photon produces a hole and electron pair that will tend to separate due to diffusion, but, as a result of the finite distance between them, will then experience a substantial Coulombic attraction. As a result of this competition between diffusion and the Coulombic attractive force, a fraction of these pairs recombine and the remainder dissociate. In the presence of an applied field, this dissociation process is enhanced at the expense of the recombination process (in effect the applied field pulls down the Coulomb well, and hence the efficiency of the dissociation is increased). The recombination between the hole and the electron created by the same photon is called geminate or initial recombination. The formulation for determining the efficiency of dissociation by the applied field in the presence of geminate recombination was developed by Onsager in connection with the study of field-enhanced dissociation in electrolytes.

The theory of geminate recombination (or initial recombination) reduces to the problem of Brownian motion in the presence of the Coulomb attraction and the applied electric field. The Onsager approach is to solve the equation of Brownian motion given by

$$\frac{\partial f(\mathbf{r}, t)}{\partial t} = \frac{kT}{e}(\mu_1 + \mu_2) \text{div} \left[\exp \left[\frac{-U}{kT} \right] \times \text{grad} \left\{ f \exp \left[\frac{U}{kT} \right] \right\} \right], \tag{14}$$

where $f(\mathbf{r}, t)$ is the distribution function of the equivalent *single* particle, $f(\mathbf{r}, t) d\mathbf{r} dt$ is the probability that the (single) particle will be found in the volume element $d\mathbf{r}$ located at \mathbf{r} in the time interval between t and $t + dt$, μ_1 and μ_2 are the mobilities of the two charge carriers, k is the Boltzmann constant and e is the electronic charge, and U is the Coulomb potential in the presence of the applied electric field in the polar coordinates and is given by

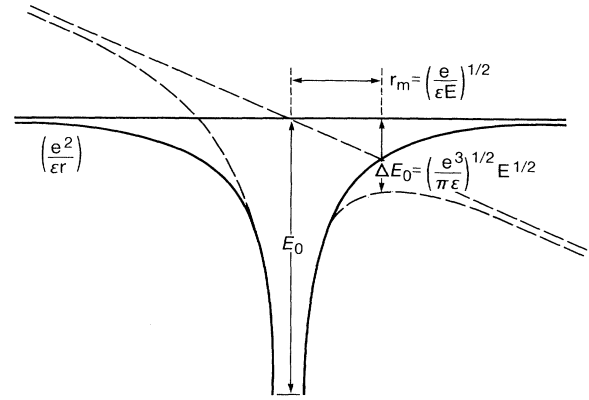


FIG. 13. Coulombic barrier (in one dimension) between oppositely charged carriers being lowered by the applied electric field.

$$U = -(e^2/4\pi\epsilon_s r) - eEr \cos\theta. \tag{15}$$

Using the solutions to the two extreme boundary-condition problems, Onsager's relation for the probability $p(r, \theta, E)$ that an ion pair thermalized with an initial separation r and at an angle θ with the applied electric-field direction will escape initial recombination and will eventually be free is given by

$$p(r, \theta, E) = e^{-A} e^{-B} \sum_{n=0}^{\infty} \sum_{m=0}^{\infty} \frac{A^m B^{m+n}}{m! (m+n)!}, \tag{16}$$

where

$$A = e^2/(4\pi\epsilon_s kTr) \text{ and } B = (eEr/2kT)(1 + \cos\theta).$$

Here we have used the rationalized mks system, and the notation used is similar to that used by Geacintov and Pope (1971).

If we now define ϕ_0 as the efficiency of production of thermalized ion pairs per absorbed photon and $g(r, \theta)$ as the initial spatial distribution of separation between ions of each ion pair, the overall generation efficiency will be given by

$$\Phi(E) = \Phi_0 \int p(r, \theta, E) g(r, \theta) d^3r, \tag{17}$$

where Φ_0 is assumed to be independent of the applied electric field. It is reasonable to begin with the assumption that the initial distribution of thermalized pairs is an isotropic δ function, so that

$$g(r, \theta) = (1/4\pi r_0^2) \delta(r - r_0). \tag{18}$$

where r_0 is a characteristic thermalization length (Batt *et al.*, 1969; Geacintov and Pope, 1971). Carrying out the integration in Eq. (16), the first few terms of the resulting equation for escape (generation) efficiency is given by

$$\Phi(r_0, E) = \Phi_0 e^{-r_c/r_0} \left[1 + \frac{e}{kT} \frac{1}{2!} r_c E + \left[\frac{e}{kT} \right]^2 \frac{1}{3!} r_c \left[\frac{r_c}{2} - r_0 \right] E^2 + \left[\frac{e}{kT} \right]^3 \frac{1}{4!} r_c \left[r_0^2 - r_0 r_c + \frac{r_c^2}{6} \right] E^3 + \dots \right], \tag{19}$$

where $r_c(T)$ is the critical Onsager distance at which Coulomb energy is equal to kT and is given by (Mozumdar and Magee, 1967)

$$r_c(T) = e^2 / 4\pi\epsilon_s kT . \quad (20)$$

It is clear from Eq. (19) that the application of Onsager's equation to the measured electric-field dependence of photogeneration requires two parameters. One is the initial distance between the hole and the electron after thermalization, r_0 , and the second is the number of thermalized carrier pairs per absorbed photon, Φ_0 . The parameter r_0 determines both the absolute efficiency and the shape of its variation with electric field. The smaller the r_0 , the lower the efficiency and the steeper the field dependence will be. At very large electric fields, the efficiency should approach Φ_0 for all r_0 . The maximum value of Φ_0 is unity and is observed in inorganic chalcogenides, such as amorphous selenium (Pai and Enck, 1975) and amorphous arsenic triselenide. However, in the case of organic materials for which this mechanism has been applied to explain photogeneration, Φ_0 is observed to be less than unity (Batt *et al.*, 1968; Melz, 1972; Chance and Braun, 1976; Borsenberger, Contois, and Hoesterey, 1978). In other words, only a fraction of the absorbed photons create the thermalized pairs that either dissociate or recombine. In summary, the main reason for the electric-field dependence in low-mobility materials is because the photogenerated hole and electron are too close to each other after thermalization. In crystalline materials, however, because of their large charge carrier mobilities, the thermalization distance between the electron and hole pair is large and the Coulombic attractive force is negligible. Hence it is not surprising that Onsager-type electric-field dependences of photogeneration efficiency have not been observed in high-mobility materials.

In Fig. 14 the circles and crosses are the measured photogeneration efficiencies of holes for amorphous selenium films of thickness 44 and 3.4 μm , respectively. The solid lines in Fig. 14 are the Onsager dissociation efficiencies calculated employing Eq. (19) with $\Phi_0 = 1$ and r_0 as indicated in the figure. The value of unity for Φ_0 is equivalent to the statement that each absorbed photon creates one pair of carriers that undergoes geminate recombination or dissociation. The thermalization distance r_0 varies from 0.84 nm at 620-nm wavelength to 7 nm at 400-nm wavelength. The larger the initial distance, the smaller the Coulomb attraction and, correspondingly, the higher the dissociation efficiency for any given field.

The variation of the photogeneration efficiency in the middle- and high-field regions is satisfactorily explained by the Onsager dissociation mechanism, as evidenced by the good fit of the measured data points with the theoretical predictions. However, it appears at first glance that there is some disagreement with the theory at low fields. Actually, the discrepancy in the low-field region is caused by recombination and/or trapping at the surface close to

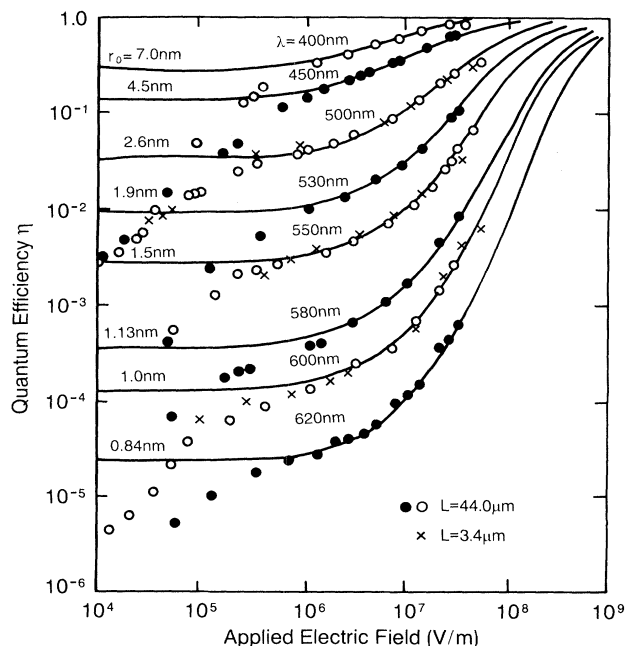


FIG. 14. Experimental quantum efficiencies of holes, shown by circles and crosses, in amorphous selenium vs applied field for different values of the wavelength of exciting radiation. Shown also are data on films of two different thicknesses. Solid lines are the theoretical Onsager dissociation efficiencies [Eq. (19)] for $\Phi_0 = 1$ and initial separation r_0 indicated in the figure (after Pai and Enck, 1975).

the photogeneration region. By employing two-photon photogeneration and delayed-voltage-application techniques, it has been found that the photogeneration in the low-field region is, indeed, that predicted by the Onsager theory (Pai and Enck, 1975). In the two-photon process, the light is bulk absorbed so that most carriers are photogenerated far from the sample surfaces, in contrast to the conventional technique (employed to generate the experimental data in Fig. 14) where the photogenerated carriers are produced by highly absorbed light in regions near the illuminated surface. In the two-photon process employing a Q-switched Nd-glass laser with a wavelength of 1.06 μm , the absorbed energy per carrier from the two photons is equal to the energy absorbed from a single highly absorbed photon used in the conventional studies (Enck, 1973). In the delayed-voltage-application technique, carriers are photogenerated by a strongly absorbed light pulse at small applied electric fields (down to zero field), but are collected by a large step-function field applied after a delay time t_d . If t_d is short compared to the trapping and recombination lifetimes, the collected charge will give the absolute quantum efficiency (Silver and Sharma, 1967; Pfister and Enck, 1976; Melnyk and Pai, 1992). The dependence of collected charge on t_d provides information on mechanisms of recombination and trapping.

The assumption that the variation of initial separation

distance r_0 with the energy of the exciting radiation occurs as a result of the initial kinetic energy of the carriers upon excitation is a reasonable one and has been applied for explaining photogeneration in liquid hydrocarbons and anthracene (Mozumdar and Magee, 1967; Silver and Jarnagin, 1968). In the case of α -Se, the variation of r_0 with the wavelength of excitation radiation has been explained by assuming that thermalization is achieved by dissipating the excess kinetic energy over the local potential by phonon emission (Davis, 1970; Knights and Davis, 1974). The motion during this process is assumed to be diffusive with a diffusion coefficient D ; so the thermalization distance $r_0 = \sqrt{Dt_0}$, where t_0 is defined as the thermalization time. It is further assumed that the rate of energy loss through phonon emission is independent of excess energy and is given by $\hbar\nu_p^2$, where ν_p is a typical phonon frequency. Assuming a band gap of E_g , the photon has an excess energy of $h\nu - E_g$ over the band edge and an excess of $h\nu - E_g + e^2/4\pi\kappa_s\epsilon_0 r$ over the local Coulomb potential. The agreement between the experimental results and this simple theory is reasonable (Pai and Enck, 1975).

The PIDC's measured on a 25- μm amorphous selenium film corona charged to a positive potential of 930 V are shown in Fig. 15. The three curves in the figure were generated with monochromatic light exposure at wavelengths of 400, 533, and 633 nm, respectively. The light-absorption depth at these wavelengths is small compared to the thickness of the photoreceptor. The three dashed lines in Fig. 15 are the contrast potentials for a 1.0 neutral density input, computed by calculating the difference in surface potentials for light exposures separated by a factor of 10 in exposure. Since there are no mobility or range limitations (high mobility and very little deep trapping) in this system, the shape of the PIDC reflects the field dependence of photogeneration efficiency. The contrast potential curves in Fig. 15 are different due to differences in the field dependence of the quantum efficiency. The contrast potential is largest for 400-nm

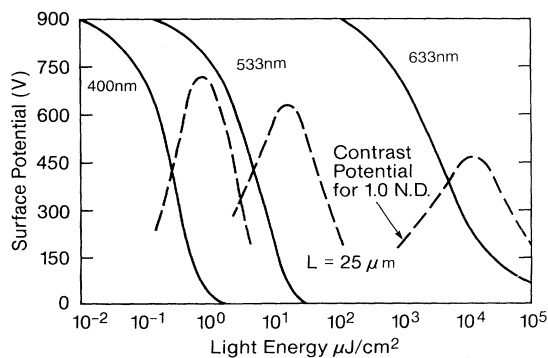


FIG. 15. Photoinduced-discharge characteristics (PIDC; solid lines) and contrast potential curves (dashed lines) for a positively charged 25- μm -thick amorphous selenium film at the indicated wavelengths (after Pai, 1980).

excitation and lowest for 633-nm excitation, indicating that the power of the electric-field dependence of photogeneration efficiency increases with increasing wavelength. The increase in exposure levels required to generate the maximum contrast as the wavelength is increased indicates that the magnitude of the photogeneration efficiency decreases with increasing wavelength. In the case of organic layered systems, the supply efficiency η_s is a product of the photogeneration efficiency η_{PG} and the efficiency of injection η_i . Field dependence of photogeneration may arise from geminate recombination, which was described earlier in connection with photogeneration in α -Se. The second limitation is seen in Fig. 16, which shows the injection efficiencies for holes in four layered systems with identical pigment layers in combination with four different charge-transport-layer materials (Melz *et al.*, 1977). The CGL in this case is a thin layer of a SeTeAs alloy. The charge-transport layers are fabricated from pyrazoline compounds with three distinctly different substituents, as shown in the inset. The pyrazolines are dispersed in polycarbonate. The fourth CTL is poly(*N*-vinyl carbazole) or PVK, a polymeric transport layer.

The field dependence in the high-field region where all the systems have the same photoinjection efficiency may be related to the field dependence of the photogeneration efficiency within the CGL. (Note that photogeneration efficiencies greater than unity are observed in SeTeAs.) In this case, all the photogenerated carriers are injected into the CTL without any further loss. In the low-field region, the efficiency depends on the CTL. Since all CTL's have approximately similar charge carrier mobili-

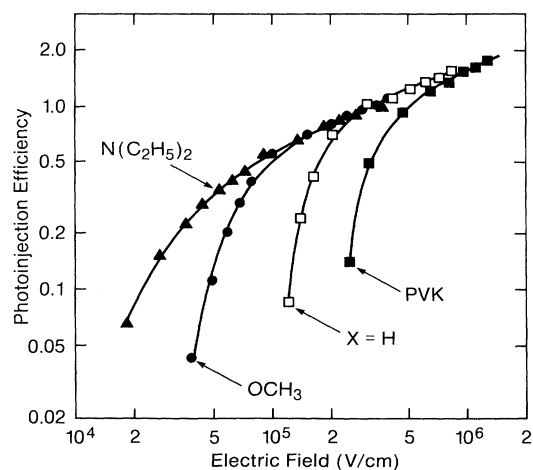


FIG. 16. Photoinjection efficiency of layered structures using SeTeAs carrier generation layer in combination with a transport layer of poly(*N*-vinyl carbazole) (marked PVK) and transport layers of three structural variants of pyrazoline molecules in polycarbonate. Structural variants of pyrazoline with substituent groups of H, OCH₃, and N(C₂H₅)₂ are employed. Illumination is at 550 nm with a photon intensity of 10¹¹ photons/cm² sec. Photogeneration efficiencies in excess of 1 are observed for SeTeAs (after Melz *et al.*, 1977).

ties, the differences in the injection rate may be related to the barrier height for injection from CGL into CTL caused by the differences in the ionization potentials. A simple model in which hole injection following photogeneration competes with a free-carrier recombination process has been employed to describe the results qualitatively.

The photoreceptor properties discussed so far have all focused on materials that can be classified as amorphous solids. One of the aspects of organic photoreceptors that makes them a challenging subject for research is that the charge-generator layer (CGL) is most commonly a granular material (see Fig. 17; for a discussion of the related problem of granular metal films, see Sheng, 1992). That is to say, it is composed of crystalline photoconducting pigments, 0.02–0.1 μm in size, dispersed in a polymer, with or without transport molecules added, and coated to a layer thickness of from 0.5–2.0 μm . When the polymer is effectively an insulator, the volume fraction of pigment is larger than 0.40 (i.e., above the effective-medium theory limit for percolative charge conduction) and more often above 0.56; which is the lowest value for random spheres to have a continuous path of contacts through the layer. Values above 0.60 are hard to achieve through conventional coating methods, due to pigment agglomeration, which is why some CGL's are vacuum evaporated.

It is interesting to examine the numerics of a CGL. First, taking the pigment volume fraction to be 0.6, the layer thickness to be 1.0 μm , and the pigment size to be 0.1 μm , the number of pigment particles per cm^2 of photoreceptor area is 6×10^{10} . The number of 780-nm photons per cm^2 required to discharge a photoreceptor 25 μm thick, charged negatively to 1000 V with a dielectric constant of 3, is about 6×10^{12} , while the number of surface charges per cm^2 is about 6×10^{11} . Thus each pigment particle is required to produce ten free carriers, and each pigment particle absorbs about 100 photons on average. (Of course, due to absorption, the top layers of pigment create the most charge.) Much of this

inefficiency is related to the difficulty in transporting charge through a granular system. For the stated geometry, the average interparticle spacing is about 18 nm. Because of the polymer coating over the pigment particles, this is the typical distance a charge must move before encountering another pigment particle. If the polymer were a pure insulator, moving charge through the system would be a very difficult matter.

Fortunately, the charge-transport molecules typically used are quite soluble in the binder polymer. The presence of solvent in the particle-coating process ensures the migration of such molecules into the CGL even if they are not intentionally included. Since the pigment particles have a dielectric constant of from 4 to 4.5, there is also electric-field enhancement across the polymer gaps between particles.

Shown in Fig. 18 are some representative molecular crystals used as photogenerating pigments. The azo pigments are typically used in copiers, as well as the dibromoanthanthrone, while the remainder are used in printers to respond to LED's (660 nm) or laser diodes (780 nm). In the case of laser diodes, sufficient pigment must be used to absorb more than 95% of the light in order to prevent image artifacts due to interference effects. The spectral absorption of these materials in the solid state is usually quite broad. Examples of the photoresponse of some of these materials is shown in Fig. 19.

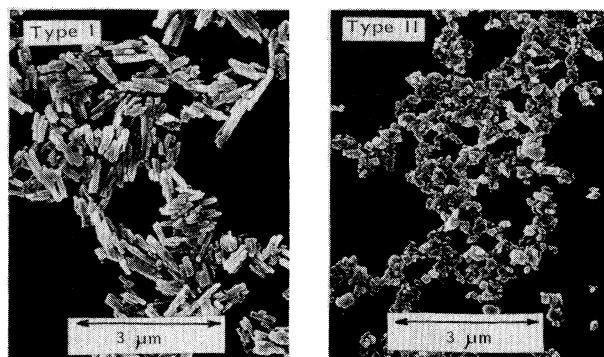


FIG. 17. Scanning electron micrograph of pigments (metal-free phthalocyanine) in the generator layer (after Enokida *et al.*, 1991).

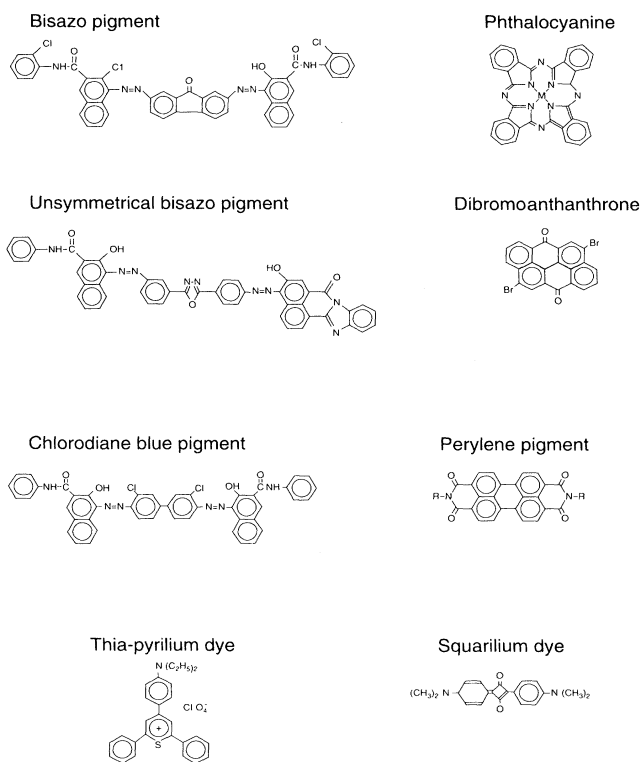


FIG. 18. Representative molecular crystals employed as pigments in the generator layer. The metal M in the center of the phthalocyanine molecule can be one of several, including TiO, VO, ClIn, ClGa, etc.

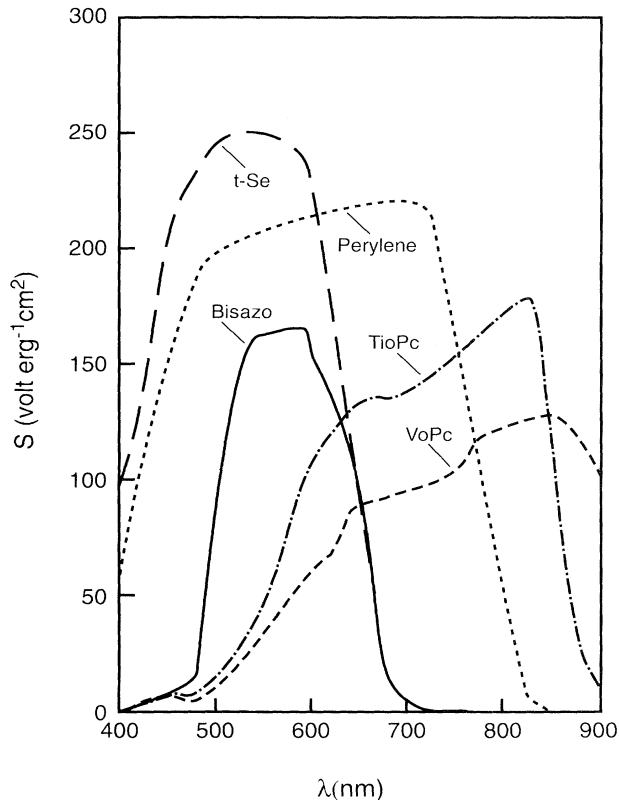


FIG. 19. Spectral response of some of the pigments employed for general use as photogenerator materials. The decrease in response at shorter wavelengths could be due in some instances to CTL absorption.

The parameter S is essentially a measure of the initial slope of the photodischarge curve (PIDC) for a photoreceptor charged negatively to 800 V. ($S=450$ corresponds to quantum efficiency of unity for a film thickness of $25 \mu\text{m}$ and an excitation wavelength λ of 600 nm). Those pigments whose photoresponse falls to zero for $\lambda < 650 \text{ nm}$ are most suited to copiers.

The charge-generation mechanism is believed to occur as depicted in Fig. 20. The crystals are usually of very high purity, but they are highly damaged as a result of manufacturing processes. Many of the materials can exist in a variety of crystal forms (Itami *et al.*, 1991). As a result, the actual photosensitivity achieved is often very dependent on the manufacturing process. Generally speaking, a singlet-state exciton is created by photon absorption and charge dissociates by an Onsager-like mechanism [Fig. 20(a)], or else it migrates to the pigment-particle surface where charge exchange with a charge-transport molecule occurs [Fig. 20(b)]. In either event, the production of charge usable for discharge is strongly field dependent once the field falls below about $10 \text{ V}\mu\text{m}^{-1}$. The actual performance in the latter case will depend on particle size (Saito *et al.*, 1991).

Production of charge from an energetic excitonlike

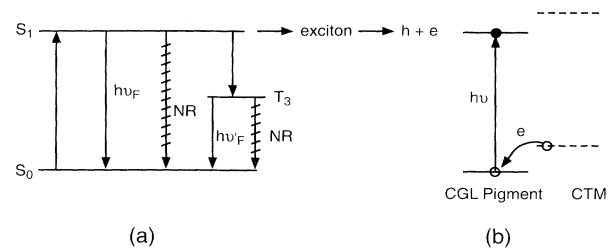


FIG. 20. Photogeneration mechanisms: (a) A singlet-state exciton created by photon absorption dissociates by an Onsager-like mechanism. The subscripts F and NR indicate fluorescent and nonradiative decay, and T is the triplet state. (b) A singlet-state exciton migrates to the pigment-particle surface where charge exchange with a transport molecule occurs.

state competes with fluorescent or nonradioactive decay (Popovic, 1984). In the figure, the subscript F indicates fluorescent decay; NR, nonradiative (phonon) decay; and T, the triplet state. Charge production occurs as the exciton diffuses to the pigment surface and a charge-transport molecule donates an electron. The hole thus created migrates away (Popovic *et al.*, 1988; Umeda *et al.*, 1990). These dispersed pigment CGL's are difficult systems to understand completely. Much of the development in this area has been empirical; part of the difficulty in achieving greater understanding is related to the fact that the CGL is only part of an even more complex structure—the photoreceptor itself.

As discussed earlier, the PIDC is a linear function of exposure for a field-independent supply efficiency. If the supply efficiency is field dependent, the PIDC is nonlinear in exposure as the discharge proceeds. The contrast potential, which is the difference in potentials between the image and background exposures, is reduced as a result of the nonlinearity. This reduces the developability. In general, the larger the power of the field dependence of the supply efficiency, the shallower and more nonlinear is the PIDC. A shallow PIDC produces lower contrast potentials.

As an example, assume that η is independent of light intensity and varies with power dependence in the electric field as (Chen and Mort, 1972)

$$\eta = \eta_0 \left(\frac{E}{E_0} \right)^p, \quad (21)$$

where $E = V/s$ and p is a parameter. Integrating Eq. (21) leads to

$$\left(\frac{V}{V_0} \right)^{1-p} = 1 - (1-p) \frac{SX}{V_0} \quad (22)$$

for $p \neq 1$, and to

$$\frac{V}{V_0} = e^{-(SX/V_0)} \quad (23)$$

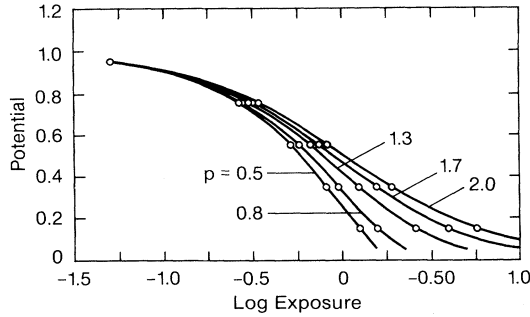


FIG. 21. PIDC's for supply-limited discharge. p is the power of the field dependence of the supply limitation [Eq. (21)]. The potential coordinate is normalized to $V_0=1$. The exposure axis is normalized to $(q/\epsilon_s)s(1-R)\eta_0$ (after Chen and Mort, 1972).

for $p=1$. The PIDC from Eqs. (22) and (23) with p as the parameter are plotted in Fig. 21. This figure illustrates how, with no mobility or range limitations, the field dependence of the photogeneration efficiency determines the entire shape of the PIDC. The steeper the field dependence (the larger the p), the shallower is the PIDC, which results in lower contrast potentials or a broader exposure range. In the treatment thus far it has been assumed that the photogenerated carrier has crossed the sample in a time short compared to the time of measurement. This is the case in *a*-Se and *a*-Si. However, in some organic photoconductor devices, the low-mobility values can have an effect on the PIDC.

E. Photoinduced-discharge curve: mobility-limited discharge

Latent-image formation in a charged photoconductive structure involves the absorption of photons and the production and transport of free carriers. In the case of positively charged single-layer amorphous photoconductive layers fabricated from Se alloys or hydrogenated amorphous silicon, the photoabsorption takes place in a narrow region close to the surface and free holes are injected into the bulk and transported to the substrate. In the case of two-layer organic photoconductors, however, free holes are photogenerated in a thin pigment layer and are subsequently injected into and transported through a thick transport layer consisting of a dispersion of organic charge-transporting molecules in an "inert," mechanically tough polymer. The effect of charge transport on the discharge shape can be seen from the simple expression for small signal discharge $\Delta V(t)$ when a photoconductor charged to a potential V_0 is exposed to a strongly absorbed short light pulse capable of generating a sheet of free charges such that $\Delta V \ll V_0$. In an ideal case, the sheet of charge transits the film thickness s , and the time dependence of discharge is given by

$$\Delta V(t) = \frac{eN_0}{C} \frac{x(t)}{s}, \quad t < t_T, \tag{24}$$

$$\Delta V(t) = \frac{eN_0}{C}, \quad t > t_T, \tag{25}$$

where N_0 is the number of photogenerated free charges that are injected into the transport layer, $x(t)$ is the position of the sheet of charge at time t and is related to the charge carrier drift mobility by

$$x(t) = \mu \frac{V_0}{s} t, \tag{26}$$

and the transit time t_T is give by

$$t_T = \frac{s^2}{\mu V_0}. \tag{27}$$

The decrease in potential, ΔV , of an exposed photoconductor [Eq. (24)] is proportional to both the number of photogenerated carriers injected into the bulk and the distance they travel. As stated earlier, the number of carriers is determined by the photogeneration and recombination in the photoabsorption region. The distance the carriers travel in a fixed time is determined by the mobility of the carriers. The previous section dealt with the shape of the discharge resulting from the field dependence of supply efficiency or N_0 being a function of electric field. It was assumed that the photogenerated carriers transited the device in times small compared to the time between the exposure and the development steps. As an example, consider amorphous selenium, which has an electric-field-independent hole mobility of 0.14 $\text{cm}^2/\text{V sec}$. With this mobility, the charge carrier transit times across a 60- μm -thick film (the thickness generally employed in electrophotographic applications) are 0.26 and 2.6 μsec at potentials of 1000 and 100 V, respectively (Spear, 1957, 1969). The hole mobility in hydrogenated amorphous silicon is $10^{-3} \text{ cm}^2/\text{V sec}$ (Spear and LeComber, 1975). For a 25- μm -thick film, this mobility produces carrier transit times of 1 msec and 0.1 second at potentials of 600 and 100 V, respectively. A typical process time between exposure and development of an image is 0.3 sec. Therefore charge carrier mobility is not a factor in determining the shape of the discharge as seen by the development system in these two materials (Pai, 1989).

The PIDC is distorted by a mobility limitation if the photogenerated carriers are still in transit across the sample at the time the photoreceptor arrives at the development station (Pai and Yanus, 1983). The discharged potential under this condition is less than that obtained had the carriers reached the substrate. The charge carrier mobility in transport layers employing a dispersion of organic charge transporting molecules is in the range of 10^{-5} to $10^{-7} \text{ cm}^2/\text{V sec}$; with material systems in the lower end of that range, the transit times are comparable to the time it takes to develop the image. The direct impact of this is to enlarge the copying machine in order to accommodate the transit time!

The incredibly low mobilities observed in amorphous molecular solids are orders of magnitude less than those in trap-free molecular crystals (Karl, 1989a, 1989b); this has been the subject of considerable research. In addition to the demonstrated technological application of such materials as transport layers in organic photoconductors, the system has been employed to study intrinsically interesting scientific questions. The molecularly doped polymers are very flexible in material design, since the concentration and type of dopant molecule can be selected that allow one to optimize certain transport properties and to vary what are thought to be the controlling parameters in a systematic way. This flexibility proves to be an essential experimental leverage for unraveling the details of charge transport in these systems (Mort and Pfister, 1978; Mort and Pai, 1987).

A host of systems have been studied and a large number of interesting features peculiar to the disordered state established. A partial list of systems studied to date include 2,4,7-trinitrofluorenone (TNF) in polyester (Gill, 1974), *N*-isopropylcarbazole (NIPC; Mort *et al.*, 1976), triphenylamine (TPA; Pfister, 1977 and Borsenberger, Mey, and Chowdhry, 1978), triphenylmethane (TPM; Pai *et al.*, 1983), hydrazone (Kakuta *et al.*, 1981), and tetraphenyldiamine (TPD; Stolka *et al.*, 1984) in polycarbonate. The molecular structures of these materials are shown in Fig. 22. The transport occurs via a sequence of charge transfer steps from one localized site to another in the presence of the applied field. There is general agreement that the charge transport is an electric-field-driven chain of reduction-oxidation processes involving neutral molecules (N) or groups and their charged derivatives: anion radicals (N^{\ominus}) in the case of electron transport, and cation radicals (N^{\oplus}) in the case of hole transport.

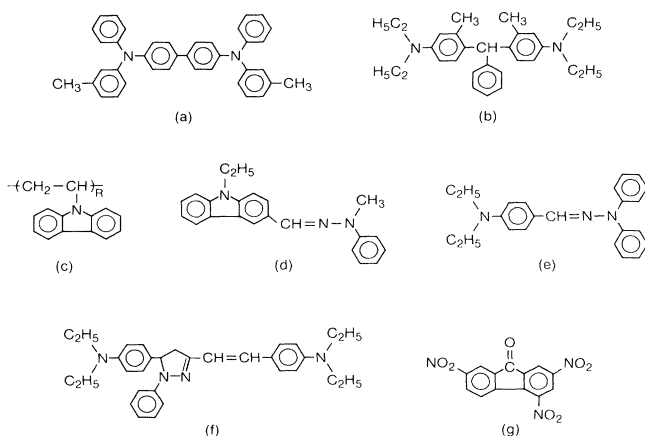
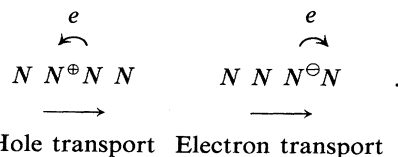


FIG. 22. Structure of electron donor and acceptor molecules employed in charge-transport layers. The structures are (a) bi-phenyldiamine (TPD), (b) bisdiethylamino triphenylmethane, (c) poly(*N*-vinyl carbazole) (PVK), (d) carbazole hydrazone, (e) benzaldehyde hydrazone, (f) pyrazoline, and (g) 2,4,7-trinitro-9-fluorenone (TNF). PVK is a polymeric transport material.



For hole transport it is therefore essential that the molecules be electron donors when neutral and have low ionization potentials so that they easily form the cation radicals and so that the redox process (oxidation/reduction/oxidation) can be completely reversible. With hole transport, for example, we may assume that as a result of the photogeneration process some dopant molecules will be positively charged (radical cation). Under the influence of the applied electric field, neutral molecules will repetitively transfer electrons to their neighboring cations. The net result of this process is the motion of a positive charge across the bulk of the film. The charge transport is an electronic process and no mass displacement is involved. On the other hand, for electron transport where electrons hop from the radical anions to their neighboring neutral molecules, the dopant molecules are acceptorlike. Indeed, for the donor molecules NIPC, TPA, TPM, hydrazone, and TPD dispersed in polycarbonate, only hole transport is observed; for the acceptor molecule TNF dispersed in polyester, only electron transport is observed. Thus the chemical nature of the dopant molecule preserved in the dispersion largely determines the sign of the mobile carrier. Since the molecules are either donorlike or acceptorlike, the molecularly doped film of one type of molecule in a binder is unipolar insofar as its charge-transport property is concerned. In this context, a one-layer photoconductor of a charge transfer complex of a donor polymer poly(*N*-vinyl carbazole) (PVK) and an acceptor molecule 2,4,7-trinitro-9-fluorenone (TNF), being ambipolar, is of interest (Gill, 1972). PVK photogenerates charge carriers when excited by UV radiation (Pai, 1970). However, the charge transfer (CT) complex with TNF is a photoconductor in visible light. The charge transfer complex of PVK:TNF has been shown to be a three-component film consisting of free TNF, uncomplexed carbazole, and charge transfer complexes (Weiser, 1972). The hole transport involves hopping between uncomplexed carbazole units, while electron transport is associated with both free and uncomplexed TNF. The unipolar nature of charge transport in systems involving molecular dispersions of one type of active molecule in an inert binder is to be contrasted with charge transport in molecular crystals in which ambipolar transport is possible (Karl, 1989a, 1989b).

The canonical experiment for measuring charge transport is the time-of-flight experiment (Spear, 1969). A pulse of strongly absorbed light generates a sheet of holes and electrons near one electrode. With the proper polarity of voltage at the far electrode, a sheet of holes (for systems containing donor molecules) moves to the far electrode. The motion of the sheet of charge gives rise to a current $i(t)$ in the external circuit given by

$$i(t) = \frac{1}{s} \int_0^s j_c(x,t) dx + \frac{\epsilon_s}{s} \frac{dV}{dt}, \quad (28)$$

where V is the voltage across the device, ϵ_s is the permittivity, and s is the thickness of the film. The first term in this expression is the current due to the drifting sheet, and the second term is the displacement current. When the experiment is carried out with V held constant, the current $i(t)$ in the external circuit is the space average current due to the drifting sheet of carriers. For normal transport, such as that which occurs in crystalline materials, the velocity of the sheet of holes is constant and the carriers travel essentially as a sheet. The current is constant until the holes arrive at the far electrode. The only spread in the charge packet is that due to normal diffusion and Coulomb repulsion. This has the effect of slightly rounding off the current pulse in the transition region where the current drops to zero.

The study of disordered materials for use as photoconductors or transport layers in organic photoconductors in electrophotography uncovered many novel features of charge transport in these materials. Generally speaking, all these features are observed in the diverse systems studied to date (Mort and Pfister, 1978; Mort and Pai, 1987; Abkowitz *et al.*, 1991). These features included (1) the occurrence of tails (broader than what can be expected due to conventional effects) in time-of-flight signals featuring well-developed plateau regions suggestive of Gaussian transport (loosely termed "nondispersive" signals); (2) transition from nondispersive to very dispersive transport observed at low temperature, indicating that the carriers cannot relax to dynamic equilibrium within a transit time; (3) dependence of mobility on the concentration of molecules; (4) dependence of mobility on the "inert" matrix material employed for dispersing the molecules; (5) a field dependence of the mobility approximately resembling $\ln \mu \propto E^{1/2}$ over an extended range of fields; (6) an electric-field-dependent activation energy, featuring activation energies from about 0.3 to 0.5 eV if analyzed in terms of the Arrhenius equation; (7) the presence of lower ionization potential molecules acting as traps when charge is transported through higher ionization potential molecules; and (8) dependence of mobility on the structure of the molecule. The similarity of field and temperature dependence of chemically very different materials synthesized via chemically very different procedures suggests a physical rather than chemical origin of these features.

The next few figures are presented to illustrate some of these features. Figure 23 shows the "nondispersive" time-of-flight signal in a TPD-polycarbonate system (Yuh and Stolka, 1988). [The molecular structure of TPD is shown in Fig. 22(a).] The spike at time $t=0$ is an artifact of the multilayer device employed to generate the free-carrier sheet before it is injected into the TPD-polycarbonate film and is not related to charge transport. The tails are much broader than what is expected from normal diffusion, and this dispersion increases as the temperature is lowered. These tails are attributed to the

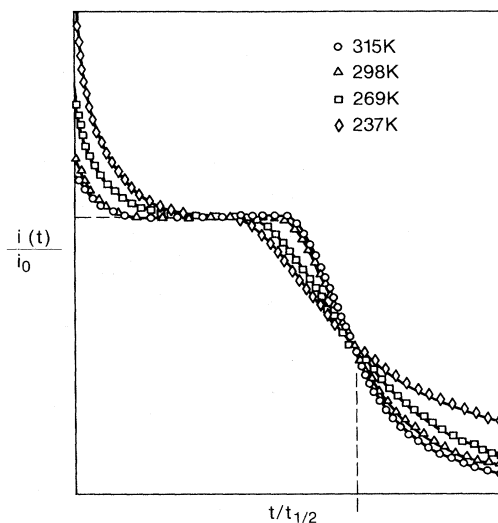


FIG. 23. Normalized time-of-flight current traces $i(t)/i_0$ vs $t/t_{1/2}$ in the CTL containing a dispersion of donor molecule TPD [Fig. 22(a)] in polycarbonate at four different temperatures. The applied field is 3×10^5 V cm $^{-1}$ and the film thickness is 74 μ m; $t_{1/2}$ is the time corresponding to $i_0/2$ (after Yuh and Stolka, 1988).

disorder inevitably contained in the amorphous systems. Figure 24 shows the room-temperature field dependence of mobility for films containing different compositions of TPD in polycarbonate (Stolka *et al.*, 1984). The mobility drops exponentially with an average intersite distance between molecules. Figure 25 illustrates the steeper field

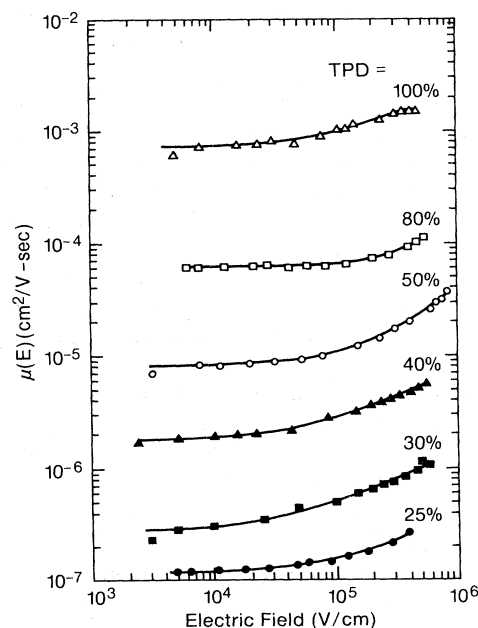


FIG. 24. Hole mobilities as a function of electric field for films of different weight compositions of donor molecule TPD [Fig. 22(a)] in polycarbonate (after Stolka *et al.*, 1984).

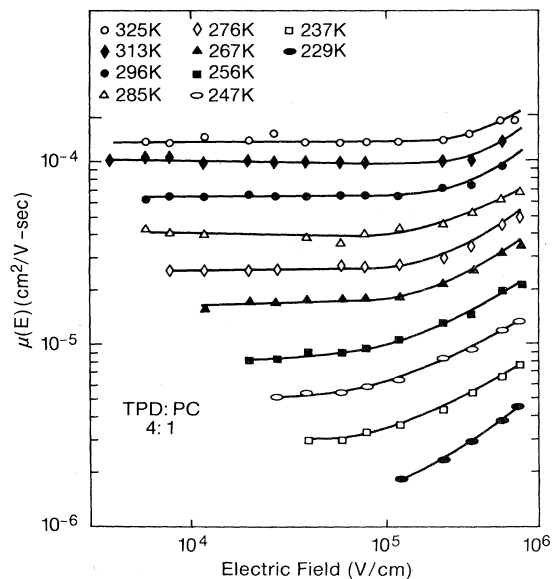


FIG. 25. Field dependence of hole mobility in 80%/20% TPD/polycarbonate film parametric in temperature (after Stolka *et al.*, 1984).

dependence as the temperature is lowered. Steeper electric-field dependence at lower temperature translates to a reduction of activation energy as the electric field is increased. Transition from hopping to trap-controlled hopping is illustrated in Fig. 26(a), which shows the mobility in films of a charge-transporting polymer PVK doped with a lower ionization potential transporting molecule, TPD (Pai *et al.*, 1984). As illustrated in Fig. 26(b,1), in the absence of TPD, holes are transported by their hopping from one carbazole site to the next. The backbone PVK does not play any direct role in the transport. At low concentration of the additive TPD [Fig. 26(b,2)], the transport is dominated by the slow release of the additive sites acting as traps for transport via carbazole groups of the polymer. As the concentration of the additive is increased, the transport is dominated by hopping via the additive sites of TPD, with the polymer PVK acting as an inert binder. The large trapping effect of small amounts of TPD, resulting in a substantial drop in mobility, is explained on the basis of the difference in ionization potentials of the two materials.

In a disordered molecular solid, the mutual orientation and intermolecular distances exhibit a distribution that generates diagonal and off-diagonal disorder. The former refers to the fluctuation of site energies $\Delta\epsilon$, the latter to the geometric parameters of the system, e.g., fluctuation in wave-function overlap parameter $\Delta\Gamma$. If $\Delta\epsilon \gg \Delta\Gamma$, the carriers become localized on individual sites; hence the conventional band picture breaks down and the transport has to be treated as a sequence of hops in an assembly of localized sites with fluctuating site energies and transition matrix elements. Several models are discussed in the literature to explain some or all of the features.

These include (1) critical-path method (Ambegaokar *et al.*, 1971); (2) continuous-time random walk (CTRW; Scher and Montroll; 1975); (3) Monte Carlo simulations in a Gaussian distribution of localized sites (Bassler, 1981; Pautmeier *et al.*, 1990); and (4) a polaron model (Holstein, 1959; Emin, 1973; Schein and Mack, 1988).

The critical-path method makes the assumption that

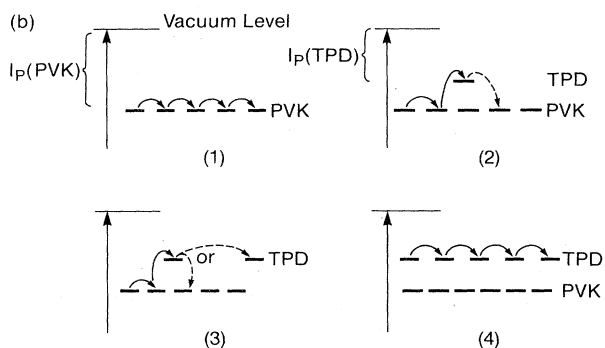
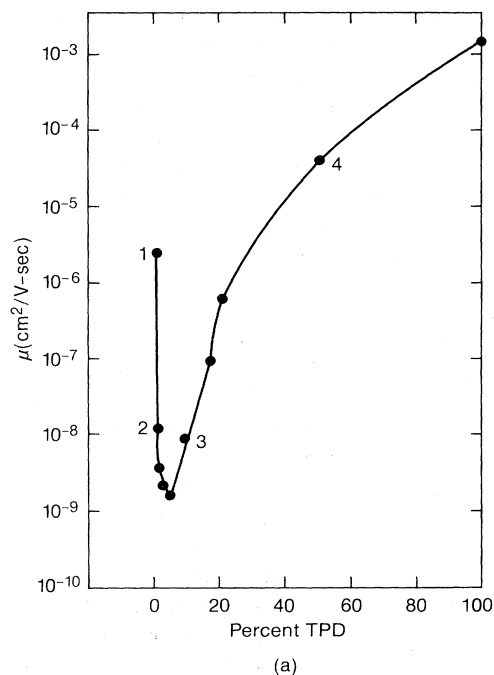


FIG. 26. Charge transport in a film containing a dispersion of two transporting materials. (a) Hole drift mobility in the hole transporting polymer PVK doped with varying amounts of TPD (in weight percent). The four regions of the data marked by 1 through 4 are explained in (b). After Pai *et al.* (1984). (b) Schematic of hopping via high ionization potential compound in the presence of low ionization potential compound: (1) hopping via high I_p material (no dopant); (2) hopping via high I_p material in the presence of a small amount of low I_p compound (trapping at the sites of low I_p material); (3) hopping via both low I_p and high I_p material; (4) hopping via low I_p compound exclusively.

the conductance between entities is the product of the probabilities for tunneling and thermal activation; i.e.,

$$g_{ij} = g_{01} \exp(-2\alpha S_{ij} - E_{ij}/kT), \quad (29)$$

where α is the WKB tunneling constant, S_{ij} the barrier thickness, and E_{ij} the energy difference between two sites. This model then gives a natural explanation of the shift of temperature and field dependence of the mobility as these external parameters are varied. The disorder is taken into account, since the path of the carrier is essentially the path of least resistance. This means the path having the lowest value of the exponent in Eq. (29); this will change as T is lowered, for example. The result is some form of power-law dependence of μ on T , and exponential dependence on field.

The basis of the CTRW model is that the transfer time between states can be a random variable (Scher and Montroll, 1975; Scher *et al.*, 1991). The probability that an individual transfer takes place between t and $t + dt$ is given by $\Psi(t)dt$. The accumulated sequence of these events as the carrier moves across the film can be viewed as a continuous-time random walk. The properties of a packet of charge propagating across a sample would then depend on the assumed functional form for the probability distribution function $\Psi(t)$ and the spatial bias introduced by the electric field. The very severe dispersion observed in some instances is explained by assuming a probability distribution with an algebraic tail

$$\Psi(t) \sim t^{-(1+\beta)}, \quad (30)$$

where β is a property of the material and may or may not be a function of temperature. It is obtained by fitting the time-of-flight current shapes to the predictions from this theory, which are

$$i(t) \sim t^{-(1-\beta)}, \quad t < t_T \quad (31)$$

and

$$i(t) \sim t^{-(1+\beta)}, \quad t > t_T. \quad (32)$$

A double-logarithmic plot of the current $i(t)$, corresponding to Eqs. (31) and (32), is two lines with slopes $-(1-\beta)$ and $-(1+\beta)$, separated by a narrow transition region. The sum of the two slopes is -2 , independent of the exponent β used to define the probability distribution function $\Psi(t)$. The time t_T , which has the meaning of transit time, is easily determined experimentally. The transit time is related to the film thickness by

$$t_T = \left[\frac{s}{l(E)} \right]^{1/\beta} \exp \left[\frac{\Delta_0}{kT} \right], \quad (33)$$

where $l(E)$ is the mean carrier displacement per hop in the direction of the field. The transit time is proportional to $(s)^{1/\beta}$, which predicts a film-thickness-dependent mobility. Equations (31) and (32) also describe band transport with extensive multiple trapping, where the total time spent in traps far exceeds the total transit time in

the conduction band (Noolandi, 1977; Schmidlin, 1977).

The basis of the third model is that, given the disorder present in the noncrystalline state, the narrow valence and conduction bands (resulting from the weak intermolecular coupling) in the corresponding molecular crystals are split into a Gaussian distribution of states (Bassler, 1981). This assumption is based on the observation of Gaussian profiles with a typical Gaussian width of 60 meV in the absorption and fluorescence bands of disordered organic materials (Rockwitz and Bassler, 1982). The electric-field and temperature dependence of drift mobility through the Gaussian distribution of states of width σ should reflect the electric-field (E) and temperature (T) dependence of the elementary transfer step between sites on adjacent molecules. The activation energy of the transfer step generally could have contributions from intermolecular and intramolecular processes. In the disorder model, the intermolecular contributions arise from the physical inequivalence of chemically identical sites due to disorder-related variations of the lattice contributions. These statistical fluctuations in the disorder energy are attributed to fluctuations of dipole-dipole and ion-dipole attractive intermolecular fluctuations. The intramolecular contribution, which is considered to be relatively less important in this model, arises from a change in the configuration of a molecule with the addition or removal of an electron.

Monte Carlo simulations and an effective-medium analysis in the disorder model showed that a particle, initially created at random within a Gaussian distribution of sites, relaxes energetically in the course of the hopping motion and ultimately reaches an energy level below the center of the Gaussian distribution; the average energy level to which the particle relaxes decreases as the temperature is lowered. The computations showed that the low-field mobility $\mu(T)$ must follow

$$\mu(T) = \mu_0 \exp - (T_0/T)^2, \quad (34)$$

where T_0 is a characteristic temperature and is related to the energy width σ of the density-of-states distribution as

$$T_0 = 2\sigma/3k, \quad (35)$$

and μ_0 is the mobility of a disorder-free (monoenergetic) hopping system having identical parameters (Movaghar *et al.*, 1986); k is the Boltzmann constant. The field dependence of mobility in a system with energetic disorder occurs as a result of tilting the manifold of hopping states which alters the barrier height for energetic uphill jumps in the field direction. Monte Carlo simulations have also been carried out for a system with fluctuations in intersite distances which give rise to fluctuations in intersite transition rates (Pautmeier *et al.*, 1990). Two characteristic features emerge from the inclusion of positional or off-diagonal disorder:

(1) The mobility increases by introducing off-diagonal disorder in an array of energetically ordered states. At low fields an indirect path may provide the charge carrier a faster down-field route, since the transition rates are

faster for more closely spaced molecules or sites. This involves hops sideways and even backward to the field.

(2) The mobility decreases with increasing field. This results from the field-imposed restriction in the choice of routes. A direct route with slower transition rates results in reduced mobility at higher fields. The simulation also predicts the two disorders will act independently, so that at low field the mobility may first decrease and then increase with electric field because the electrostatic energy lowering mechanism due to diagonal disorder becomes dominant. In the presence of both diagonal and off-diagonal disorders the model predicts the high-field mobility as

$$\mu(\hat{\sigma}, \Sigma, E) = \mu_0 \exp\left[-\left(\frac{2}{3}\hat{\sigma}\right)^2\right] \times \begin{cases} \exp C(\hat{\sigma}^2 - \Sigma^2)E^{1/2}, & \Sigma > 1.5 \\ \exp C(\hat{\sigma}^2 - 2.25)E^{1/2}, & \Sigma < 1.5 \end{cases} \quad (36)$$

where $\hat{\sigma} = \sigma/kT$, $C = 2.9 \times 10^{-4} \text{ (cm/V)}^{1/2}$, and Σ is a parameter that characterizes the degree of off-diagonal disorder. Σ accounts for variations of intersite coupling due to random variations of both intersite distances and wave-function overlap. The theoretical predictions are illustrated in Fig. 27 for a system parametric in Σ and assuming $\hat{\sigma} = 3$ (Borsenberger and Bassler, 1991).

The transport through a Gaussian distribution of states has also been employed to explain shape changes of time-of-flight transients between materials and temperature dependence of the shapes. The initial drop in

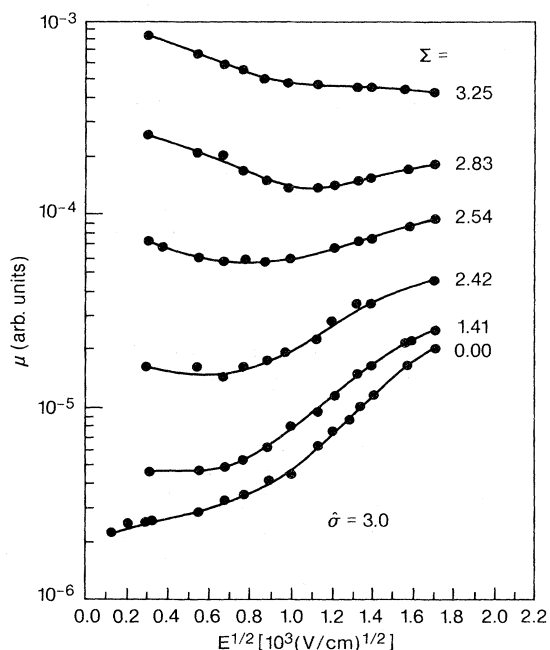


FIG. 27. Theoretical field dependence of mobility employing Monte Carlo simulations in a Gaussian distribution of states for the case of both diagonal and off-diagonal disorder (Borsenberger and Bassler, 1991).

current is a consequence of energetic relaxation of the carrier packet to the equilibrium distribution. The current subsequently reaches a nondispersive plateau before decaying when the carriers begin to exit at the far electrode. The shape of the signal in a particular situation would then depend on the relative values of the relaxation t_{rel} and the transit time t_T : $t_{rel}/t_T \ll 1$ results in a plateau at long times; t_{rel} is higher for systems with larger energetic disorder, resulting in very dispersive signals, without a plateau on a linear ($i-t$) plot. These can be plotted on a log-log presentation in order to obtain a transit time. $t_{rel}/t_T \gg 1$ is the regime, discussed under CTRW theory, in which carriers have not relaxed to the dynamic equilibrium condition by the time they exit at the far electrode.

The basis of the fourth model, identified as the polaron model, is that the contribution of intramolecular deformation energy is relatively more important than the disorder energy. The polaron theory is based on the idea that the geometry of a molecule is dependent on whether the molecule is neutral or ionized. The configuration of a dopant molecule relaxes reversibly with the addition or removal of an electron, which means that electron transfer will require the dragging of the associated molecular distortion (Holstein, 1959; Emin, 1973). The rationale for the application of this theory for charge transport in disordered molecular systems seems to be based on the similarity between some features of the equation for the mobility of a small polaron and the experimentally obtained functional relationships of mobility with temperature, electric field, and the average spacing between molecules (Schein and Mack, 1988). The theory does not address the issue of the shape of the time-of-flight transients nor the role the disorder plays in the transport. Although the physical mechanisms underlying charge transport through molecularly doped systems seem intractable and unraveling them remains a very active field of research, the selection of materials for charge-transport layers in OPC is made by combining scientific insight with empirical optimization, together with factors such as cost and simplicity in the manufacturing process. In the final analysis, as far as the charge-image-formation step is concerned, what matters is the absolute value of the mobility and whether the carriers photogenerated in the pigment layer and injected into the transport layer at the time of the exposure exit the far surface by the time of the development step (Pai and Yanus, 1983). Another important consideration in the use of these materials is whether there are any deep traps, be they impurity related or related to inhomogeneity resulting from incompatibility between the material constituents. The hole mobilities in some of the systems employed commercially are shown in Fig. 28. The data are obtained by time-of-flight experiments on films containing a 50 wt % (note volume % also) solution of the organic molecular material in the polycarbonate binder. The mobility is electric-field dependent and varies between 3×10^{-5} and $10^{-7} \text{ cm}^2 \text{V}^{-1} \text{sec}^{-1}$ for the five electron donor molecules

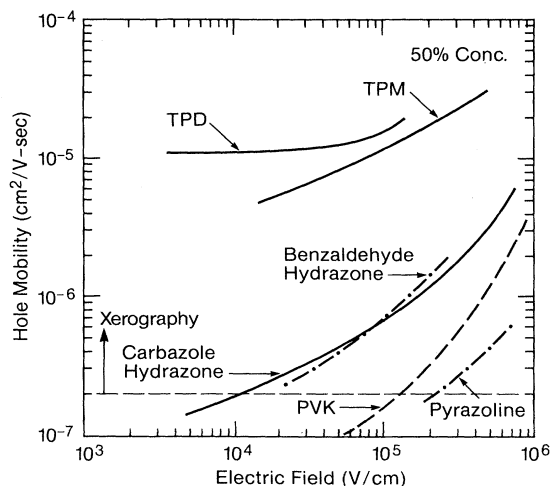


FIG. 28. Hole mobility in five transport layers containing 50 wt % concentration of donor molecules shown in Fig. 22. The binder is polycarbonate (after Pai and Yanus, 1983). The mobility required for reasonable imaging machine design is shown by the dashed line.

shown in Fig. 22. Also shown is the line corresponding to the mobility requirement for use of these systems as transport layers in OPC for high-speed electrophotographic applications. This value for the mobility requirement is calculated by assuming that the transport layer of the OPC is $20\ \mu\text{m}$ thick and that the device is initially charged to 900 V and discharged by the background exposure to a potential of 50 V. The time duration between exposure and development is assumed to be 0.5 sec. The charge carrier mobility has to be larger than $2 \times 10^{-7}\ \text{cm}^2\text{V}^{-1}\text{sec}^{-1}$ for a carrier to drift $20\ \mu\text{m}$ in less than 0.5 sec. To the extent mobility values are lower than this value, the carriers photogenerated at the exposure time will be part way through the transport layer by the time of the development step, thus reducing the sensitivity of the device [Eq. (24)]. Detailed analytical treatment of the impact of the carrier mobility on the discharge shape of the photoreceptor has appeared in several publications (Batra *et al.*, 1970; Chen, 1972). The goal of this subsection has been to provide a conceptual discussion of the key points. For more information on photoconductivity, the reader is referred to several books and chapters on the topic: Bube (1960, 1992), Rose (1963), Ryvkin (1964), Patsis and Seanor (1976), Mort and Chen (1975), and Mort and Pai (1976), to name only a few.

F. Measurement technique

Photoreceptors are characterized by a very powerful technique that simulates the xerographic process. The schematic is shown in Fig. 29 (Scharfe *et al.*, 1989; Melnyk and Pai, 1992). The photoconductor in the form of a film on a substrate is mounted on a metallic cylindrical drum, which can be rotated on a shaft. It is charged by a

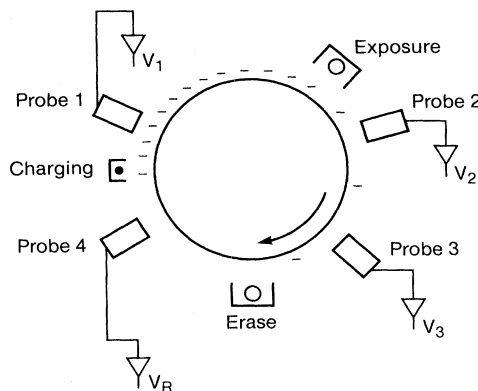


FIG. 29. Scanner that measures PIDC and cyclic stability of photoreceptors. The probes are one of several forms of electrostatic (noncontacting) voltmeters.

corotron mounted along the circumference. The surface potential is measured as a function of time by several capacitively coupled probes placed at different locations around the drum. The probes are calibrated by applying a known potential to the drum substrate. The sample is exposed and erased by light sources located at appropriate positions around the drum.

The measurement consists of charging the photoreceptor in a constant current or constant voltage mode. In the constant current mode, the corotron places a known charge on the photoconductor, and the resulting potential is measured. In the constant voltage mode the photoconductor is charged to the required potential, and the charge required to accomplish this is measured. As the drum rotates, the initial charging potential is measured by probe 1. Further rotation leads to the exposure station where the photoconductor is exposed to monochromatic or broadband radiation of known intensity. The surface potential after exposure is measured by probes 2 and 3. The photoconductor is finally exposed to an erase lamp of appropriate intensity, and any remaining residual potential is measured by probe 4. In some situations, the residual potential is a direct measure of the carrier range or schubweg. The process is repeated with the magnitude of exposure automatically changed for the next cycle. A photoinduced-discharge characteristic (PIDC) is obtained by plotting the potential at probes 2 or 3 as a function of exposure. Further experimentation might involve either changing the wavelength of the exposure and repeating the procedure or eliminating the exposure and monitoring the dark decay.

The equipment is mounted so that the corotron, exposure lamp, and the probes can be moved along the circumference and easily clamped. PIDC plots and plots of potentials of probes 1 through 4 as a function of cycles are used to study several features of the photoreceptor properties. These include (1) dark decay, which may either be related to the presence of charge-generating sites within the photoconductor or be due to injection from

the appropriate surface; (2) sensitivity and the shape of the PIDC, which may be related to the absolute quantum efficiency of carrier supply and its electric-field dependence (Fig. 14); (3) spectral response (Fig. 19); (4) dark decay after exposure to light and the buildup of dark decay with cycles, which may be related to shallow-trap concentration; and (5) residual potential and buildup of residual potential with cycles, which may be due to the accumulation of trapped charge at the deep-trapping centers. These measured quantities have been employed to study unambiguously the fundamental photoconductor parameters, such as photogeneration efficiency (Pai and Enck, 1975), deep-trapping lifetime and release time, gap-state distribution, etc. (Abkowitz, 1987). The traditional steady-state photoconductivity measurements with two electrodes provide information on products of several parameters of interest, and separate measurements are necessary to disentangle the product of parameters. In addition, the ambiguity of the contact in traditional steady-state measurements makes the interpretation of measurement difficult. Surprisingly, the powerful xerographic technique employed in the reprographic industry to characterize thin films is not well known outside the industry (Dolezalek, 1976; Melnyk and Pai, 1992).

IV. DEVELOPMENT FIELDS

The electric field in the space above the photoreceptor surface is the driving force for the development process. An electric-field pattern is produced by the charge pattern on the photoreceptor. A surface charge pattern does not ensure the presence of an electric field in the space above the photoreceptor. In the absence of a development electrode, it exists only as a fringe field in regions corresponding to sharp boundaries of the charge pattern. The nature and behavior of the fringe electric field is illustrated for the case of a single line image. The lines of electric force and of equipotentials above a 30- μm -wide charged line are shown in Fig. 30 (Neugebauer, 1964). The calculation was performed by means of series expansions using the method of images for a charged line on a dielectric film of 25 μm thickness and a dielectric constant of 6.6. The charge density on the line is assumed to be $2.34 \times 10^{-8} \text{ C/cm}^2$. A solid patch of this charge density results in a potential of 100 V in the center of the patch. The center of the line of infinite length perpendicular to the plane of the paper coincides with the origin of the coordinate system which lies on an axis of symmetry. The lines of force are essentially perpendicular at the center of the line and almost parallel at the edge of the line. The forces experienced by a toner, either triboelectrically attached to a carrier or stripped from the carrier, vary depending on whether it finds itself on the center of the line, the edge, or beyond. With a distant electrode, the field above a charge pattern corresponding to a solid dark area is very small. Since development takes place through the attraction of the charged toner particles,

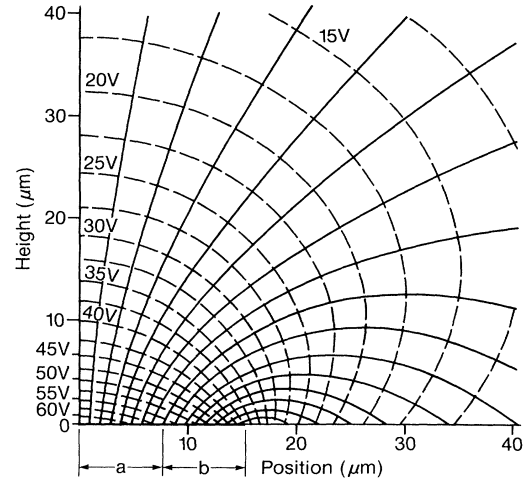


FIG. 30. Electric-field pattern above a 30- μm -wide line charge pattern. Shown is the half plane with the x axis marking the top surface of the photoconductor. The charge pattern extends from $x = -15$ to $x = +15 \mu\text{m}$. The height above the photoconductor is marked along the y axis. The half plane is symmetrical about the y axis (after Neugebauer, 1964).

toner is attracted only to the fringe of the wide image areas. This situation is rectified by the introduction of a development electrode. The field lines emanating from the surface charge corresponding to a solid area are shared between the photoconductive layer and the space above the photoconductor. When the developer is insulating, the average electric field driving magnetic-brush development (in the presence of the development electrode) at the air gap between the photoconductor and developer is

$$E_{\text{ave}} = \frac{V_0}{s/\kappa_s + d/\kappa_d}, \quad (37)$$

where s/κ_s is the dielectric thickness of the photoconductor, d/κ_d is the dielectric thickness of the photoconductor to developer roll (rotating shell in Fig. 10) spacing, and V_0 is the initial potential on the photoconductor which is related to the surface charge density by Eq. (8). The mean dielectric constant of the developer itself is typically 5 to 7. The photoreceptors employed in electrophotography are relatively thin, typically 60 μm with Se alloys with dielectric constant ranging from 6 to 10 and organic photoreceptors of 15 to 30 microns thickness with dielectric constant of 3 and hydrogenated amorphous silicon of thickness 25 μm and dielectric constant of 11. The spacing of the electrode above the photoconductors is determined by the physical limitations of the development systems, including the size of the carrier beads. For an insulating magnetic-brush development system, the electrode (developer roll surface) is placed typically at a distance of 1000 to 1500 μm , with the carrier bead sizes in the 100 to 200 μm diameter range. The practical limit of electrode distance for powder-cloud de-

velopment which has no carrier beads is $250\ \mu\text{m}$. The dielectric thickness of the photoreceptor is therefore more than an order of magnitude smaller than the dielectric thickness of the space between the photoreceptor surface and the development electrode.

When the developer is a conductive magnetic brush, the effective distance of the development electrode to the photoconductor surface is reduced considerably, increasing the strength of the average value of the development field. Assuming the average dielectric thickness of the air gap is equal to the toner diameter D plus a fraction ($\sim \frac{1}{2}$) of a bead radius R , the average value of the electric field for a conducting developer is given by

$$E_{\text{ave}} = \frac{V_0}{s/\kappa_s + (D + R/2)} \quad (38)$$

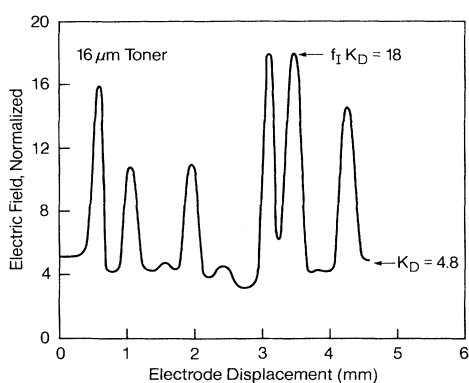
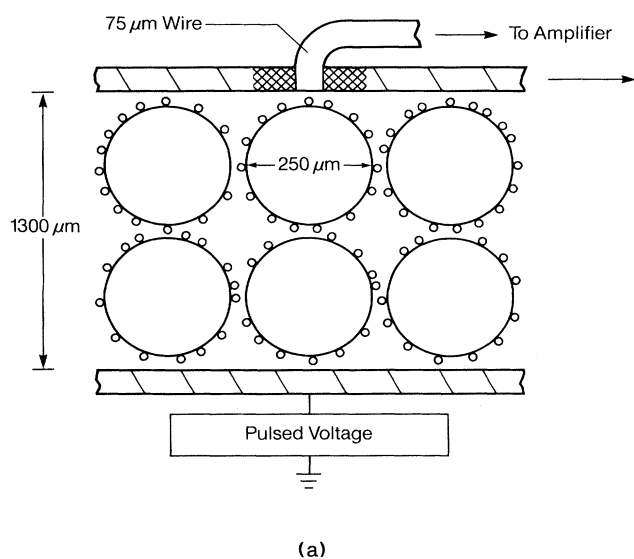


FIG. 31. Electric field profile at a photoconductor developer interface. (a) Apparatus for measuring the electric-field profile. A high-voltage pulse unit applies 1 msec pulse every 250 msec. The electrode moves at a speed of 2 mm/min. (b) Profile of the electric field (normalized to the empty cell field) as a function of the electrode displacement. K_D is the mean dielectric constant of the developer (after Hays, 1978).

The dielectric constant in the air gap is unity.

The electric field acting on the toner and responsible for development can be highly structured due to the discreteness of the carrier beads. The electric-field intensification occurs when a bead chain is centered directly in the middle of the development zone. This intensification occurs for both insulating and conducting developers (Schein, 1975a) and has been measured by equipment shown in Fig. 31(a) (Hays, 1978). A wire probe is embedded in a movable electrode of a cell containing the developer mixture. A voltage pulse is applied periodically and the charge induced in the probe during the motion of the electrode is measured. The electric-field profile is shown in Fig. 31(b) for a development mixture consisting of $250\text{-}\mu\text{m}$ -diameter polymer-coated steel carrier beads and toners with an average diameter of $16\ \mu\text{m}$. The peak field E_p occurs when a toned bead is directly under the probe. The peak electric field is

$$E_p = f_I E_{\text{ave}} \quad (39)$$

where f_I , the field intensification factor, is found to vary between 2.6 and 5.8 as the average toner diameter is varied from 28 to $8\ \mu\text{m}$.

Although the electric field in the center of a solid-area patch is increased by several orders of magnitude, the fringe field at the edge of the solid and above the center of a line charge is almost unaffected by the electrode. Generally the electrode is biased to a voltage somewhat higher than the white image background potential in order to prevent toner development in the white areas.

The discussion on the nature of the electric field thus far has been qualitative. Exact calculations that shed more insight into the characteristic features and limits of resolutions of electrophotographic images have been performed for specific charge patterns (Neugebauer, 1964, 1965; Schaffert, 1962, 1975; Schmidlin, 1972; Kao, 1973; Williams, 1982). A typical object is a line-copy document in which there is sharp demarcation between black and white regions. In an ideal case of equal linewidths, this would result in a square-wave charge pattern on the photoconductor. However, some loss of sharpness is to be expected from the optical system employed to illuminate the charged photoconductor. Some very slight charge spreading is expected in organic photoreceptors when the charge photogenerated in the pigment layer transits the transport layer (Yarmchuk and Keefe, 1989; Chen, 1990). These edge effects are more severe for narrow lines and thick photoreceptors. One approach employed is the method of images and series expansions for a square-wave charge pattern (Neugebauer, 1964, 1965). A second approach, which is outlined below, has been to obtain image fields and potentials as closed solutions of Laplace's equation for images of sinusoidal charge patterns (Schaffert, 1962, 1975). By varying the frequency and combining harmonics, it is possible to produce charge distributions corresponding to different linewidths and solid-area gray scale. The magnitude of the electric field depends strongly on the dielectric properties of the pho-

toconductor and developer, the thicknesses of photoconductor and developer region, the size and shape of the latent image (solid area or narrow line), the bias on the developer delivery roller, and the magnitude of the surface charge associated with the electrostatic image. The interaction of these parameters in modulating the development field was first considered in detail by considering three dielectric slabs between two plane electrodes, the lower dielectric representing the photoconductor, and two slabs representing the developer region with two distinct permittivities. Since then the analysis has been carried out in a model assuming five dielectric slabs consisting of photoreceptor, developed toner, air gap, an active brush region in which toner migration occurs, and an inactive brush region in which there is no toner migration (Benda and Wnek, 1981). Since the salient features of the nature and behavior of electric field and its dependence on the important parameters can be obtained by considering a homogeneous development system, here we shall only consider a two-slab model consisting of the photoconductor and developer region shown in Fig. 32 (Schaffert, 1962, 1975). As explained before, the effect of inhomogeneity such as that which occurs due to bead chaining can be described by an effective permittivity [Fig. 31(b)]. In Fig. 32, the upper electrode is maintained at a potential V_b and the lower electrode is at zero potential.

The electrostatic latent image on the surface of the photoreceptor is represented by a sinusoidal charge pattern. The charge pattern is given by

$$\sigma = \sigma_0 + \sigma_k \cos ky, \quad (40)$$

where σ is the surface charge density, σ_0 is the amplitude of a nonvarying component, and σ_k is the amplitude of a spatially varying surface charge component. The line frequency k is equal to $2\pi/\lambda$, where λ is the period of the charge pattern.

The cosine function enables one to solve for the electric field in both slabs, using boundary-value techniques. In this way, one can obtain a closed-form solution for the electric-field equation. In addition, the cosine function is

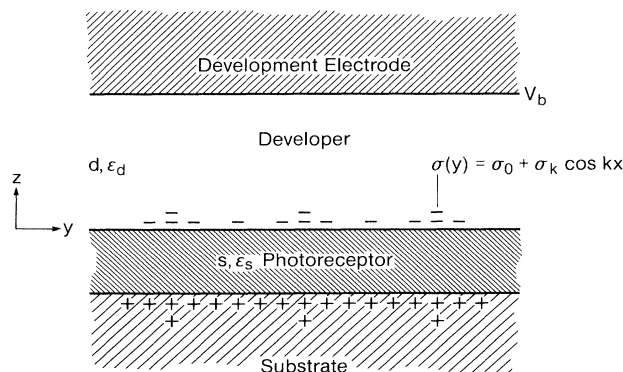


FIG. 32. Dielectric slab model used in the calculation of electric field in the development zone above the photoconductor.

an excellent approximation to real electrostatic line charge-image patterns on the surface of the photoconductor. For example, when the cosine function is positive, it represents the electrostatic charge of a dark line. When the cosine function is negative, it represents the background area between dark lines. The width of the line is approximately $\lambda/2$. The width of the line can be changed by simply changing k , the line frequency. When k is zero, the cosine function approximates a large, solid-area image ($\lambda \rightarrow \infty$). As k increases, it represents lines of smaller and smaller width. Consequently, the cosine function provides a solution for all linewidths without having to solve for each individually. Finally, more complex images, such as sharp boundaries, produced by exposures to high contrast input images, can be deduced by simply performing a Fourier expansion of the input image and applying the solutions obtained for the cosine case discussed in this section.

The goal is to solve Laplace's equation

$$\nabla^2 V = 0 \quad (41)$$

for the electric field in the region above the surface of the photoconductor by applying proper boundary conditions, where V is the potential in the region between the substrate and the development electrode. A schematic of the geometry is defined in Fig. 32 in which x direction is perpendicular to the plane of the figure. Since there is no variation in the x direction, Laplace's equation is solved in two dimensions (y and z) by assuming the dielectric slabs to be homogeneous. For each region, solutions are of the form (Neugebauer, 1965)

$$V = A + A_0 z + (A_1 e^{kz} + A_2 e^{-kz}) \cos ky. \quad (42)$$

There are two such equations for the two regions requiring determination of eight constants. Assuming the dielectric to be linear, the harmonic portion may be separated from the solutions to the constant part, and the total solution may be obtained as the sum of the two solutions. The eight constants are determined by employing four boundary conditions for the set of equations dealing with the harmonic and constant components. The four boundary conditions are potential of the lower and upper conductor, which should be constant, continuity of potentials across the photoconductor-dielectric interface, and the change in the normal component of electric displacement at the photoconductor-dielectric interface, which is equal to the charge density on the photoconductor surface.

In the absence of the development electrode ($d = \infty$), the normal component of the field above the image is given by

$$E_z = \frac{\sigma_k \tanh ks e^{-k(z-s)}}{\epsilon_d \tanh ks + \epsilon_s} \cos ky, \quad (43)$$

where ϵ_s and ϵ_d are the permittivities of the photoconductive layer and air, respectively, and s is the thickness of the photoconductive layer. The normal component of

the field has the highest value on the photoreceptor surface and drops off exponentially with the height above the photoreceptor. The rate of loss of field with height is greater for higher-frequency images. The horizontal component of the field is given by

$$E_y = \frac{\sigma_k \tanh ks e^{-k(z-s)}}{\epsilon_d \tanh ks + \epsilon_s} \sin ky . \quad (44)$$

Figure 33(a) shows the flux lines for a sinusoidal charge pattern of 100 lines per mm ($\lambda=10$). The sinusoidal charge pattern is shown in Fig. 33(c). The rest of the parameters are indicated in the figure caption. The lines of force trace the direction of the field, and the density of the lines represent the magnitude. The normal and horizontal component of the electric field in the presence of a development electrode biased at a potential V_b is given by

$$E_z = \frac{\sigma_0 - V_b \frac{\epsilon_s}{s}}{\epsilon_d + \frac{d}{s} \epsilon_s} + \frac{\sigma_k \cosh k(z-s-d) \cos ky}{\epsilon_s \left[\frac{\epsilon_d}{\epsilon_s} + \frac{\tanh kd}{\tanh ks} \right] \cosh kd} , \quad (45)$$

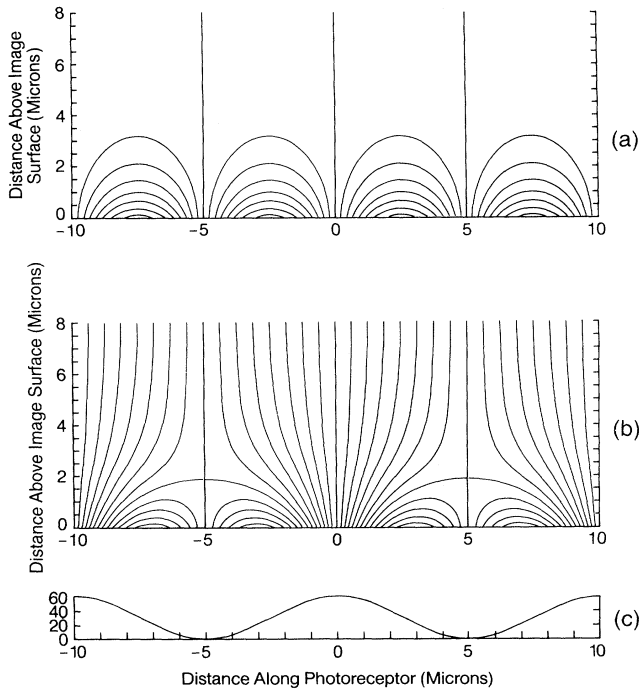


FIG. 33. Field flux lines above the photoreceptor surface. (a) Field flux lines in the absence of a development electrode. The photoconductor is assumed to be $25 \mu\text{m}$ thick with a dielectric constant of 3.0. The sinusoidal charge pattern has 100 line pairs per millimeter or $\lambda=10 \mu\text{m}$. Charge density is $\sigma_0=2.93 \times 10^{-4} \text{ C/m}^2$; $\sigma_k=2.93 \times 10^{-4} \text{ C/m}^2$ (after Jeyadev, 1991). (b) Field flux lines in the presence of a development electrode placed $100 \mu\text{m}$ above the photoreceptor surface. The rest of the parameters are the same as those shown in Fig. 33(a). After Jeyadev (1991). (c) The sinusoidal charge pattern. The amplitude is $\sigma_0 + \sigma_k=58.6$ in units of 10^{-3} C/m^2 .

$$E_y = \frac{\sigma_k}{\epsilon_s} \frac{\sinh k(d+s-z) \sin ky}{\left[\frac{\epsilon_d}{\epsilon_s} + \frac{\tanh kd}{\tanh ks} \right] \cosh kd} . \quad (46)$$

Excellent agreement has been obtained experimentally by employing electrostatic probes to measure electric field above charge patterns of various spatial frequencies (Junginger *et al.*, 1978). Equation (45) for the normal component can be simplified further by making the following substitutions (Schmidlin, 1972; Scharfe and Schmidlin, 1975):

$$V_0 = (\sigma_0 + \sigma_k) \frac{s}{\epsilon_s} \quad \text{and} \quad V_{bg} = (\sigma_0 - \sigma_k) \frac{s}{\epsilon_s} , \quad (47)$$

where V_0 and V_{bg} are the surface potentials corresponding to the solid-area image and background, respectively;

$$E_z = [f_0 + p(z)f_k] \frac{V_c}{2} + f_0(V_b - V_{bg}) , \quad (48)$$

where

$$f_0 = \frac{1}{\frac{\epsilon_d}{\epsilon_s} s + d} , \quad (49)$$

$$f_k = \frac{1}{s} \frac{1}{\left[\frac{\epsilon_d}{\epsilon_s} + \frac{\tanh kd}{\tanh ks} \right]} , \quad (50)$$

$$p(z) = \frac{\cosh k(d-z) \cos ky}{\cos kd} ; \quad (51)$$

and the contrast potential,

$$V_c = V_0 - V_{bg} . \quad (52)$$

As k approaches zero, the field that determines the solid-area density is given by

$$E_z = f_0(V_0 - V_b) ; \quad (53)$$

f_0 is the capacitance division between the photoconductor and development regions. Similarly $p(z)$ is the parameter that describes the variation of electric field with height above the photoconductor surface, and f_k is the parameter that shows how the dielectric properties of the components determine the field for line development.

In Fig. 33(b) the lines of flux represent the field configuration for a sinusoidal charge pattern of 10 lines per mm with a development electrode placed $100 \mu\text{m}$ from the photoconductor surface and biased to zero volts ($V_b=0$). The shape and intensity of the image field are changed considerably by the introduction of the electrode. The intensity of the normal component increases when an electrode is brought closer to the image surface, whereas the horizontal component is essentially unaffected. The normal component of the image field has its peak value on the photoconductor surface and is a function of the spacing between the photoconductor and the development electrode, and the spatial frequency.

The development process, however, is dominated by events occurring at a finite range of heights above the image surface; the image field drops from a maximum value with height, and the rate of decrease of image field with height is a function of the proximity of the development electrode and the spatial frequency of the image. This effect is shown graphically in Fig. 34 for two cases: (a) without electrode and (b) electrode placed $100\ \mu\text{m}$ above the photoreceptor surface. The falloff seen at the higher frequencies is not observed if the electrode is brought to within 10 to $20\ \mu\text{m}$ of the image surface (not shown in the figure). Such short distances are not practical for most of the development systems employed commercially. In fact, the effect shown in Fig. 34 along with the size of the toner may be two of the dominant effects limiting resolutions of the electrophotographic images made by dry toners employing two-component magnetic-brush development. The development electrode can be brought closer and smaller-size toners employed without encountering dirt problems in development systems employing liquid medium.

The reason for discussing this purely electrostatic problem in some detail is that it is these electric fields which drive the toner to the photoconductor surface. The detailed mechanistic of this process will be discussed shortly in Sec. VI after we discuss how toner acquires an electric charge.

V. CONTACT ELECTRIFICATION

When two materials are brought into contact or rubbed against each other and then separated, charge is usually transferred from one material to the other. This phenomenon of contact electrification or triboelectricity has been known since 600 B.C., when the Greeks observed that amber when rubbed with silk attracted small

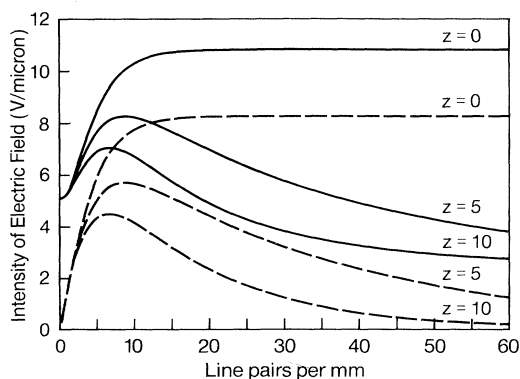


FIG. 34. Effects of spatial frequency on image field for three heights (image surface, and 5 and $10\ \mu\text{m}$ above the image surface). Dashed lines are for the case without electrode, and solid lines are for the case with electrode placed $100\ \mu\text{m}$ above the photoreceptor surface. The photoreceptor thickness is $25\ \mu\text{m}$, with a dielectric constant of 3.0 and $\sigma_0 = 2.93 \times 10^{-4}\ \text{C/m}^2$ (after Jeyadev, 1991).

pieces of straw. Although triboelectric charging between toners and carriers is a key element in the xerographic process, it remains the least understood and most controversial (Loeb, 1958; Harper, 1967; Fabish and Duke, 1977; Cottrell *et al.*, 1979; Lowell and Rose-Innes, 1980; El-Kazzaz and Rose-Innes, 1985, 1987; Akande and Lowell, 1987; Fabish and Duke, 1988; Lowell and Akande, 1988; Lowell, Rose-Innes, and El-Kazaaz, 1988; Terris *et al.*, 1989; Yu and Watson, 1989; Mizes *et al.*, 1990). For a general review, see Schein (1988). In the two-component developer system, toners typically $10\ \mu\text{m}$ in diameter are charged by carrier beads that are typically $100\ \mu\text{m}$ in diameter. The main constituent of the toner is an insulating polymer. The carriers are made from magnetic materials coated with a different insulating polymer. By the proper selection of the two polymers, the toner can be charged to either positive or negative polarity. The carrier is charged to a polarity opposite to that of the toner, and the toner-carrier mixture is neutral. The charge exchange between toners and carriers during the mixing and agitation in the development station.

Contact charge exchange takes place between all materials and can be classified into three classes: metal-metal, metal-insulator, and insulator-insulator. The charge exchange for metal-metal contacts is quite well understood (Harper, 1967; Lowell, 1975). In this case electrons are transferred from the metal with the lower work function Φ_A to the metal with the higher work function Φ_B , so as to bring the two Fermi levels into coincidence (Fig. 35). A thermodynamic equilibrium is

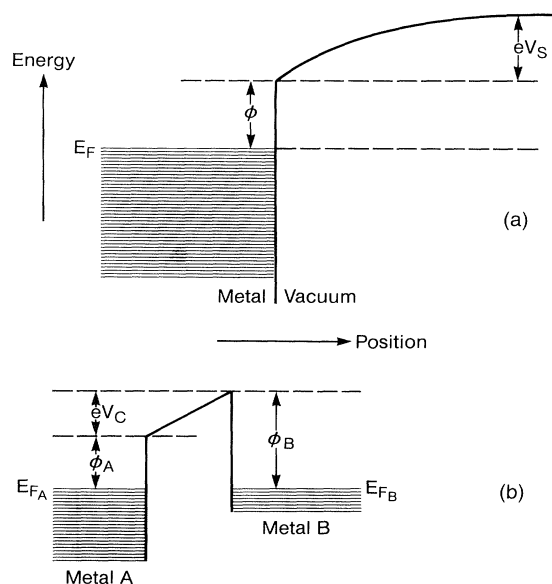


FIG. 35. Energy of an electron inside and outside a metal (a), with the image potential ignored. Φ is the work function, V_s is the surface potential, and E_F is the Fermi level. Two metals in close proximity (b) exchange charge until their Fermi levels are coincident. The transferred charge causes a contact potential difference of V_C equal to $(\Phi_B - \Phi_A)/e$ (after Harper, 1967).

maintained with a contact potential difference given by

$$V_c = \frac{\Phi_B - \Phi_A}{e} \quad (54)$$

The charge exchange between the two metals is given by the product of this potential and the effective capacitance between them. As the two materials are separated, electrons will transfer back by tunneling to maintain a potential difference of V_c . The tunneling current is cut off at a distance of approximately 1 nm between the two materials (Harper, 1951). Therefore the net charge transferred between the two materials is given by

$$Q = CV_c, \quad (55)$$

where C is the capacitance between the two materials at a spacing of 1 nm. The essential predictions of Eqs. (54) and (55) have been confirmed by measuring the charge exchange between a chromium sphere and a variety of metals. Charge measured on the chromium sphere as a function of the contact potential difference between the chromium and contacted metal is shown in Fig. 36 (Harper, 1967). The theoretical predictions based on tunneling between closely spaced metals is also shown. The slight discrepancy is attributed to the roughness of the surfaces (Harper, 1967; Lowell, 1975).

When one of the contacting materials is an insulator, significant discrepancies arise between experimental results and theoretical explanations. Metal-insulator contact electrification has been the subject of a large number of investigations (Inculet and Wituschek, 1967; Cressman *et al.*, 1974; Hays, 1974; Fabish and Duke, 1977; Cottrell *et al.*, 1979; Lowell and Rose-Innes, 1980; Akande and

Lowell, 1985). On the other hand, studies on insulator-insulator contacts are not extensive. The lack of a clear-cut explanation of the metal-insulator contact phenomenon has to do with the reliability of experimental results as well as the poor state of understanding of the electronic states of the insulator surface. The concept of a Fermi level is unclear in an insulator where excess charge transferred to the insulator might not reach equilibrium for very long times. The magnitude of the charge exchange is small, typically 10^{-8} C/cm², which means that one in 10^4 or 10^5 of the surface atoms or molecules takes part in the charge-exchange process. Moreover, insulating materials are typically very poorly characterized. If experimental precautions are not taken and the experiments are carried out under normal atmospheric conditions, contact electrification is likely to be affected by surface contaminants and adsorbed water layers. The oxidation of a polymeric surface can have a significant effect on charge exchange (Hays, 1974). Surfaces are very rough on a microscopic scale and the materials make contact only on the high spots, so that the actual contact area is considerably less than is indicated by a simple size measurement. These and other experimental difficulties have led to major uncertainties as to whether electrons or ions are involved in the charge-exchange process, and whether the states involved are intrinsic, extrinsic, surface, or bulk. Experimental results on nominally the same kind of polymer have been employed to substantiate the many theories that predict totally different relationships between the charge exchanged and the work function of the contacting material. Because of scientific and practical interest, there is considerable activity in this field, and the experimental techniques are becoming more refined (Binnig *et al.*, 1986; Schein, 1988).

It is to be expected that, with so much uncertainty in the measurements and interpretation of the metal-insulator case, the insulator-insulator charge exchange has received less attention. There is some evidence to indicate that the basic mechanism underlying the metal-insulator system is also operative in the case of the insulator-insulator system and that advances in the understanding of the former will lead to a better understanding of the insulator-insulator system (see Horn and Smith, 1992, for a specific example involving mica and silica). The insulator-insulator contact charge exchange has been handled on an empirical basis by arranging the materials in a triboelectric series such that a material higher in the list will charge positively when contacted or rubbed with a material lower down in the list (Henniker, 1962). The fact that the same trends in the triboelectric series are observed for the same materials prepared under different conditions in different laboratories implies that the charge exchange is intrinsic to the material and that a single mechanism is operating at both donor and acceptor surfaces. A selected list of polymers used frequently for toner or carrier fabrication is presented in Table II. Although the positions of a few materials are erratic,

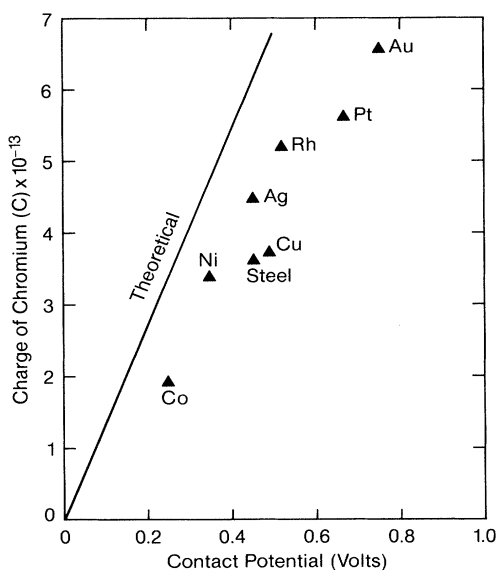


FIG. 36. Charge on a 5/32-inch chromium sphere after contact with a 1/2-inch sphere of another metal, plotted against the contact potential difference between the metal and Cr. The line corresponds to a theory based on tunneling between closely spaced smooth metal surfaces (after Harper, 1967).

TABLE II. Triboelectric series.

Polyamide (nylon)
Polymethyl methacrylate
Styrene butadiene copolymer
Styrene butylmethacrylate copolymer
Polyethylene terephthalate
Polyacrylonitrile
Polycarbonate
Polystyrene
Polyethylene
Polypropylene
Polyvinylchloride
Polytetrafluoroethylene

there is general agreement on the relative positions of the majority of polymers. The triboelectric series shows no correlation with dielectric constant or the dipole moment. Attempts have been made to correlate the chemical structure of model organic compounds with charging behavior. In some studies, a systematic quantitative relation has been shown between the charge-to-mass ratio (Q/M) of beads cascaded over the material as a function of the Hammett substituents constant σ , which is a measure of the electron withdrawing power of the group (Cressman *et al.*, 1974; Gibson, 1975; Gibson and Bailey, 1977). These results suggest that the triboelectric charging of solids is directly related to the molecular structure of the solids.

Certain polymer classes have been empirically identified as positive charging materials. These include polyamides, polyamines, and polyacrylates. Highly halogenated polymers, such as poly(tetrafluoroethylene) and poly(chlorotrifluoroethylene), are found to be negative charging materials. Positive charging polymers typically have nucleophilic sites such as nitrogen or oxygen atoms attached to the polymer backbone or within the backbone of the polymer. Strongly negative charging atoms, such as fluorine, chlorine, and bromine, are electrophilic in nature. Although highly halogenated polymers are not well suited for toner applications, they are commonly used as carrier coatings when positively charged toners are required.

The insulator-insulator charge exchange is not sufficient to predict the outcome of the toner/carrier charge exchange, since toner is composed of many different additives. These include colorant (carbon black for black toners), plasticizers, and flow aids (Barby, 1976; Nash and Bickmore, 1989). Charge control agents are also added to toners for the explicit purpose of controlling the toner charge. Charge control agents based on the phosphonium ion and various metal complexes have been reported (Yourd *et al.*, 1985). In addition to the organic acids, various metal complexes have also been reported as negative charge control agents (Nimura *et al.*, 1984; Gregory, 1985; Birkett and Gregory, 1986). In all cases charge control agents stabilize the charge level,

narrow the toner charge distribution, and improve the rate of toner charging.

There are several semiquantitative explanations of the toner charging process in two-component systems (Lee, 1978; Anderson, 1989) that rely upon the ideas of charge exchange between acceptor and donor sites on the toner and carrier to affect a lining up of the chemical potentials so that there results an electric field across the toner-carrier interface. Each carrier is dressed with many toner particles, and the tumbling or mixing action in the developer housing is necessary to achieve charge equilibrium. This charge equilibrium state is well described phenomenologically by (Kurita, 1992)

$$q_s = \epsilon_0 E_{ic} (1 + f A_{ic} t_c)^{-1}, \quad (56)$$

where $q_s = (S_t r / 3)(Q/M)$ is the surface charge density of the toner, S_t is the toner surface area, r is the effective toner radius, E_{ic} is the interfacial equilibrium electric field, t_c is the toner concentration in the developer mixture, A_{ic} is the ratio of carrier surface area to toner surface area, and f is the shape factor to account for non-spherical particles. Equation (56) shows that charge-to-mass ratio, Q/M , depends explicitly on surface area geometry and that, as t_c increases, Q/M decreases. This is why t_c control is such an important function in a xerographic machine. It is the parameter E_{ic} which is controlled by varying the surface material properties of both toner and carrier.

Another important property of the developer system is that it reach the equilibrium state described by Eq. (56) quickly, since toner is continually used up and fresh toner is supplied to the developer mixture. Unless the toner has achieved its equilibrium state, the theory of toner detachment explained below will not properly apply because there will be a bimodal charge distribution at worst and a very broad distribution (approaching zero) at best. The processes governing the approach to equilibrium depend largely on the many-body statistics of the situation and can only be described phenomenologically in an average manner.

The charge distribution of toner particles can be measured by the charge spectrograph, as shown in Fig. 37 (Lewis *et al.*, 1983). The instrument is essentially a compact low-speed wind tunnel with an electric field across the direction of the air flow. A small air jet strips the charged toners from a two-component carrier/toner mixture, and the sample is introduced at the top of the instrument. Toner particles introduced at the axis with a downward airflow drift down and laterally according to their charge and Stokes mobility and are deposited on a filter paper through which the air stream leaves the chamber. During the drift of the toner particles, the Coulomb force qE moves the toner against the viscous air drag force given by the Stokes law. The toner terminal velocity in the direction of the electric field can be calculated from

$$qE = 6\pi\eta r v, \quad (57)$$

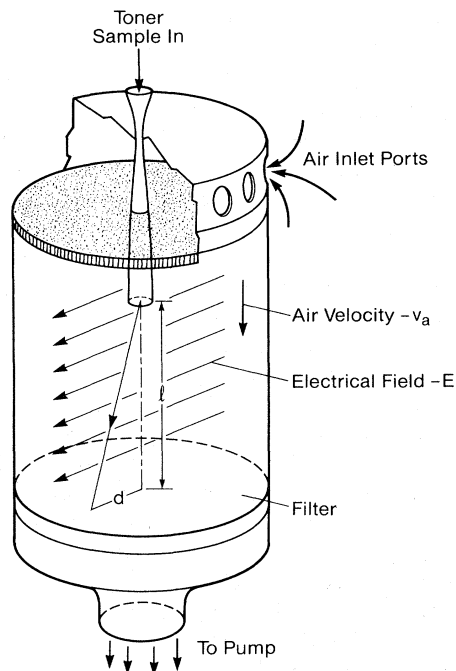


FIG. 37. Charge spectrograph chamber employing laminar air flow and crossed electric field. The toner is collected on the filter paper at the bottom of the chamber (after Lewis *et al.*, 1983).

where η is the viscosity of air and r is the toner radius. If the air velocity is v_a and the axial length is l_a , the toner displacement y during the axial transit time of l_a/v_a is given by

$$y = \left[\frac{q}{r} \right] \left[\frac{E}{6\pi\eta} \right] \left[\frac{l_a}{v_a} \right]. \tag{58}$$

The displacement is proportional to the ratio of the toner charge to diameter. The toner deposited on the exit filter is scanned and analyzed for both size and displacement by a computer-driven microscope-based particle analysis system. The information generated by this technique is displayed in a charge spectrograph, shown in Fig. 38 (Lewis *et al.*, 1983). Figure 38(a) shows the distribution of charge/diameter for those toners in the size distribution with a diameter of $10 \pm 0.5 \mu\text{m}$. The figure shows a narrow distribution of charge, since the toner was well mixed in the fresh carrier. Figure 38(b) shows the distribution after the carrier in the developer has been worn out by use. The charge distribution is very broad, and the toner even contains zero as well as reverse charged particles. Zero and wrong-sign particles are not easily controlled by the latent-image field and cause machine-dirt contamination as well as dark image background problems. The carriers have to be replaced when the toner charging degenerates. Figure 38(c) shows the distribution of charge soon after the addition of fresh toner to

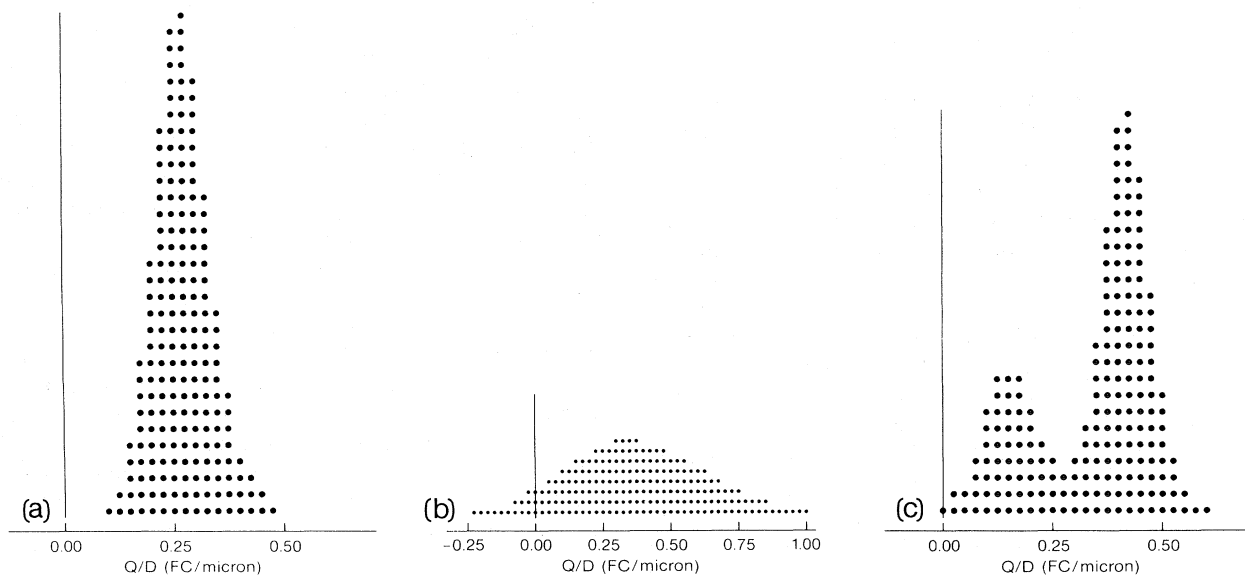


FIG. 38. Toner charge distribution. (a) A $10 \pm 0.5\text{-}\mu\text{m}$ -diameter toner fraction from a working developer showing a sharp peak. The ordinate is a normalized number (of toner particles). (b) A $10 \pm 0.5\text{-}\mu\text{m}$ -diameter toner fraction from a worn-out developer showing a large number of uncharged and reverse charged particles. (c) A $10 \pm 0.5\text{-}\mu\text{m}$ -diameter fraction from a running developer shortly after the addition of uncharged toner. The added toner has low charge and causes copy quality problems (after Lewis *et al.*, 1983).

the developer. The added toner has low charge, which can create a copy quality problem.

VI. TONER-CARRIER ADHESION FORCES AND DETACHMENT OF TONERS

In Sec. IV, the electric-field distribution in the space above the photoreceptor corresponding to line frequency and solid areas of charge pattern was calculated with particular attention given to the characteristic features of edge effects and spatial resolution. The development process is based on the electric-field detachment of charged toner particles from the oppositely charged carrier beads. The surface charge pattern formed after exposure of the charged photoconductor does not remain constant and changes continuously (Junginger and Strunk, 1976). The dark decay of the photoconductor reduces the magnitude of the charge pattern during the time interval between the exposure and development stations and also during the time of the development process. The magnitude of the charge pattern diminishes further as a result of the shielding effect of the developer material. Since the electric field parallel to the surface is spatially varying and any currents near the surface of the photoconductor are electric-field dependent, the magnitude and shape of the charge pattern may vary in time due to this effect also. As the development proceeds, the electric field driving development diminishes further as a result of neutralization by the developed toner and the tribo interaction with the developer. This is the dominant cause of electric-field diminution. Measurement of developed toner mass per unit area of a dense path shows that development does not proceed until the charge on the photoconductor is neutralized. In most cases approximately 40% of the photoconductor charge is neutralized.

As shown in Fig. 34 the magnitude of the electric field above the photoconductor corresponding to a line charge pattern depends strongly on the distance above the photoconductor. The physics of the toner detachment and the amount of toner detached depends on the process by which toner is delivered in terms of proximity of the developer to the photoconductor surface. The quantitative description of the resulting deposition of toner on lines and solids is contained in a frequency- and voltage-dependent function called a "modulation transfer function." Essentially, it describes the developer density resulting from each of the Fourier components of a given electrostatic image. Since the toners are expected to follow the electric-field lines once detached, the modulation transfer function will be affected by the range of heights above the photoconductor at which toner is released. Since the electric field is involved in the release mechanism, this function is also affected by the magnitude of the field in that height range. With reference to the field pattern in Fig. 30, consider the two extreme cases of development systems employing very small (1 or 2 μm) toner particles (Goren, 1976). The first is a liquid development system in which the toners are transported by a hy-

drocarbon medium close to the photoconductor surface. The agitation of the liquid provides sufficient mechanical energy, and the small toner particles penetrate the fringing field to develop the entire linewidth, marked a and b in Fig. 30. The second case is that of a development system known as a powder-cloud system in which charged toner particles are released at a much greater distance from the photoconductor and arrive on the photoconductor surface under the influence of gravity and electric field. The field lines at the large distances from the photoreceptor develop only the center region of the line marked a . The gravity force is too weak to penetrate the fringing field on the edges of the line, and the streamlines concentrate the toner in the center. Liquid development systems are employed in high-resolution color proofing systems and also in electrophotographic systems employed in dental x rays. Powder-cloud development is used commercially in xeromammography to develop x-ray-exposed photoconductor plates. The two-component magnetic-brush development system employed in most commercial applications lies between the two extreme cases of liquid and powder-cloud development with regard to the size of the toner and the height at which the dominant mechanism is operative. Toners in the size range of 5 to 20 μm are stripped from the carrier and launched into the field pattern above the photoconductor in the height range of 5 to 200 μm . The electric-field stripping of the toners is assisted by contributions from inertial forces associated with collisions between carrier beads or collisions between the carrier bead and the photoconductor.

Some properties of the toner release mechanism have been demonstrated by a simple experiment. A developer mixture dropped several millimeters releases a small amount of toner. As shown in Fig. 39, in the presence of an electric field as small as 10^3 V/cm, the toner release efficiency increases significantly. In the absence of mechanical agitation, an electric field of that magnitude strips a negligible amount of toner. Electrophotographic image development, then, results from a combination of mechanical and electrostatic forces. This is especially the case in the cascade development process employed in the early versions of the copying machines. In this system, glass or sand beads mixed with toners were cascaded over the latent-image charge pattern. During the agitation the combined effect of the mechanical impulses and the electric field stripped the less tightly held toners from the carrier surfaces and deposited them on the charge pattern on the photoconductor surface. The adhesion force holding the toner to the carrier has been investigated experimentally using a centrifuge (Donald, 1969) and electric-field detachment (Hays, 1978). The total adhesive force F_A that binds the toner to the carrier with a conductive core can be described by

$$F_A = F_I + F_{\text{SRC}} = \alpha Q^2 / 16\pi\epsilon_0 r^2 + F_{\text{SRC}}, \quad (59)$$

where F_I is the image force and F_{SRC} is a short-range van der Waals force. The image force can be described in

terms of a point charge Q , radius r of the toner, ϵ_0 , the permittivity of free space, and a constant α that depends on the dielectric constant of the toner and the properties of the carrier. Development occurs when the electrostatic development force QE exceeds the total adhesion force F_A . The graph of F_A as a function of Q is shown in Fig. 40 (Schmidlin, 1972). Also shown are the lines corresponding to the development force for two different electric fields E_1 and E_2 . In the absence of inertial forces and three-body collisions, the development force QE_1 in this example is too small to strip the toner from the carrier. On the other hand, assuming F_{SRC} and r to be constant, the development force corresponding to electric field E_2 is sufficient to overcome the adhesion forces for toner in the charge range Q_1 to Q_2 . The threshold electric field required to pull the toner from the carrier is given by

$$E = \frac{\alpha Q}{16\pi\epsilon_0 r^2} + \frac{F_{SRC}}{Q} \tag{60}$$

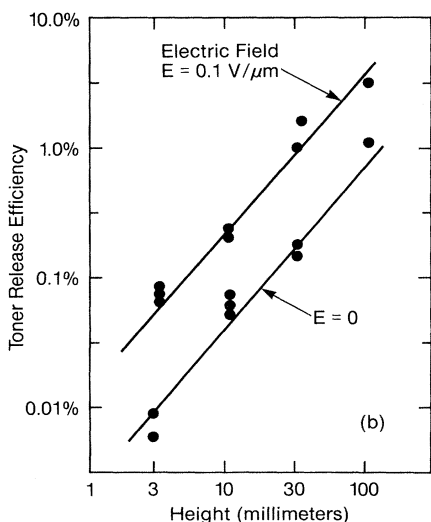
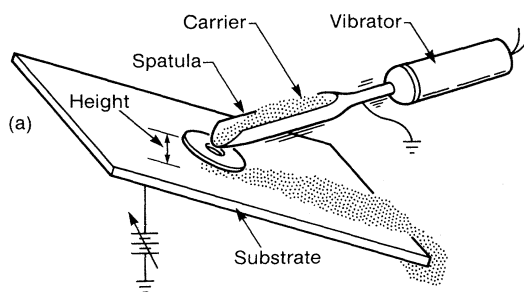


FIG. 39. Influence of the impact of carrier beads in the presence of an electric field. (a) Experimental setup for dropping carrier onto a substrate in the presence of an electric field; (b) efficiency of toner release as a function of the drop height with and without an electric field (after Donald and Watson, 1972).

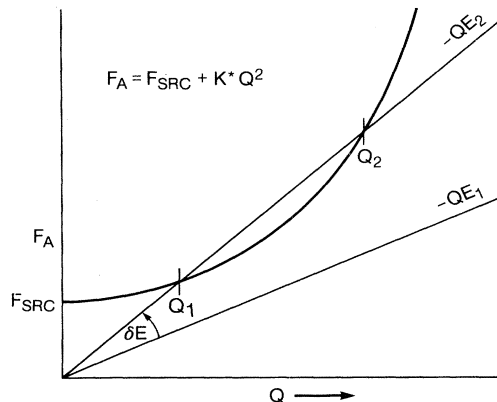


FIG. 40. Relationship between the adhesive force, which holds the toner particles of charge Q to a carrier, and the electrostatic force $(-QE)$, which tends to remove it. In this example, all toners with charge between Q_1 and Q_2 will be separated from the carrier for the field E_2 (after Schmidlin, 1972).

The optimal toner charge to minimize the development field is obtained by differentiating Eq. (60) with respect to Q . Q_{opt} and E_{min} are given by (Scharfe *et al.*, 1989)

$$Q_{opt} = \left[\frac{16\pi\epsilon_0 F_{SRC}}{\alpha} \right]^{1/2} r \tag{61}$$

$$E_{min} = 2 \left[\frac{\alpha F_{SRC}}{16\pi\epsilon_0} \right]^{1/2} \left[\frac{1}{r} \right] \tag{62}$$

Unless the toner charge varies linearly with the radius of the toners, a distribution of toner sizes leads to a distribution of adhesion forces. In the manufacture of toners, the very large and very small toners are removed to obtain a narrow distribution of sizes. The minimum detachment electric field is usually inversely proportional to the toner radius and therefore very high electric fields are required to free small toners. Toners of radius much smaller than $5 \mu\text{m}$ tend to remain in the developer mixture and eventually are impacted (permanently stuck) on the carrier surface, resulting in changes in the toner charging after extended developer usage. At that point the carriers have to be replaced by a fresh batch.

The electric field required to detach a toner in the absence of mechanical forces has been measured under well-defined conditions (Hays, 1978). A $250\text{-}\mu\text{m}$ spherical carrier bead with attached toner particles of $13 \mu\text{m}$ in size is held in an electrode structure shown in Fig. 41(a). High-voltage pulses are employed to detach toners which can pass through the $150\text{-}\mu\text{m}$ hole in the grounded electrode into a field-free region. The charged particle induces a charge in the bottom electrode and this induced charge is amplified and measured by a transient recorder. The particle bounces back and forth in the field-free region between the charge-sensing bottom electrode and the grounded electrode. The bouncing results from conversion of kinetic energy to elastic energy and back to ki-

netic energy. The electric field required to detach toners with an average charge of 3×10^{-14} C was found to be 7×10^4 V/cm, considerably higher than the peak electric field available in the development zone employing insulating developers. It was concluded that either mechanical forces or three-body collisions between toner, carrier, and photoconductor are required to strip the toner. For conductive developers the electric field in the development zone is high enough that one can expect toner detachment from noncontacting particles.

Another conclusion from the above experiment is that the electrostatic image force in Eq. (59) accounts for only a fraction of the total adhesion force. Figure 41(b) shows a comparison of the total adhesion force to the electrostatic image force. The total adhesion force is calculated as the product of the applied field at which toner detachment occurs and the measured toner charge. The image force is calculated from the expression for F_I in Eq. (59) where $\alpha = 1.9$ corresponds to a toner dielectric constant

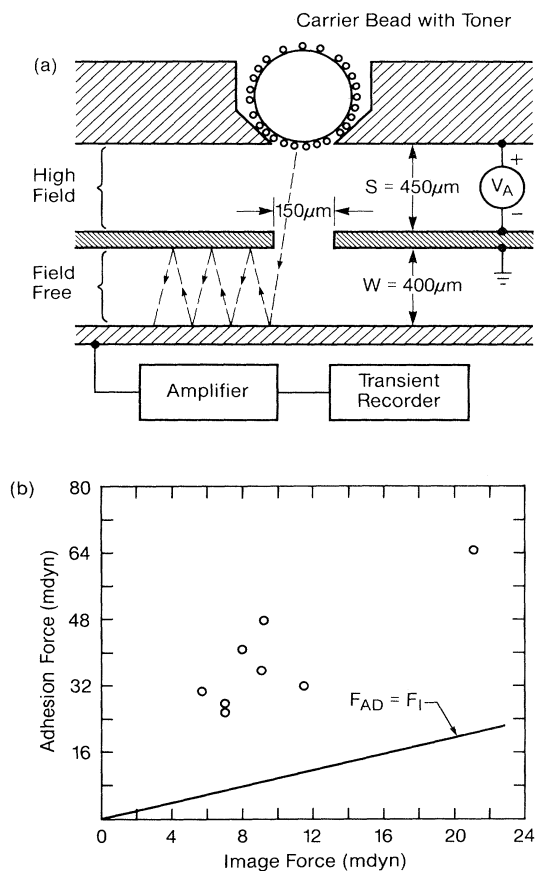


FIG. 41. Adhesive force between the carrier and the toner. (a) Experimental setup for measuring the adhesion and charge of toner detached from a single carrier bead. The toner is detached by the high electric field and allowed to pass into the field-free cavity where its charge is measured. (b) A comparison of the adhesive force to the electrostatic image force of $13\text{-}\mu\text{m}$ toner. The data would be near the solid line if the adhesive force were dominated by the image force (after Hays, 1978).

of 4. If the spherical toner is uniformly charged, the electrostatic force only accounts for one-quarter of the total adhesion force. It has been suggested that a nonuniform charge distribution on the particle can provide the enhanced adhesion. A technique for measuring the nonuniform charge distribution in a $100\text{-}\mu\text{m}$ dielectric sphere has been described by Hays and Wayman (1989) and Hays (1991).

Three models have been considered for solid-area development in a two-component development system (Schein, 1975a, 1975b; Burland and Schein, 1986; Hays, 1989): (1) powder cloud, (2) field stripping, and (3) field collapse. In the powder-cloud model, a powder cloud of toner particles is produced as a result of mechanical impulses associated with the carrier-carrier and carrier-photoconductor collisions. The charged toners then move along the electric-field lines associated with the latent image and deposit on the photoconductor surface. This model predicts a superlinear relationship of the developed toner mass with the developer roller velocity. (This velocity determines the delivery rate of toner to the development zone.) However, the measured toner mass varies linearly as a function of roller velocity. In the field stripping model, the electrostatic forces QE stripping the toner particles has to exceed the adhesion forces in Eq. (59). Since the typical toners contain a distribution of size and charge which results in a distribution of adhesion forces, all toners with adhesion forces less than QE will be developed. Therefore the developed mass versus photoreceptor potentials should be the integral over adhesion distributions and therefore a nonlinear function. Experimentally the developed mass is found to vary linearly with potential.

The model that seems to fit most of the experimental observations is the field collapse model. The experiment described earlier on the measurement of electric field required to detach a toner in the absence of all other forces suggested that in the absence of inertial forces or three-body collisions the electric field in the development zone of an insulating magnetic-brush development system will be insufficient to overcome the adhesion forces between the toner and the carrier (Hays, 1978). The expression for the three-body collision model is given by (Scharfe *et al.*, 1989)

$$F_{\text{SRP}} + \frac{\alpha_2 Q^2}{16\pi\epsilon_0 r^2} + QE > F_{\text{SRC}} + \frac{\alpha Q^2}{16\pi\epsilon_0 r^2}, \quad (63)$$

where F_{SRP} is the short-range van der Waals force between the toner and the photoconductor, and α_2 is a constant that describes the strength of the image charges induced in the photoconductor. The contact between the photoconductor and the toner attached to the carrier provides an additional adhesion force that lowers the magnitude of the threshold electric field.

During the development step, charged toners migrate toward the photoconductor surface, leaving a countercharge on the carrier beads. For example, in the case of charged-area development of a negatively charged organ-

ic photoconductor, the migrating toner is positively charged and the bead charge is negative. This reverse field buildup in the development zone due to the accumulation of charge on the beads results in a reduction of the net electric field driving development. The development stops when the net electric field near the photoconductor interface is lower than the value required to satisfy the inequality in Eq. (63). An estimate of the developed toner mass per unit area, m , can be obtained by assuming that the development proceeds until the electric field at the photoconductor collapses completely (Hays, 1989). As Fig. 42(a) shows, the electric field at the photoconductor interface before the onset of development is given by

$$E_A = -f_1 \frac{\kappa_d V_A}{d}, \tag{64}$$

where f_1 is the field intensification factor defined in Eq. (39), V_A is the potential difference between the photoconductor and the development electrode, and d/κ_d is the dielectric thickness of the photoconductor to developer roll spacing; the permittivity of the developer is $\epsilon_d = \kappa_d \epsilon_0$. The dielectric thickness of the photoconductor is assumed to be much smaller than the dielectric thickness of the developer. If the corresponding bead charge σ_B is at a position δ above the photoconductor surface [Fig. 42(b)], the reverse field due to the developed toner is given by

$$E_B = -f_1 \sigma_B \frac{d - \delta}{\epsilon_0 d}. \tag{65}$$

If the net field, $E_A + E_B = 0$,

$$\sigma_B = \frac{-\kappa_d \epsilon_0 V_A}{d - \delta} = \frac{-\sigma_T}{v}, \tag{66}$$

where σ_T is the charge density of the toner layer on the photoreceptor and v is the ratio of the developer surface velocity to photoconductor surface velocity. The toner-layer charge density is related to the developed toner charge-to-mass ratio Q/M by

$$\sigma_T = \left(\frac{Q}{M} \right) m; \tag{67}$$

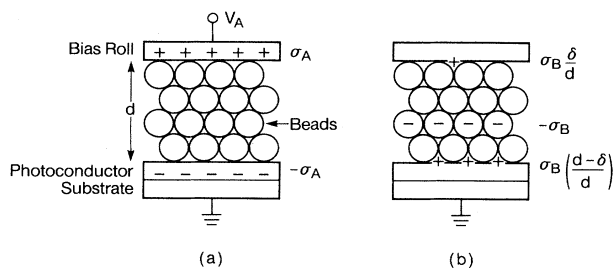


FIG. 42. Field collapse in the development zone. (a) Applied field charge densities at the bias electrode photoconductor interfaces; (b) charge densities at electrodes due to bead charge density σ_B at position δ after positive charges have migrated to the photoconductor surface (after Hays, 1989).

substituting from Eq. (66), the developed toner density m is given by

$$m = \frac{\kappa_d \epsilon_0 V_A v}{\left[\frac{Q}{M} \right] (d - \delta)}. \tag{68}$$

The field collapse model predicts that the developer toner density will be proportional to both the development potential difference and the speed ratio, and inversely proportional to the developer tribo. Q/M from Eq. (56) can be further substituted into Eq. (68) to display the dependence on toner and carrier geometric factors.

The measured solid-area-developed mass per unit area (M/A) as a function of the potential difference between the photoconductor and the bias roll shows essentially a linear relationship with both the potential and roller velocity. The measured Q/M of the developed toner as a function of the potential difference is essentially independent of potential (Schein and Fowler, 1985). The data are consistent with the bead-charging equilibrium model (Schein, 1975a, 1975b; Hays, 1989). A model for solid-area development is easier to formulate, since the electric field in the development zone is constant and easily verified by measurement. For line development, on the other hand, the electric field depends on the position within the development zone, and the final response may be dominated by events in other regions.

The measurements relating to lines in a two-component magnetic-brush development have been carried out by exposure of a charged photoconductor to a sinusoidal density image which forms a periodic charge image on the photoconductor (Witte and Szczepanik, 1978). The response of the system as a function of the line frequency is measured directly on the photoconductor plate by monitoring the change in specular reflectance from the plate surface due to the presence of toner using a bright field microdensitometry system. Figure 43 shows the xerographic response as a function of spatial frequency, the modulation transfer function for

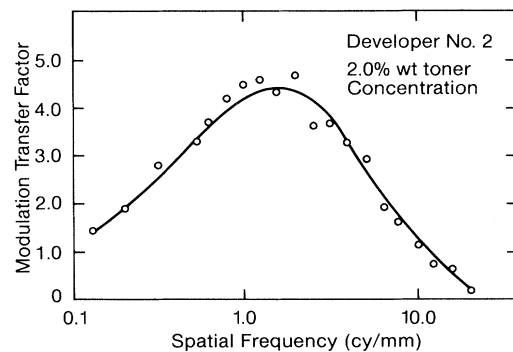


FIG. 43. Experimentally measured xerographic development transfer function for two-component magnetic-brush development system, which roughly expresses development efficiency as a function of image linewidth (after Witte and Szczepanik, 1978).

this particular system. The initial characteristic rise from zero frequency is due to the edge enhancement effect resulting from the markedly high fringe fields compared to the dc field in the solid area and the development physics associated with two-component magnetic-brush system with insulative developer. The high-frequency falloff results from the loss of fringe field at the appropriate tone detachment height range as well as the toner size employed in this experiment. The 15- μm toner employed in this study is expected to produce a limiting resolution of 30 cycles/mm. Apart from the limitations due to toner size, the response in Fig. 43 closely parallels the electric field at a height of 20 μm above the photoreceptor (similar to the data shown for 10- μm height in Fig. 34), suggesting that the development physics is dominated by events in this region. For a general reading on the adhesion of particles and dust, see Krupp (1967) and Zimon (1969).

VII. TONE REPRODUCTION CURVE

Thus far the physics of two key subsystems and their impact on subsystem transfer functions has been discussed. The transfer function of the latent-image formation has been subdivided into that of the exposure step and the photoinduced-discharge characteristics or the PIDC of the photoreceptor. The transfer function of the exposure step is the relationship between the density of the optical input image and the exposure incident on the photoreceptor. The PIDC is the relationship between the broad area surface potential of the photoreceptor and the exposure. In general, the PIDC is determined by (1) the field dependence of the carrier supply, which includes both the physics of the photogeneration step and the physics associated with the injection of the photogenerated carrier into the bulk of the photoconductor, and (2) the limitations imposed by the charge carrier mobility if it falls below a minimum value. The transfer function of the development subsystem is the relationship between image development and the surface potential on the photoconductor and is different for line and solid-area development; it can be represented from Eqs. (48), (53), and (68) by (Scharfe and Schmidlin, 1975; Scharfe *et al.*, 1989)

$$D_s = v_0(V - V_b), \quad (69)$$

$$D_l = (v_0 + v_1)V_c/2 - v_0(V_b - V_{bg}). \quad (70)$$

In these equations, which were developed for charged-area development (CAD), D_s is the developed density for large solid areas; D_l is the developed density for line images; V is the surface potential on the photoconductor produced by exposure to the input image; V_b is the bias on the development roller; V_{bg} is the potential on the photoconductor corresponding to exposure to background areas of the image; $V_c = (V - V_{bg})$ is the contrast potential; v_0 is a slope constant that depends on the toner

delivery rate, toner size, triboelectric and dielectric constants and thickness of the photoconductor, and the development region and the physics of the toner stripping mechanism; and v_1 is similar to v_0 and, in addition, has the linewidth information in the form of the spatial frequency dependence of electric field.

The tone reproduction curve is the relationship between the output and input densities and can be graphically generated and optimized from transfer functions of the exposure, photoconductor, and development subsystems by what is known as the Jones or four-quadrant plot (Fig. 44). As shown in Fig. 44, the transfer functions of the exposure, photoconductor, and development subsystems are plotted in quadrants 4, 3, and 2 respectively. The lamp intensity determines the background and contrast potentials and is chosen to optimize contrast potentials for a range of densities. Once the lamp intensity is chosen, the bias potential V_b is chosen to be about $(V_{bg} + 100)$, so that the field in the background region is in a direction to move the toner away from the photoreceptor to ensure a clean background. From the transfer function plots in quadrants 4, 3, and 2, the tone reproduction curve is easily obtained and is displayed in quadrant 1. A variety of considerations beyond those shown in Fig. 44 enter into the selection of the development system and developer design. These include desired copy quality in terms of fidelity, the process speed, the number of development rollers in the machine, the conductivity of the developer in terms of the extent of the insulator

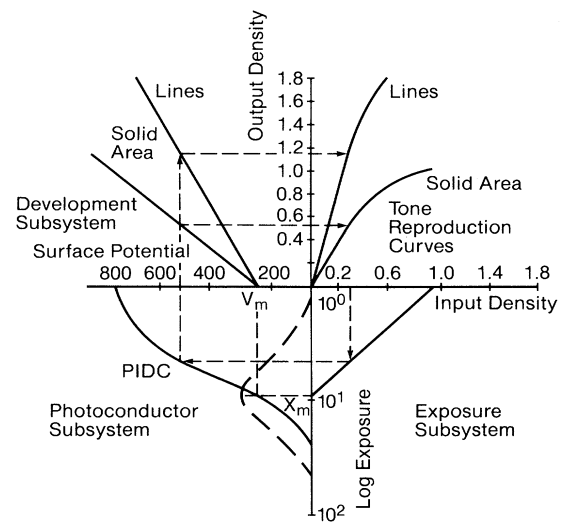


FIG. 44. Four-quadrant plot of tone reproduction curve in a xerographic system. The exposure subsystem defined by Eqs. (6) and (7) is plotted in the lower right-hand quadrant. The photoconductor PIDC is plotted in the lower left-hand quarter. The development equations, as defined by Eqs. (69) and (70), are plotted in the upper left-hand quarter. The resulting tone reproduction curves for both typewritten lines and solid areas are shown in the upper right-hand quadrant. The dashed lines represent the development of 0.3 input density images (after Scharfe *et al.*, 1989).

coating on the developer beads, the fusing process, and the cost. The thickness of the photoconductor and the potential to which it is charged are two parameters required to satisfy the image density requirements. The thickness of the photoconductor is limited to a value between 5 and 100 μm due to manufacturing and material property constraints. The maximum field to which the photoconductor can be charged is governed by the occurrence of image defects resulting from localized breakdown, which in some instances may be defect induced. For more details on system optimization, see *Electrophotography Principles and Optimization* by M. E. Scharfe (1984).

VIII. COLOR ELECTROPHOTOGRAPHY

So far, it has been explicitly assumed that we have been addressing black and white (B&W) copying and printing. This brief section will comment on the impacts that color has on photoconductors and development systems, and the xerographic system as a whole. However, the basic process remains as indicated in Fig. 3.

The first point to note is that the eye readily perceives variations in color; so the system as a whole is placed under much more stringent requirements as to stability and control of the process. The second point to note is that color images are composed of four basic colors—cyan, magenta, yellow, and black (CMYK set). The imaging process is, in consequence, a subtractive one as opposed to CRT screens, which use an additive process with the primary colors being red, blue, and green (RBG). Thus not only must tighter control be achieved, but there are also now four development steps and four transfer steps as opposed to one each for B&W. Basically, each color separation is imaged, developed, and transferred to paper separately. The printing speed is thus typically 4 times slower than for B&W.

The color electrographic systems use DAD development and digital imaging; the color gamut is achieved by traditional halftone methods. This means that the development systems not only must be more stable and uniform, they must also respond well to electrostatic images with a lot of high-frequency components and utilize toners in the 5–10- μm -size range, since a typical one bit dot at 300 dpi (dots per inch) is about 80 μm in diameter. In addition, due to the shift in fusing requirements from matte to glossy (or semigloss), the material properties and color pigment loadings of the toner must change. And lastly, if the color printing speed is to be the same as B&W is currently, the development process must occur in one-quarter of the time presently allotted.

From a photoconductor point of view, this last point means intrinsically faster responding devices are required, implying higher effective photoefficiencies and higher mobilities. Due to the stability requirements, the photoconductor must be capable of being made highly uniform (to less than 1% thickness variation) and should have very low dark decay and fatigue characteristics.

Since the imaging is digital and the development system has to contend with high-frequency images, the PIDC should approach being linear with a sharp cutoff at low voltages as opposed to the much softer shape required for B&W copying.

The electronic system of the printer must also be capable of keeping each color in excellent register, which means tight control of all motions within the printer, including the very difficult issue of the paper movement. For some general references on the topic of color and color electrophotography, see, for example, Yule (1967), Wyszecski and Stiles (1982), Durbeck and Sherr (1988), Sahni (1991).

IX. GAIN: PHOTOGRAPHY VERSUS ELECTROPHOTOGRAPHY

Photography requires a photoreceptor of sufficient sensitivity to capture a momentary pattern of dim light arriving through a lens, momentary because the exposure times are short and dim light because optical systems are very inefficient and light sources are of limited intensity. Practical light sources and optics can provide about 10^{14} photons per square centimeter per second at the photoreceptor surface, which for exposure times of 10^{-2} seconds translates into 10^{12} photons per square centimeter. Assuming the conversion of one molecule per incident photon, the direct imaging process can at most convert 10^{12} light-absorbing molecules per square centimeter. Because about 10^{17} converted molecules per square centimeter are required to give an optical density of 2.0 (99% light absorption), an amplification of 10^5 is required (Mees and James, 1966; Shaw, 1975; Goren, 1976; Weigl, 1977; Pai and Melnyk, 1989). Both photography (employing silver halide emulsion) and xerography (utilizing photoconductors) resort to amplification in the image-development step. In photography, light absorbed in a micron-size grain of silver halide produces an invisible latent image of silver if the light exposure is above a threshold level. Development converts the entire grain with this latent image into a black mass of silver by chemical reduction. The development gain can be enhanced by increasing the grain size, thereby sacrificing resolution. Typically ASA 100 films require 100 photons per grain to form the latent image. Although the primary quantum efficiency of photogeneration is unity, the net efficiency is about 1% (Sahyun, 1974). This is because a complex series of reactions are required to produce the cluster of four silver atoms necessary for the latent image. Since a monolayer of silver grains contains 10^8 grains per square centimeter, 10^{10} photons per square centimeter are required to produce an image.

Xerography, on the other hand, requires 10^{12} photons per square centimeter or has an ASA of about 1. In xerography, a photoreceptor 25 μm in thickness with a dielectric constant $\epsilon=3$ has a surface charge density of 90 nano coulombs per square centimeter (nC/cm^2) or 0.5×10^{12} ions/ cm^2 when corona charged to 800 V. Thus

for 50% quantum efficiency, a light exposure of 10^{12} photons per square centimeter is required to discharge the photoreceptor. Typically the charge image is developed with toner particles $10\ \mu\text{m}$ in diameter with a charge of approximately 2 or 3×10^{-5} C/g to a coverage of 10^{-3} g/cm³. This layer of 10^6 toner particles/cm² corresponds to a surface charge of 20 – 30 nC/cm² or about 30% neutralization. Note that while xerographic photoreceptors are nearly 100 times more efficient than silver halide, the final sensitivity is determined by the development process (Schmidlin, 1972). In principle, the development process, and hence the xerographic speed, can be enhanced by increasing surface charge neutralization and reducing the toner charge from 5×10^3 electrons per particle to 10^3 or lower.

X. CONCLUSIONS

Chester Carlson's invention of electrophotography is based on several apparently unrelated areas of physics that were obscure backwaters at the time of the invention. These include contact electrification, photoconductivity, and amorphous solids and polymers. Contact electrification, which plays a major role in the development process, had been known at least since 600 B.C. Although it had been explored during the 18th and 19th centuries, the underlying physics was poorly understood. Systematic treatment of the area of photoconductivity, which was discovered by Willoughby Smith (1873), was initiated by the investigations of Gudden and Pohl and the Göttingen School (Nix, 1932; Hughes, 1936), principally with zinc sulfide, diamond, alkali halides, and crystalline selenium. On the other hand, physics of the amorphous or disordered state in all kinds of materials was nonexistent at the time of the invention. These last two, photoconductivity and amorphous materials, turned out to be critical to the successful maturation of Carlson's invention, since they involve predictable image formation with low-energy sources and the fabrication of uniform large area photoconductors. It is not surprising that the technical people who evaluated the process at some of the major corporations were not impressed and did not see the potential of the process on the basis of the material properties known at that time, since the strong emphasis was then on crystals and metals and the associated fabrication processes. Similarly, the idea of a controlled room air discharge was only a curiosity which has since become commercially important in electrostatic precipitators.

The early stages of the research and development required to transform Carlson's invention into a product were carried out primarily by technologists and empiricists. The vigorous interaction between scientifically oriented research aimed at elucidating microscopic physical properties of the material and the empirical information obtained from the need to optimize the performance of the materials in devices resulted in major advances in the technologies and related sciences from about 1963

onward. The multidisciplinary nature of the electrophotographic process demanded collaborative research with contributions from scientists in many fields, especially physics, chemistry, materials science, imaging science, computer science, and chemical engineering. Major advances have since been made in the physics of the amorphous state, the physics of adhesion between particles, contact electrification, and the generally related issues of the structure-property relationships in relevant materials, mainly polymers.

The stringent material properties required of xerographic photoreceptors have been a major catalyst in the emergence and growth of the science and technology of disordered materials. The current understanding of the electro-optical and material properties of amorphous selenium and its alloys, and those of amorphous organic materials, and, more recently, the structure-property relationships of photoactive organic pigments resulted from the need for high-sensitivity, large-area, and low-cost photoconductors. As a result of these advances in the material technology, organic photoconductors with quantum efficiency of unity have been identified and commercially used. The characterization of disordered materials is no longer viewed as a challenge. The concept of molecular doping of polymers to transport charge is a case of molecular design and engineering which has resulted in the identification and modification of large numbers of charge-transporting organic material systems. Remarkably, some of these systems are devoid of deep traps for charge carriers. The increased understanding of the electronic properties of, and charge transport in, disordered solids has directly benefited from research on xerographic photoconductors. The application of disordered materials as photoconductors in electrophotography has also led to considerable advances in the measurement techniques for unambiguously characterizing these materials.

The complexity of the xerographic development process and the difficulties associated with understanding tribocharging have posed significant scientific challenges in elucidating the physics of the development step. The development step has to balance the conflicting requirements of supplying a large amount of charged toner with a narrow distribution of adhesive force that can be developed at the available fields without causing contamination of the rest of the subsystems. Small toners improve copy quality, reduce image graininess, and reduce fusing-induced stresses which distort the paper. However, small toners are hard to deliver to the photoconductor surface when in a dry state, and they are more costly to produce. In the two-component system, the adhesive forces on the carrier are approximately inversely proportional to the toner radius, requiring large image fields to develop these toners. Once developed, the small toner particles are hard to transfer from the photoconductor surface to the copy medium. The latter results from the increased adhesive force of smaller-diameter toner to the photoconductor surface and the inherent roughness of

paper. Uncharged small toners in the dry development system are likely to cause contamination of the rest of the hardware. The liquid development system, which is capable of delivering small-size toner without dust problems, suffers from the disadvantage of solvent vapors, which need to be recovered, and the aforementioned transfer problem. The innovations in the systems for toner delivery and the material advances needed to meet the requirements of these varied systems have been dramatic. The cascade system, which employed gravity to cascade the carrier beads on the photoconductor surface, was supplanted by the two-component magnetic-brush development system. The replacement of spherically shaped carrier beads with the irregular-shaped beads resulted in a significant increase in the image fields and image density. Advances have also been made in the monocomponent development systems. Toner materials in this case are charged by induction or triboelectric interaction against a suitable donor roll with or without an applied electric field. Although the standard procedure is still to optimize both hardware and material parameters by empirical means, considerable strides have been made in understanding the physics of solid-area development in a very complex and largely uncontrolled environment.

The structure and property relationships that create the delicate balance between adhesive and electrostatic forces in the development step are another instance of technology based on scientific insight and empirical optimization. The advances in the understanding of many features of contact electrification have resulted in more reliable experimental techniques required for optimum selection of materials. The experimental techniques allow one to quantify the rate, equilibrium value, the distribution of charge exchange, and the processes affecting the degradation of charge exchange. Considerable chemical expertise is required to design the toners so that they operate in a stable manner over their useful life. In general, it can be said that sufficient empirical knowledge has been acquired so that phenomenological algebraic descriptions can now be written down and used for simulation purposes, as exemplified by the plots in Fig. 44.

The evolution of electrophotographic imaging technology has been and continues to be influenced by the parallel invention and development of two other technologies: (1) the invention of transistors and the revolution in solid-state electronics and computers, and (2) the invention and development of lasers, both gas and solid state, and light-emitting diodes. Xerographic printing resulted from the successful marriage of the three technologies. As an example, in order to employ a solid-state laser for raster scanning, infrared-sensitive organic photoreceptors had to be developed. Further advances are being made in polymer design and processing for toners in response to an increased use of color in business communications.

Solid-state electronics has been identified as an innovation based on science (Braun and MacDonald, 1978; Mort, 1989). Such is not the case with electrophotography, where innovation and technology lead science. J.

Bronowski (1973), in *The Ascent of Man*, stresses the role of ritual in developing technology when he describes the making of the samurai sword, a process in existence since 800 A.D. The quality control required to produce high-tensile steel was maintained by a "precise ceremonial which fixes the sequence of operations so that they are exact and memorable." Much later, scientific understanding of the metallurgy determined the essential steps of the operation, thereby simplifying the process and improving the product. Modern technology, including electrophotography, is not without art. Deeper scientific understanding of underlying physical processes of the interactive nature of various subsystems enables progress in optimizing materials properties, thereby significantly improving electrophotographic process speed and image quality. Future advances in the understanding and applications of the electronic properties of these materials must involve a closer interdisciplinary collaboration between synthetic chemists, physicists, and materials-manufacturing engineers. In order to fully capitalize on these advances, this interdisciplinary collaboration must extend to those scientists and engineers involved in solid-state optical devices and image processing.

ACKNOWLEDGMENTS

The authors are grateful to Ms. Joanne Fitzmaurice for her assistance in the preparation of this manuscript. We should like to express our appreciation to Dr. Surender Jeyadev of Xerox Corporation for performing the calculations of electric-field profiles within the development zone.

APPENDIX: OTHER ELECTROPHOTOGRAPHIC IMAGING SYSTEMS

1. Electrofax

Electrofax[®] is the trade name of a xerographic system that uses a photosensitive paper on which the final image appears, eliminating the transfer and cleaning steps (Young and Grieg, 1954; Amick, 1959). The photoconductor layer, consisting of zinc oxide particles in a silicone resin binder, is coated on a paper substrate treated with a conducting solution. The scattering of visible light by the zinc oxide particles gives it a white color. Because zinc oxide absorbs only ultraviolet light, the zinc oxide is dyesensitized with, for example, Rose Bengal, fluorescein, or methylene blue dyes, and the appearance of the paper is made as close to plain paper as possible by selecting an appropriate mixture of dyes to produce a light gray color. During the operation, the coated paper is charged to a negative polarity corona and imagewise exposed. The light absorbed in the dye excites electrons, which are transferred to zinc oxide particles and transported through the particle contact network of zinc oxide

particles. The latent image is developed and fused on the coated paper.

For *transparencies*, the final image may be formed directly on a transparent organic photoreceptor. By using liquid development and omitting the transfer step, very high image resolution can be achieved. Another variant is to peel the thin photoconductor layer, with the fused image, from the substrate and laminate it to the paper (Nylund *et al.*, 1986).

2. Overcoated xerography

Overcoated xerography is a variant of the xerographic process which forms the image on a photoreceptor overcoated with an insulating layer. The charge pattern is formed by conventional means and remains across both layers in the unexposed region and only across the insulator in the exposed region. Through the use of an alternating current corotron, the charge is altered so that the electrostatic image remains only in the exposed region. The point of using an insulator, which may be 5–20 μm thick, is as a protective layer for the underlying photoconductor. The electrostatic image is developed with toner and transferred to paper by the conventional steps (Rice and Schaffert, 1972; Mark, 1974). Several variations of this charge-image formation have been proposed and one has been used extensively in copiers. A related process, called TESI (for transfer of electrostatic image), transfers the charge pattern of the electrostatic image onto another insulating layer that is separate from the photoreceptor.

3. Ionography

Ionography is a xerographic process wherein the light-exposure step is eliminated and the charged image pattern is created directly on the insulating dielectric by ion deposition (Selenyi, 1938; Pressman, 1974; Fotland, 1990). An array of addressable charging pins or ion apertures is used to electronically create the charge pattern, which is then developed by liquid or dry toner in the manner already described. The process whereby the ions are created is quite similar to that described in Sec. II.A. The ion flow is directed or controlled by electrostatic forces achieved by voltages applied to microelectrodes. Addressabilities of 300 dots per inch (dpi) are currently being achieved. Several commercial printers use this process.

4. Photoelectrophoresis and particle migration

These electrophotographic processes are based on the electrophoretic motion of charged pigment particles in a liquid or near-liquid dielectric medium. The charge on a pigment particle and hence its motion can be controlled by absorbed light; that is, charge is generated in the pigment and exchanged with the dielectric medium. As

mentioned before, the principle of this process is based on the second term in Eq. (2). Photoelectrophoresis is unique in that it offers the possibility of single-step full-color imaging (Tulagin, 1969; Cressman and Hartmann, 1974; Hartmann and Schmidlin, 1975; Warter *et al.*, 1987). Red, green, and blue wavelengths of light are selectively absorbed by properly formulated cyan, magenta, and yellow pigments. Thus a suspension of these pigments in a dielectric medium layer, with an electric field across the layer, forms a positive color image on one electrode and a corresponding negative image on the other (Fig. 45). The positive image can be transferred and fixed to the paper. Although considerable development work has been carried out to perfect this system, it has not been commercially exploited. A monochromatic variation of this process incorporates an inert pigment with the photoactive pigment (Weigl, 1977). Charge exchange between the two types of particle results in their deposition on the opposite electrode. This process permits the use of a very sensitive pigment, such as phthalocyanine, with an inert pigment of the desired color.

Another variant of this process is based on the principle of particle migration through a thermoplastic that has been temporarily softened by heat or solvent vapor (Fig. 46; see also Goffe, 1971; Pundsack, 1974; Tam *et al.*, 1992). A thin, densely packed film of submicrometer-sized amorphous selenium spheres is embedded near the surface of a 10- μm -thick thermoplastic layer on a metallized base. When negatively charged and exposed in the conventional manner, the α -Se particles in the exposed region become negatively charged. Softening the thermoplastic layer allows the negatively charged particles to migrate into the bulk while in the unexposed region the particles stay near the surface region, resulting in a transmitted light density contrast. A variant of this process can be employed to make master plates for lithography (Bugner, 1991).

Another variant is a process wherein a thin layer of photoactive pigment particles deposited on an electrode is charged and exposed (Weigl, 1977). In the unexposed regions, the pigment adheres electrostatically to the substrate, whereas the pigment in the exposed region ex-

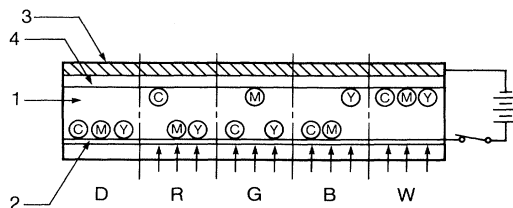


FIG. 45. Polychrome photoelectrophoretic process. A suspension of cyan (C), magenta (M), and yellow (Y) pigments in a liquid dielectric medium is contained between a transparent injecting electrode (2) and a blocking electrode (4). The particle migration under the influence of red (R), green (G), blue (B), white (W), and dark areas is schematically illustrated (after Weigl, 1977).

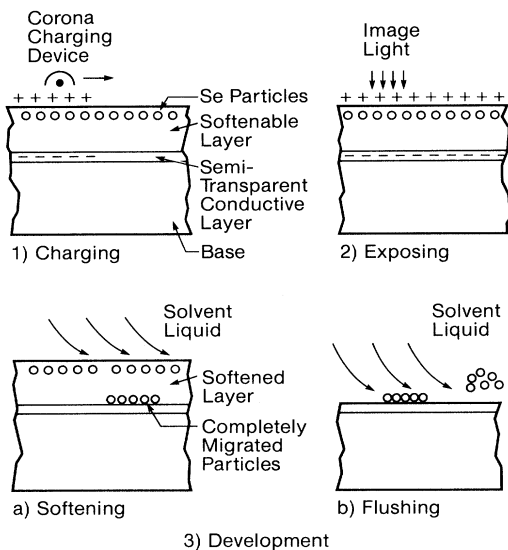


FIG. 46. Imaging steps for a liquid development particle migration system.

changes charges and becomes loose. The loose pigment can be blown away, forming the image.

5. Thermoplastic electrophotography

Thermoplastic electrophotography produces images by surface deformation of a thermoplastic. The photoreceptor can consist of an organic thermoplastic photoconductor or a photoconductive layer overcoated with a thin layer of thermoplastic material (Cressman, 1963; Gundlach and Claus, 1963). In the latter instance, the charge pattern, formed by conventional means (Fig. 47), remains across both layers in the dark regions and across the thermoplastic layer in the light-exposed areas. By charging with an alternating current corotron to zero potential,

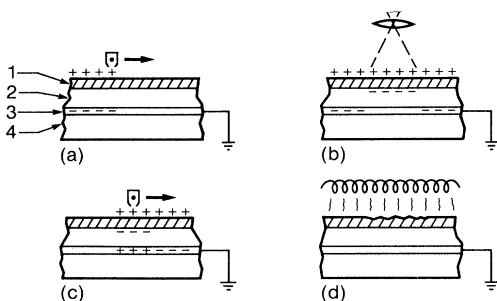


FIG. 47. Steps in the process of overcoated thermoplastic xerography: (a) The structure consisting of insulating substrate (4), conducting layer (3), photoconductor layer (2), and thermoplastic overcoat (1) is uniformly charged. (b) The structure is imagewise exposed; (c) Charge with an ac corotron to zero potential. The charge is removed in the unexposed regions. (d) Upon heating, the electric field in the exposed region causes the thermoplastic to deform.

tential, the charge is removed in the unexposed region but remains in the exposed region [Fig. 47(c)]. Upon heating, the electric-field stress in the exposed region causes the thermoplastic to deform into a wrinkling pattern [Fig. 47(d)], and differential light scattering renders the image visible.

6. Magnetography

This is a scheme that parallels ionography. In this case the receptor is a magnetizable film that can be written on in bitwise fashion to create a digital replica of an image (Eltgen, 1990). The toner in this case is heavily loaded with magnetic material. The image is developed as the magnetic toner dipoles respond to the magnet-field gradient created by the magnetic latent image. This scheme has a drawback for color, since the necessity to magnetically load the toner significantly reduces the achievable color gamut. The main advantage of this process is high speed and the fact that the magnetic material is essentially an erasable master.

REFERENCES

- Abkowitz, M. A., 1987, in *Disordered Semiconductors*, edited by M. A. Kastner, G. A. Thomas, and S. R. Ovshinsky (Plenum, New York), p. 205.
- Abkowitz, M. A., H. Bassler, and M. Stolka, 1991, *Philos. Mag.* **8**, 201.
- Akande, A. R., and J. Lowell, 1985, *J. Electrostat.* **16**, 147.
- Akande, A. R., and J. Lowell, 1987, *J. Phys. D* **20**, 565.
- Ambegaokar, V., B. I. Helperin, and J. S. Langer, 1971, *Phys. Rev. B* **4**, 2612.
- Amick, J. A., 1959, *RCA Rev.* **20**, 770.
- Anderson, J. H., 1989, *J. Imaging Sci.* **33**, 200.
- Barby, D., 1976, in *Characterization of Powder Surfaces*, edited by G. D. Parfitt and R. S. W. Sing (Academic, New York), p. 353.
- Bassler, H., 1981, *Phys. Status Solidi B* **107**, 9.
- Batra, I. P., K. K. Kanazawa, and H. Seki, 1970, *J. Appl. Phys.* **41**, 3409.
- Batt, R. H., C. L. Braun, and J. F. Hornig, 1968, *J. Chem. Phys.* **49**, 1967.
- Batt, R. H., C. L. Braun, and J. F. Hornig, 1969, *Appl. Phys. Suppl.* **3**, 20.
- Bean, L. F., and R. L. Miller, 1978, U.S. Patent 4,124,287.
- Benda, J. A., and W. J. Wnek, 1981, *IEEE Trans. Ind. Appl.* **IA-17**, 610.
- Berger, S. B., R. C. Enck, M. E. Scharfe, and B. E. Springett, 1979, in *The Physics of Selenium and Tellurium*, Proceedings of the International Conference on the Physics of Selenium and Tellurium, Konigstein, Fed. Rep. of Germany, edited by E. Gerlach and P. Grosse (Springer-Verlag, New York), p. 256.
- Bhateja, S. K., and S. K. Gilbert, 1986, *J. Imaging Technol.* **12**, 156.
- Bickmore, J. T., K. W. Gunther, J. F. Knapp, and W. A. Sullivan, 1970, *Photogr. Sci. Eng.* **14**, 42.
- Bickmore, J. T., M. Levy, and J. Hall, 1960, *Photogr. Sci. Eng.*

- 4, 37.
- Binnig, G., C. F. Quate, and C. Gerber, 1986, *Phys. Rev. Lett.* **56**, 930.
- Birkett, K. L., and P. Gregory, 1986, *Dyes Pigm.* **7**, 341.
- Bixby, W. E., 1961, U.S. Patent 2,970,906.
- Borsenberger, P. M., and H. Bassler, 1991, *J. Imaging Sci.* **35**, 79.
- Borsenberger, P. M., L. E. Contois, and D. C. Hoesterey, 1978, *J. Chem. Phys.* **68**, 647.
- Borsenberger, P. M., W. Mey, and A. Chowdry, 1978, *J. Appl. Phys.* **49**, 273.
- Braun, E., and S. MacDonald, 1978, *Revolution in Miniature* (Cambridge University Press, Cambridge).
- Bronowski, J., 1973, *The Ascent of Man* (Little Brown, Boston).
- Bube, R. H., 1960, *Photoconductivity in Solids* (Wiley, New York).
- Bube, R. H., 1992, *Photoelectric Properties of Semiconductors* (Cambridge University Press, Cambridge).
- Bugner, D. E., 1991, *J. Imaging Sci.* **35**, 377.
- Burland, D. M., and L. B. Schein, 1986, *Phys. Today* **39**, No. 5, 46.
- Burne, J. F., 1974, U.S. Patent 3,816,118.
- Burne, J. F., and P. F. Kurz, 1967, U.S. Patent 3,357,989.
- Carlson, C. F., 1940, *Electron Photography*, U.S. Patent 2,221,776.
- Carlson, C. F., 1942, *Electrophotography*, U.S. Patent 2,297,691.
- Chance, R. R., and C. L. Braun, 1976, *J. Chem. Phys.* **64**, 3573.
- Chen, I., 1972, *J. Appl. Phys.* **43**, 1137.
- Chen, I., 1982, *Photogr. Sci. Eng.* **26**, 153.
- Chen, I., 1990, *J. Imaging Sci.* **34**, 15.
- Chen, I., and J. Mort, 1972, *J. Appl. Phys.* **43**, 1165.
- Cheung, L., G. M. T. Foley, P. Fournia, and B. E. Springett, 1982, *Photogr. Sci. Eng.* **26**, 245.
- Cheung, L., and B. E. Springett, 1981, *IEEE Trans. Ind. Appl.* **IA-17**, 502.
- Comizzoli, R. B., S. L. Lozier, and A. R. Ross, 1972, *Proc. IEEE* **60**, 348.
- Cottrell, G. A., J. Lowell, and A. C. Rose-Innes, 1979, *J. Appl. Phys.* **50**, 1374.
- Cressman, P. J., 1963, *J. Appl. Phys.* **34**, 2327.
- Cressman, P. J., and G. C. Hartmann, 1974, *J. Chem. Phys.* **61**, 2740.
- Cressman, P. J., G. C. Hartmann, J. E. Kuder, F. D. Saeva, and D. J. Wychick, 1974, *J. Chem. Phys.* **61**, 2740.
- Dahlquist, J., and I. Brodie, 1969, *J. Appl. Phys.* **40**, 3020.
- Davis, E. A., 1970, *J. Non-Cryst. Solids* **4**, 107.
- Demizu, H., T. Saito, and K. Aoki, 1987, in *Proceedings of the Third International Congress on Advances in Non-Impact Printing Technologies*, edited by J. Gaynor (SPSE, Springfield, VA), p. 84.
- DePalma, V. M., 1982, *Photogr. Sci. Eng.* **26**, 198.
- Dessauer, J. H., 1971, *My Years With Xerox, The Billions Nobody Wanted* (Doubleday, Garden City, NY).
- Dessauer, J. H., and H. E. Clark, 1965, Eds., *Xerography and Related Processes* (Focal, New York).
- Dessauer, J. H., G. R. Mott, and H. Bogdonoff, 1955, *Photogr. Eng.* **6**, 250.
- Diamond, A. S., 1991, Ed., *Handbook of Imaging Materials* (Marcel Dekker, New York).
- Dolezalek, F., 1976, in *Photoconductivity and Related Phenomena*, edited by J. Mort and D. M. Pai (Elsevier, New York), Chap. 1.
- Donald, D. K., 1969, *J. Appl. Phys.* **40**, 3013.
- Donald, D. K., and P. K. Watson, 1972, *IEEE Trans. Electron Devices* **19**, 458.
- Durbeck, R. C., and S. Sherr, 1988, *Output Hardcopy Devices* (Academic, New York).
- El-Kazzaz, A. M., and A. C. Rose-Innes, 1985, *J. Electrostat.* **16**, 157.
- El-Kazzaz, A. M., and A. C. Rose-Innes, 1987, *J. Phys. D* **20**, 1616.
- Eltgen, J. P., 1990, in *Hard Copy and Printing Technologies*, SPIE Proceedings Vol. 1252, edited by K. I. Shimazu (SPIE, Bellingham, WA), p. 104.
- Emin, D., 1973, in *Electronic and Structural Properties of Amorphous Semiconductors*, edited by P. G. LeComber and J. Mort (Academic, New York), Chap. 7.
- Enck, R. C., 1973, *Phys. Rev. Lett.* **31**, 220.
- Enokida, T., R. Hirohashi, and S. Mizukami, 1991, *J. Imaging Sci.* **35**, 235.
- Fabish, T. J., and C. B. Duke, 1977, *J. Appl. Phys.* **48**, 4256.
- Fabish, T. J., and C. B. Duke, 1988, *J. Appl. Phys.* **64**, 2218.
- Felty, E. J., 1967, in *Proceedings of the Second International Congress on Reprography*, edited by O. Helwich (Vertag Dr. Othman Helwich, Darmstadt, Germany), p. 40.
- Fletcher, G. M., 1991, in *Proceedings of the 7th International Congress on Advances in Non-Impact Printing Technologies*, Vol. 1, edited by K. Pietrowski (IS&T, Springfield, VA), p. 157.
- Folkins, J. J., 1985, IEEE-IAS Meeting Conf. Proc. 1510.
- Fotland, R. A., 1990, in *Hard Copy and Printing Technologies*, SPIE Proceedings Vol. 1252, edited by K. I. Shimazu (SPIE, Bellingham, WA), p. 18.
- Gaimo, E., 1957, U.S. Patent 2,786,440.
- Geacintov, N. E., and M. Pope, 1971, in *Proceedings of the 3rd International Conference on Photoconductivity*, edited by P. J. Warter (Pergamon, New York), p. 311.
- Gibson, G. A., R. H. Luebbe, and Y. Kelvin, 1991, in *Proceedings 7th International Congress on Advances in Non-Impact Printing Technologies*, edited by K. Pietrowski (IS&T, Springfield, VA), p. 540.
- Gibson, H. W., 1975, *J. Am. Chem. Soc.* **97**, 3832.
- Gibson, H. W., and H. W. Bailey, 1977, *Chem. Phys. Lett.* **51**, 352.
- Gill, W. D., 1972, *J. Appl. Phys.* **43**, 5033.
- Gill, W. D., 1974, in *Proceedings of the 5th International Conference on Amorphous and Liquid Semiconductors*, edited by J. Stuke and W. Brenig (Taylor and Francis, London), p. 901.
- Goffe, W. L., 1971, *Photogr. Sci. Eng.* **15**, 304.
- Goren, R. N., 1976, *J. Appl. Photogr. Eng.* **2**, 17.
- Gotlieb, M., C. L. M. Ireland, and J. M. Ley, 1983, *Electro-optic and Acousto-optic Scanning and Deflection* (Marcel Dekker, New York).
- Gregory, P., 1985, *Dyes Pigm.* **7**, 1.
- Gruber, R. J., T. J. Pacansky, and J. F. Knapp, 1982, U.S. Patent 4,318,974.
- Gundlach, R. W., 1989, *J. Electrostatics* **24**, 3.
- Gundlach, R. W., and C. J. Claus, 1963, *Photogr. Sci. Eng.* **7**, 14.
- Haas, W. E., 1983, *Mol. Cryst. Liq. Cryst.* **94**, 1.
- Harper, W. R., 1951, *Proc. R. Soc. London, Ser. A* **205**, 83.
- Harper, W. R., 1967, *Contact and Frictional Electrification* (Oxford University, Oxford).
- Hartmann, G. C., and F. W. Schmidlin, 1975, *J. Appl. Phys.* **46**, 266.
- Hays, D. A., 1974, *J. Chem. Phys.* **61**, 1455.
- Hays, D. A., 1977, *J. Appl. Phys.* **48**, 4430.

- Hays, D. A., 1978, *Photogr. Sci. Eng.* **22**, 232.
- Hays, D. A., 1987, *IEEE Trans. Ind. Appl.* **IA-23**, 970.
- Hays, D. A., 1989, *J. Imaging Technol.* **15**, 29.
- Hays, D. A., 1991, *J. Imaging Technol.* **17**, 252.
- Hays, D. A., and D. H. Wayman, 1989, *J. Imaging Sci.* **33**, 160.
- Henniker, J., 1962, *Nature (London)* **196**, 474.
- Hida, M., J. Nakajima, and H. Takahasi, 1982, *IEEE-IAS Meeting Conf. Proc.* 1225.
- Holstein, T., 1959, *Ann. Phys. (N.Y.)* **8**, 325.
- Horn, R. G., and D. T. Smith, 1992, *Science* **256**, 362.
- Hughes, A. L., 1936, *Rev. Mod. Phys.* **8**, 294.
- Incullet, I. I., and E. P. Wituschek, 1967, *Inst. Phys. Conf. Ser.* **4**, 37.
- Itami, A., A. Kinoshita, N. Hirose, K. Watanabe, and K. Sawada, 1991, U.S. Patent 5,039,586.
- Jewett, W. S., 1977, *IEEE-IAS Meeting Conf. Proc.* 557.
- Jeyadev, S., 1991, private communication.
- Johnson, J. L., 1986, *Principles of Non-Impact Printing* (Palatino, Irvine, CA).
- Julien, P. C., 1982, in *Carbon Black-Polymer Composites*, edited by E. K. Sichel (Marcel Dekker, New York), p. 189.
- Junginger, H. G., R. F. Schmidt, and R. Strunk, 1978, *Photogr. Sci. Eng.* **22**, 213.
- Junginger, H. G., and R. Strunk, 1976, *J. Appl. Phys.* **47**, 3021.
- Kakuta, A., T. Mori, and H. Morishita, 1981, *IEEE Trans. Ind. Appl.* **IA-17**, 4.
- Kamimura, T., and I. Itoh, 1991, *Electrophotography* **30**, 318.
- Kanemitsu, Y., and S. Imamura, 1990, *J. Appl. Phys.* **67**, 3728.
- Kao, C. C., 1973, *J. Appl. Phys.* **44**, 1543.
- Karl, N., 1989a, *Mol. Cryst. Liq. Cryst.* **171**, 31.
- Karl, N., 1989b, *Mol. Cryst. Liq. Cryst.* **171**, 157.
- Kasper, G. P., and J. W. May, 1978, U.S. Patent 4,076,857.
- Khe, N. C., O. Takenuchi, T. Kawara, H. Tanaka, and S. Yokota, 1984, *Photogr. Sci. Eng.* **28**, 196.
- Kiyota, K., A. Teshima, and M. Tanaka, 1980, *Photogr. Sci. Eng.* **24**, 289.
- Knights, J. C., and E. A. Davis, 1974, *J. Phys. Chem. Solids* **35**, 543.
- Krupp, H., 1967, *Adv. Colloid Interface Sci.* **1**, 111.
- Kuo, Y., 1984, *Polym. Eng. Sci.* **24**, 9.
- Kurita, T., 1992, *J. Imaging Sci. Technol.* **36**, 209.
- Larson, J. R., 1989, in *Proceedings of the Fourth International Congress on Advances in Non-Impact Printing Technologies*, edited by A. Jaffe (IS&T, Springfield, VA), p. 142.
- Lee, L. H., 1975, in *Adhesion Science and Technology*, edited by L. H. Lee (Plenum, New York), p. 831.
- Lee, L. H., 1978, *Photogr. Sci. Eng.* **22**, 228.
- Lewis, R. B., E. W. Connors, and R. F. Koehler, 1983, *Jpn. J. Electrophotography* **22**, 85.
- Lewis, R. B., and H. M. Stark, 1972, in *Current Problems in Electrophotography*, edited by W. F. Berg and K. Hauffe (de Gruyter, Berlin), Chap. 10.
- Light, W. A., 1971, U.S. Patent 3,615,414.
- Loeb, L. B., 1958, *Static Electrification* (Springer, Berlin).
- Loeb, L. B., 1965, *Electrical Coronas* (University of California, Berkeley).
- Loutfy, R. O., A. M. Hor, and A. Rucklidge, 1987, *J. Imaging Sci.* **31**, 31.
- Lowell, J., 1975, *J. Phys. D* **2**, 53.
- Lowell, J., and A. R. Akande, 1988, *J. Phys. D* **21**, 125.
- Lowell, J., and A. C. Rose-Innes, 1980, *Adv. Phys.* **29**, 947.
- Lowell, J., A. C. Rose-Innes, and A. M. El-Kazzaz, 1988, *J. Appl. Phys.* **64**, 1957.
- Macholdt, H. T., and A. Sieber, 1988, *Dyes Pigm.* **9**, 119.
- Mark, P., 1974, *Photogr. Sci. Eng.* **18**, 254.
- Mees, C. E. K., and T. H. James, 1966, *The Theory of the Electrophotographic Process*, 3rd ed. (Macmillan, New York).
- Melnyk, A. R., 1980, *J. Non-Cryst. Solids* **35-36**, 837.
- Melnyk, A. R., J. H. Neyhart, and R. H. Sperry, 1976, in *Proceedings of the Electrophotographic Conference*, edited by M. Tubbs (Cambridge University, Cambridge, England), p. 99.
- Melnyk, A. R., and D. M. Pai, 1990, in *Proceedings of the SPIE/SPSE Symposium on Electronic Imaging, Santa Clara, USA*, edited by J. Gaynor (SPIE, Bellingham, WA), p. 141.
- Melnyk, A. R., and D. M. Pai, 1992, in *Physical Methods of Chemistry*, Vol. 8, edited by B. W. Rossiter, J. F. Hamilton, and R. C. Baetzold (John Wiley and Sons), in press.
- Melz, P. J., 1972, *J. Chem. Phys.* **57**, 1694.
- Melz, P. J., R. B. Champ, C. Chiou, G. S. Keller, L. C. Licican, P. R. Nieman, M. D. Shattuck, and W. J. Weiche, 1977, *Photogr. Sci. Eng.* **21**, 73.
- Metcalfe, K. A., 1955, *J. Sci. Instrum.* **32**, 74.
- Mitsuya, T., and T. Kumasaka, 1992, *J. Imaging Sci. Technol.* **36**, 88.
- Mizes, H. A., E. M. Conwell, and D. P. Salamida, 1990, *Appl. Phys. Lett.* **56**, 1597.
- Mort, J., 1989, *The Anatomy of Xerography, Its Invention and Evolution* (McFarland, Jefferson, NC).
- Mort, J., and I. Chen, 1975, in *Applied Solid State Science, Vol. 5*, edited by R. Wolfe (Academic, New York), p. 69.
- Mort, J., and D. M. Pai, 1976, *Photoconductivity and Related Phenomena* (Elsevier, New York).
- Mort, J., and D. M. Pai, 1987, in *Amorphous Molecular Solids, Non-Crystalline Solids*, edited by M. Pollak (CRC, Boca Raton), p. 35.
- Mort, J., and G. Pfister, 1978, in *Polym. Technol.* **12**, 89.
- Mort, J., G. Pfister, and S. Grammatica, 1976, *Solid State Commun.* **18**, 693.
- Movaghar, B., M. Grunewald, B. Ries, and H. Bassler, 1986, *Phys. Rev. B* **33**, 5545.
- Mozumdar, A., and J. L. Magee, 1967, *J. Chem. Phys.* **47**, 939.
- Naidis, G. V., 1992, *J. Phys. D* **25**, 477.
- Nakamura, S., 1991, *Electrophotography* **30**, 312.
- Narusawa, T., N. Sawatari, and H. Okuyama, 1985, *J. Imaging Technol.* **11**, 284.
- Nash, R. J., and J. T. Bickmore, 1989, in *Proceedings of the Fourth International Congress on Advances in Non-Impact Printing Technologies*, edited by A. Jaffe (SPSE, Springfield, VA), p. 113.
- Nelson, R. A., 1984, U.S. Patent 4,469,770.
- Neugebauer, H. E. J., 1964, *Appl. Opt.* **3**, 385.
- Neugebauer, H. E. J., 1965, in *Xerography and Related Processes*, edited by J. H. Dessauer and H. E. Clark (Focal, New York), Chap. 8.
- Neyhart, J. H., 1966, *Photogr. Sci. Eng.* **10**, 126.
- Nimura, I., H. Smagoma, H. Yamaga, N. Akuzawa, K. Yuta, and T. Kurasaki, 1984, U.S. Patent 4,433,040.
- Nix, F. C., 1932, *Rev. Mod. Phys.* **4**, 723.
- Noolandi, J., 1977, *Phys. Rev. B* **16**, 4466.
- Nylund, T., C. Cowan, J. Spence, and L. Steele, 1986, in *The Third International Congress on Advances in Non-Impact Printing Technologies*, edited by J. Gaynor (SPSE, Springfield, VA), p. 74.
- Onsager, L., 1934a, *Phys. Rev.* **54**, 554.
- Onsager, L., 1934b, *J. Chem. Phys.* **2**, 599.
- Pai, D. M., 1970, *J. Chem. Phys.* **52**, 2285.
- Pai, D. M., 1980, in *Proceedings of the Tokyo Symposium on Advances in Photography*, edited by K. Honda (Society of Photo-

- graphic Science and Technology of Japan, Tokyo), p. 109.
- Pai, D. M., 1989, in *Proceedings of the Fourth International Congress on Advances in Non-Impact Printing Technologies*, edited by A. Jaffe (SPSE, Springfield, VA), p. 41.
- Pai, D. M., and R. C. Enck, 1975, *Phys. Rev. B* **11**, 5163.
- Pai, D. M., and A. R. Melnyk, 1989, in *Imaging Technology*, Ullmann's Encyclopedia of Industrial Chemistry, edited by (VCH Verlagsgesellschaft, mbH, Weinheim), Vol. A **13**, p. 571.
- Pai, D. M., and J. Yanus, 1983, *Photogr. Sci. Eng.* **27**, 14.
- Pai, D. M., J. Yanus, and M. Stolka, 1984, *J. Chem. Phys.* **88**, 4714.
- Pai, D. M., J. Yanus, M. Stolka, D. Renfer, and W. W. Limburg, 1983, *Philos. Mag. B* **48**, 505.
- Pake, G. E., 1992, *Phys. Today* **45**, No. 4, 56.
- Patsis, A. V., and D. A. Seanor, 1976, *Photoconductivity in Polymers, An Interdisciplinary Approach* (Technomic, Westport, Connecticut).
- Pautmeier, L., R. Richert, and H. Bassler, 1990, *Synth. Met.* **37**, 271.
- Pell, E. M., and K. J. Teegarden, 1969, Eds., *Electrophotography*, Appl. Opt. Suppl. **3**.
- Pfister, G., 1977, *Phys. Rev. B* **16**, 3676.
- Pfister, G., and R. C. Enck, 1976, in *Photoconductivity and Related Phenomena*, edited by M. Mort and D. M. Pai (Elsevier, New York), Chap. 7.
- Popovic, Z. D., 1984, *Chem. Phys.* **86**, 311.
- Popovic, Z. D., A. M. Hor, and R. O. Loutfy, 1988, *Chem. Phys.* **127**, 451.
- Pressman, G. L., 1974, *Second International Conference on Electrophotography, Washington, D.C.*, SPSE **38**, edited by D. R. White (SPSE, Springfield, VA), p. 37.
- Prime, R. B., 1983, *Photogr. Sci. Eng.* **27**, 1.
- Pundsack, A. L., 1974, *Photogr. Sci. Eng.* **18**, 642.
- Regensburger, P. J., 1968, *Photochem. Photobiol.* **8**, 429.
- Rice, P., and R. M. Schaffert, 1972, *Electrophotographic Processes*, IEEE Trans. Electron Devices **19**.
- Rockwitz, K. D., and H. Bassler, 1982, *Chem. Phys.* **70**, 307.
- Rose, A., 1963, *Photoconductivity and Related Processes* (Interscience, New York).
- Ross, D. A., 1979, *Opto-Electronic Devices and Optical Imaging Techniques* (MacMillan, London).
- Ryvkin, S. M., 1964, *Photoelectric Effects in Semiconductors* (Consultants Bureau, New York).
- Sahni, O., 1991, in *Printing Technologies for Images, Gray Scale and Color*, SPIE Proceedings Vol. 1458, edited by D. B. Dove (SPIE, Bellingham, WA), p. 4.
- Sahyun, M. R. V., 1974, *J. Chem. Educ.* **51**, 72.
- Saito, T., T. Kawanishi, and A. Kakuta, 1991, *Jpn. J. Appl. Phys.* **30**, L1182.
- Schaffert, R. M., 1962, *Photogr. Sci. Eng.* **6**, 197.
- Schaffert, R. M., 1975, *Electrophotography*, 2nd ed. (Focal, London).
- Schaffert, R. M., and C. D. Oughton, 1948, *J. Opt. Soc. Am.* **38**, 991.
- Scharfe, M. E., 1984, *Electrophotography Principles and Optimization* (Research Studies, Letchworth, England).
- Scharfe, M. E., D. M. Pai, and R. J. Gruber, 1989, in *Imaging Processes and Materials*, Neblette's 8th ed., edited by J. Sturge, V. Walworth, and A. Shepp (Van Nostrand Reinhold, New York), p. 135.
- Scharfe, M. E., and F. W. Schmidlin, 1975, in *Advances in Electronics and Electron Physics*, edited by L. Marton (Academic, New York), Vol. **38**, p. 83.
- Schein, L. B., 1975a, *Photogr. Sci. Eng.* **19**, 3.
- Schein, L. B., 1975b, *Photogr. Sci. Eng.* **19**, 255.
- Schein, L. B., 1988, *Electrophotography and Development Physics* (Springer-Verlag, New York).
- Schein, L. B., and K. J. Fowler, 1985, *J. Imaging Technol.* **11**, 295.
- Schein, L. B., and J. X. Mack, 1988, *Chem. Phys. Lett.* **149**, 109.
- Scher, H., and E. W. Montroll, 1975, *Phys. Rev. B* **12**, 2455.
- Scher, H., M. F. Shlesinger, and J. T. Bendler, 1991, *Phys. Today* **44**, No. 1, 26.
- Schlosser, G., 1978, *J. Appl. Photogr. Eng.* **4**, 118.
- Schluesener, M., 1991, in *Proceedings of the 7th International Congress on Non-Impact Printing Technologies*, Vol. 1, edited by K. Pietrowski (IS&T, Springfield, VA), p. 167.
- Schmidlin, F. W., 1972, *IEEE Trans. Electron Devices* **4**, 448.
- Schmidlin, F. W., 1977, *Phys. Rev. B* **16**, 2362.
- Schmidt, S. P., J. R. Larson, and R. Bhattacharya, 1991, in *Handbook of Imaging Materials*, edited by A. S. Diamond (Marcel Dekker, New York), p. 227.
- Seanor, D. A., 1978, *Photogr. Sci. Eng.* **22**, 240.
- Selenyi, P., 1938, *J. Appl. Phys.* **9**, 637.
- Shahin, M. M., 1969, in *Electrophotography*, edited by E. M. Pell and K. J. Teegarden (Appl. Opt. Suppl. **3**), p. 106.
- Shaw, R., 1975, *J. Appl. Photogr. Eng.* **1**, 1.
- Sheng, P., 1992, *Philos. Mag. B* **65**, 357.
- Shimizu, I., T. Komatsu, K. Santo, and E. Inoue, 1980, *J. Non-Cryst. Solids* **35/36**, 773.
- Sigmond, R. S., and M. Goldman, 1981, in *Electrical Breakdown and Discharge in Gases*, edited by E. E. Kunhardt and L. H. Luesser (Plenum, New York), p. 1.
- Silver, M., and R. C. Jarnagin, 1968, *Mol. Cryst. Liq. Cryst.* **3**, 461.
- Silver, M., and R. Sharma, 1967, *J. Chem. Phys.* **46**, 692.
- Smith, M., R. Radler, and C. Hackett, 1973, U.K. Patent 1,337,228.
- Smith, Willoughby, 1873, *Nature* **7**, 303.
- Spear, W. E., 1957, *Proc. Phys. Soc. London* **70**, 669.
- Spear, W. E., 1969, *J. Non-Cryst. Solids* **1**, 197.
- Spear, W. E., and P. G. LeComber, 1975, *Solid State Commun.* **17**, 1193.
- Springett, B. E., 1988, *Phosphorus Sulfur* **38**, 341.
- Springett, B. E., F. M. Tesche, A. R. Davies, and J. A. L. Thompson, 1978, *Photogr. Sci. Eng.* **22**, 200.
- Starkweather, G. K., 1980, *Laser Appl.* **4**, 125.
- Starkweather, G. K., 1991, in *Printing Technologies for Images, Gray Scale and Color*, SPIE Proceedings Vol. 1458, edited by D. B. Dove (SPIE, Bellingham, WA), p. 120.
- Stolka, M., J. F. Yanus, and D. M. Pai, 1984, *J. Phys. Chem.* **88**, 4707.
- Sullivan, W. A., and T. L. Thourson, 1967, *Photogr. Sci. Eng.* **11**, 115.
- Takahasi, T., N. Hosomo, J. Kanbe, and T. Toymono, 1982, *Photogr. Sci. Eng.* **26**, 5.
- Tam, M. C., R. O. Loutfy, G. J. Kovacs, A. L. Pundsack, J. Meestor, and H. Aboushaka, 1992, *J. Imaging Sci. Technol.* **36**, 81.
- Tateishi, K., and Y. Hoshino, 1981, *IEEE Trans. Ind. Appl.* **IA-17**, 606.
- Terris, B. D., J. E. Stern, D. Rugar, and H. J. Mamin, 1989, *Phys. Rev. Lett.* **63**, 2669.
- Thourson, T. L., 1972, *IEEE Trans. Electron Devices* **19**, 495.
- Tulagin, V. C., 1969, *J. Opt. Soc. Am.* **59**, 328.
- Umeda, M., T. Niimi, and M. Hashimoto, 1990, *Jpn. J. Appl. Phys.* **29**, 2746.
- Vahtra, V., and R. F. Wolter, 1978, *IBM J. Res. Dev.* **22**, 34.

- Walkup, L., 1952, U.S. Patent 2,618,551.
- Warner, P., V. Tulagin, and L. Carreira, 1987, in *The Third International Congress on Advances in Non-Impact Printing Technologies*, edited by J. Gaynor (SPSE, Springfield, VA), p. 419.
- Watanabe, Y., K. Okada, M. Sato, and S. Namekata, 1991, *Electrophotography* **30**, 439.
- Waters, R. T., and W. B. Stark, 1975, *J. Phys. D* **8**, 416.
- Watson, P. K., 1979, *Inst. Phys. Conf. Ser.* **48**, 1.
- Weigl, J., J. Mammino, G. L. Whittaker, R. W. Radler, and J. F. Byrne, 1972, in *Current Problems in Electrophotography*, edited by W. F. Berg and K. Hauffe (De Gruyter, Berlin), p. 287.
- Weigl, J. W., 1977, *Agnew. Chem. Int. Ed. Engl.* **16**, 374.
- Weiser, G., 1972, *J. Appl. Phys.* **43**, 5028.
- Williams, E. M., 1982, *Photogr. Sci. Eng.* **26**, 88.
- Williams, E. M., 1984, *The Physics and Technology of Xerographic Processes* (Wiley, New York).
- Williams, E. W., and R. Hall, 1978, *Luminescence and Light Emitting Diode* (Pergamon, Oxford).
- Wise, E., 1952, U.S. Patent 2,618,552.
- Witte, J. C., and J. F. Szczepanik, 1978, *J. Appl. Photogr. Eng.* **2**, 52.
- Wyszecki, G., and W. S. Stiles, 1982, *Color Science*, 2nd ed. (Wiley & Sons, New York).
- Yang, C. C., and G. C. Hartmann, 1976, *IEEE Trans. Electron Devices* **23**, 308.
- Yarmchuk, E. J., and G. E. Keefe, 1989, *J. Appl. Phys.* **66**, 5435.
- Young, C. J., 1957, U.S. Patents 2,786,439 and 2,786,441.
- Young, C. J., and H. G. Grieg, 1954, *RCA Rev.* **15**, 441.
- Yourd, R. A., D. Majumdar, and R. J. Gruber, 1985, U.S. Patent 4,537,848.
- Yu, Z., and P. K. Watson, 1989, *J. Phys. D* **22**, 798.
- Yuh, H. J., and M. Stolka, 1988, *Philos. Mag. B* **58**, 539.
- Yule, J. A. C., 1967, *Principle of Color Reproduction* (Wiley & Sons, New York).
- Zaretsky, M. C., 1991, in *Proceedings of the 7th International Congress on Advances in Non-Impact Printing Technologies*, Vol. 1, edited by K. Pietrowski (IS&T, Springfield, VA), p. 73.
- Zimon, A. D., 1969, *Adhesion of Dust and Powder* (Plenum, New York).



FIG. 1. Chester Carlson's first image, consisting of the date and location (Astoria, NY), which he used as a successful demonstration of the electrophotographic process (after Carlson, 1942).

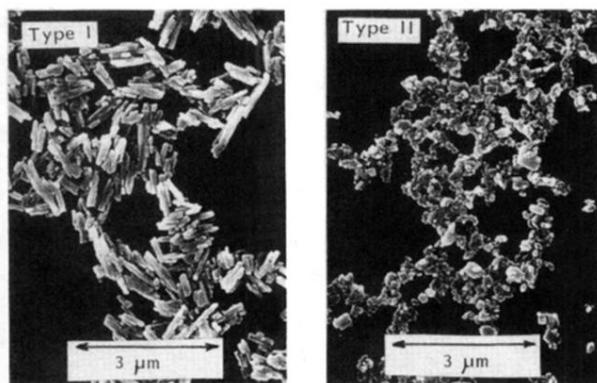


FIG. 17. Scanning electron micrograph of pigments (metal-free phthalocyanine) in the generator layer (after Enokida *et al.*, 1991).

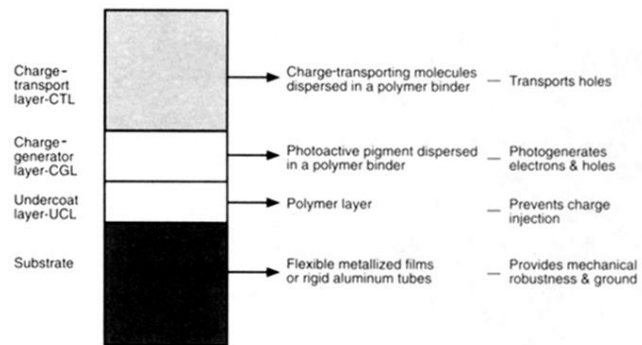


FIG. 7. Generic structure of a typical organic photoconductor found in today's copiers and printers. The functions of the different layers are indicated on the right. This type of design permits flexibility in the choices of materials in order to optimize overall device performance.

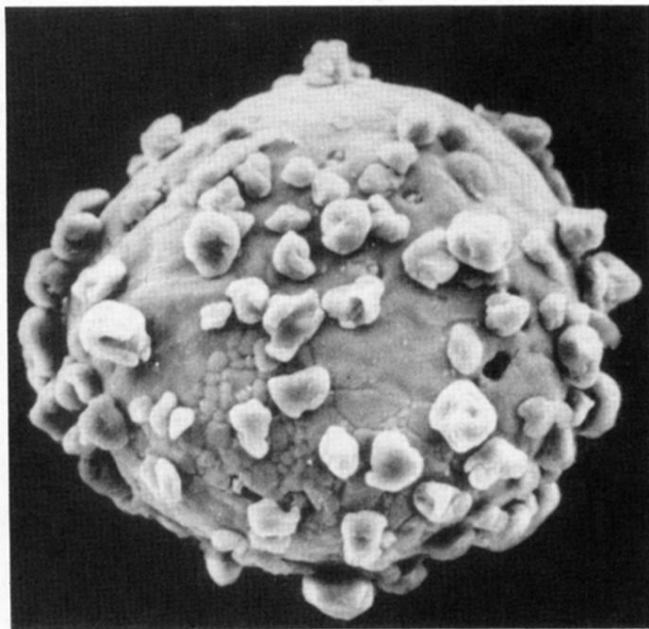


FIG. 8. Photomicrograph of a charge developer bead. Toner particles are held to the polymer-coated carrier bead primarily by electrostatic forces. Toner diameter is 5–20 μm . Carrier beads are 50–150 μm in diameter (after Scharfe *et al.*, 1989).